

## ABSTRACT

ZWILLING, JACOB, DENNIS. Fundamental Understanding of the Formation of Lignin Colloids by Nanoprecipitation and Their Potential for Antimicrobial Applications. (Under the direction of Dr. Ronalds Gonzalez, Dr. Richard Venditti, and Dr. Hasan Jameel,)

Colloids are a heterogeneous mixture of compounds in which one or more compounds are dispersed within a continuous medium. Colloids allow for what would normally be a two-phase immiscible mixture of materials to exist as a stable homogenous dispersion of the two phases. Colloids are crucial in food systems, healthcare, energy, and materials manufacturing and unlock a greater versatility of applications for immiscible compounds. Lignin, a plant-derived aromatic polymer, possesses self-assembly characteristics in aqueous systems that allow for colloid formation. This transformation of lignin expands its uses in aqueous environments and may be a viable candidate for antimicrobial carrier solutions.

The transformation of lignin as an industrial waste product to a functional lignin nanoparticle (LNP) and its potential applications in antimicrobial formulations was investigated from a fundamental perspective in this work. To better understand the formation mechanisms and colloidal interactions of LNPs, a fractionation method was implemented to isolate specific physical and chemical characteristics of lignin and their relationship to the nanoscale. The fundamental understanding of LNPs allows for the development of other colloid formulations such as nanocomplexes with small molecules for antimicrobial applications.

Firstly, an observational study of the persistence of foodborne-related bacterial organisms on lignocellulosic surfaces was performed by inoculating bleached and unbleached paper surfaces with bacterial cultures. This provided the motivation for future work to develop biobased antibacterial solutions to foodborne outbreaks. It was determined that two model organisms for bacterial foodborne pathogens, *Salmonella enterica* serovar Typhimurium and

*Listeria innocua* can survive on lignocellulosic surfaces for over 40 days, with little reduction in the viable bacteria populations. Contrary to our initial hypothesis that lignin's aromatic structure may yield antibacterial activity, it was found that the lignin-containing surfaces yielded higher bacterial growth compared to fully bleached paper surfaces. This was attributed to the higher hydrophobicity of the lignin-containing surface, providing enhanced nutrient accessibility to the organisms.

Secondly, to promote the design of antimicrobial biobased nanomaterials, the synthesis and characteristics of lignin nanoparticles was investigated. A nanoprecipitation method was implemented using a solvent exchange process by solubilizing lignin in a water-miscible organic solvent followed by the rapid addition of excess water, to which lignin has negligible solubility. To dive deeper into the formation mechanisms, different fractions of lignin were isolated, each with a unique chemical and molecular weight distribution. It was determined that LNPs formed from more hydrophilic lignin were 67% larger on average than those formed from less hydrophilic lignin. This was attributed to a particle swelling and fusion phenomenon due to higher interactions between the lignin fraction and the aqueous medium. It was also determined that less hydrophilic LNPs possess a higher surface free energy, resulting in the aggregation of individual particles driven by hydrophobic forces. In this work we investigated the surface forces that play a role in the formation and stability of soft colloids that can be extrapolated to other colloidal systems.

Thirdly, to develop antibacterial solutions from biobased materials, lignin was coprecipitated with a known antibacterial essential oil compound, isoeugenol, at a high oil-to-lignin ratio. This coprecipitation was engineered using concepts from the ouzo effect in which a submicron droplet is spontaneously formed by supersaturated nucleation. The lignin

nanocomplex (LNC) configuration was suggested to follow the unique case of “trapped species in a droplet”, in which lignin stabilizes an isoeugenol droplet from within by balancing the surface interactions at the oil-water interface. It was determined that lignin greatly increases the stability of an isoeugenol dispersion through ripening inhibition, as evidenced by the consistent turbidity at high ionic strengths and elevated temperatures. The improved stability of the isoeugenol dispersion translated to twice the antibacterial activity against *Salmonella enterica* serovar Typhimurium and *Listeria innocua* in solution and on dry paper surfaces. Lignin was also fractionated to tune the LNC characteristics and stability. Less hydrophilic lignin fractions enhanced the stability of isoeugenol to a greater degree than more hydrophilic lignin fractions. This work elucidates the versatility of lignin as a nanomaterial and potential for lignin valorization in antimicrobial applications.

Finally, the design of a continuous nanoprecipitation mixer ( $NP_{cont}$ ) to produce LNPs was reported using concepts from the Venturi effect. The Venturi effect employs a laminar flow of fluid through a constricted volume to generate a drop in static pressure that may be exploited to generate a flow of a second stream. The two streams used for LNP formation were a continuous flow of water and an aqueous acetone lignin solution. In this research, the solvent effects of LNP formation were investigated and the determine optimal parameters were used for LNP scaled-up synthesis. The  $NP_{cont}$  showed potential to produce much smaller particles than at the bench scale and at a rate of 225 g/hour on a dry basis.

© Copyright 2022 by Jacob Dennis Zwilling

All Rights Reserved

Fundamental Understanding of the Formation of Lignin Colloids by Nanoprecipitation and Their  
Potential for Antimicrobial Applications

by  
Jacob Dennis Zwilling

A dissertation submitted to the Graduate Faculty of  
North Carolina State University  
in partial fulfillment of the  
requirements for the degree of  
Doctor of Philosophy

Forest Biomaterials

Raleigh, North Carolina  
2022

APPROVED BY:

---

Dr. Ronalds W. Gonzalez  
Committee Co-Chair

---

Dr. Richard A. Venditti  
Committee Co-Chair

---

Dr. Hasan Jameel  
Committee Co-Chair

---

Dr. Orlin Velev

---

Dr. Orlando J. Rojas

---

Dr. Amy Grunden  
Graduate School Representative

## **DEDICATION**

To my parents, Stephen and Lisa, who have always loved and supported me in the best of times and in the worst of times.

To my late brother Jeff, who inspired me to start my academic journey in the sciences.

To my lifelong friends I have developed at NC state.

“Only a life lived for others is a life worthwhile” – Albert Einstein

## **BIOGRAPHY**

Jacob Dennis Zwilling was born on April 29<sup>th</sup>, 1996 in Delaware, USA. He started his college career after high school in 2014 at the University of North Carolina at Charlotte. He transferred the following year to the University of North Carolina at Wilmington where he completed his Bachelors of Science in Chemistry and Minor in Mathematics in 2018. During his undergraduate studies, he conducted research under the direction of Dr. Bart Jones, and Dr. Robert Hancock on the formation constants of organometallic coordination complexes. He finished his undergraduate degree with research honors in chemistry. He became interested in nanomaterials towards the end of his undergraduate degree and pursued a Ph.D. in Forest Biomaterials at North Carolina State University under the guidance of Dr. Ronalds Gonzalez, Dr. Hasan Jameel, and Dr. Richard Venditti.

## ACKNOWLEDGMENTS

First and foremost, I would like to acknowledge the guidance I have been given throughout the PhD at NC State. I came to NC State with a strong curiosity and work ethic but lacked direction. I am grateful to Dr. Ronalds Gonzalez, Dr. Hasan Jameel, and Dr. Richard Venditti who were pivotal in providing me with that direction. They guided me not only on an academic level but at a personal level and this has resulted in lifelong skills as a professional and as an individual.

To Dr. Ronalds Gonzalez, who challenged me beyond where I believed I could go and gave me the freedom to explore my curiosity. To Dr. Hasan Jameel, who kept me grounded and always brought my research back to reality when it began to runoff. To Dr. Richard Venditti, who taught me the fundamentals of becoming a scientific researcher and how to think critically and be brave with your ideas. To Dr. Orlin Velez, who always put an effort into really understanding my research and helping to develop the more complex ideas. To Dr. Amy Grunden, who aided me in my transition to working in the microbiology sphere, which was outside of my comfort zone. To Dr. Orlando Rojas, who founded the topic of my research and inspired my curiosity.

I would like to give a special thanks to Xiao Jiang, who was always willing to sit with me during my early days as a researcher and helped guide my research and rationale. His patience and understanding did not go unnoticed. I have great gratitude to all my friends I have earned in the Department of Forest Biomaterials, many of which I can consider my family now.

Finally, to my family who never doubted my success and provided me the confidence and resources to challenge myself beyond what I thought was possible.

## TABLE OF CONTENTS

LIST OF TABLES .....	viii
LIST OF FIGURES .....	ix
1 INTRODUCTION .....	1
1.1 Lignin description .....	1
1.2 Lignin availability and commercial isolation.....	2
1.3 The rise of paper packaging .....	4
1.4 Foodborne pathogens and their prevalence.....	6
1.4.1 Foodborne infections .....	9
1.4.2 Essential oils entrapment .....	12
2 BACKGROUND .....	16
2.1 Nanoprecipitation method.....	16
2.2 Mechanisms of nanoparticle formation.....	17
2.2.1 Classical nucleation and growth .....	17
2.2.2 Solid-liquid phase transitions.....	22
2.3 The Ouzo effect.....	25
2.4 Ostwald ripening .....	27
3 SURVIVABILITY OF <i>SALMONELLA</i> TYPHIMURIUM (ATCC 14208) AND <i>LISTERIA</i> <i>INNOCUA</i> (ATCC 51742) ON LIGNOCELLULOSIC MATERIALS FOR PAPER PACKAGING .....	31
3.1 Abstract .....	31
3.2 Introduction .....	31
3.3 Materials and Methods.....	35
3.3.1 Materials .....	35
3.3.2 Fabrication of Paper Samples .....	36
3.3.3 Characterization of Paper Samples .....	36
3.3.4 Inoculation of Microbes on Paper.....	36
3.3.5 Bacterial Enumeration .....	38
3.3.6 Statistical Analysis.....	38
3.4 Results .....	39
3.4.1 Survivability of bacteria on lignocellulosic materials .....	39
3.5 Discussion .....	46

3.6	Conclusions .....	49
4	UNDERSTANDING LIGNIN MICRO- AND NANOPARTICLE NUCLEATION AND GROWTH BY SOLVENT FRACTIONATION <sup>1</sup> .....	51
4.1	Abstract .....	51
4.2	Introduction .....	52
4.3	Materials and Methods.....	56
4.3.1	Materials .....	56
4.3.2	Methods.....	57
4.3.3	Fractionation of Kraft Lignin.....	58
4.3.4	Molecular Weight Determination of Lignin Fractions by Gel-Permeation Chromatography. ....	59
4.3.5	Lignin Hydroxyl Group Content by <sup>31</sup> P-NMR Analysis .....	60
4.3.6	Derjaguin-Landau-Verwey-Overbeek (DLVO) Model of Lignin Particles .....	60
4.3.7	Preparation of Kraft Lignin Particles.....	61
4.3.8	Dynamic Light Scattering.....	61
4.3.9	Transmission Electron Microscopy (TEM) .....	62
4.4	Results and Discussion.....	62
4.4.1	Lignin Fractionation and Molecular Weight Distribution .....	62
4.4.2	NMR Analysis of Solvent Fractionated Kraft Lignin.....	65
4.4.3	Fractionation Effects on Lignin Particle Formation .....	67
4.4.4	Concentration Effects on Lignin Particle Formation .....	74
4.5	Conclusions .....	81
5	ANTISOLVENT PRECIPITATION OF SURFACTANT-FREE ISOEUGENOL LIGNIN NANOCOMPLEXES FOR ANTIMICROBIAL APPLICATIONS .....	83
5.1	Abstract .....	83
5.2	Introduction .....	83
5.3	Materials and Methods.....	87
5.3.1	Materials .....	87
5.3.2	Solvent fractionation of kraft lignin.....	88
5.3.3	Essential oil loaded lignin nanocomplex synthesis.....	89
5.3.4	Particle Size Distribution .....	89
5.3.5	Stability .....	89
5.3.6	Isoeugenol release profile .....	89
5.3.7	Antibacterial activity.....	91
5.3.8	Transmission electron microscopy of Bacteria.....	92

5.3.9	Antibacterial activity on surfaces.....	92
5.4	Results .....	93
5.4.1	Particle Characteristics.....	93
5.4.2	Antimicrobial activity of LNCs .....	102
5.5	Discussion .....	106
5.5.1	Trapped Species in a Droplet Hypothesis.....	107
5.5.2	Antibacterial activity.....	110
5.6	Conclusions .....	111
6	HIGH-THROUGHPUT CONTINUOUS NANOPRECIPITATION DESIGN FOR LIGNIN NANOPARTICLE PRODUCTION UTILIZING THE VENTURI EFFECT .....	112
6.1	Abstract .....	112
6.2	Introduction .....	112
6.3	Materials and Methods.....	115
6.3.1	Materials .....	115
6.3.2	Methods.....	115
6.3.3	Particle size analysis .....	118
6.4	Results and discussion.....	118
6.4.1	Solvent effects on LNP formation .....	118
6.4.2	Scalability of LNP production .....	121
6.5	Conclusions .....	123
7	CONCLUSIONS.....	125
8	FUTURE WORK.....	127
9	REFERENCES .....	129
10	APPENDICES .....	157
	APPENDIX A: Supplementary Information for Chapter 3 .....	158
	Short term effects of storage conditions .....	158
	JSL code for comparison of slopes test.....	159
	Non-linear model of bacterial growth and decay.....	160
	Microscopic images of paper specimens .....	162

## LIST OF TABLES

Table 1-1. Estimated cost of foodborne illness from bacterial pathogens.....	8
Table 1-2. Examples of recent outbreaks of foodborne illness in the U.S. (FDA, 2020).....	10
Table 3-1. Paper characteristics and extraction efficiencies ( $\epsilon$ ) of microbes from bleached (SBSK) and unbleached (UBSK) pulps. The arithmetic extraction efficiency is the average CFU extracted from each paper type divided by the average CFU in the inoculum.....	40
Table 3-2. Fitting parameters for each of the linear regressions displayed in Fig. 3-2. Values for the parameters were calculated using JMP standard least squares fit model with paper and bacteria as fixed effects as well as the interaction term. The comparison of slopes test was computed using a customized least squares regression (see supplementary material, Section 2). A p-value $< 0.05$ is considered a statistically significant difference.....	44
Table 3-3. Comparison of least squares means for each of the four conditions tested. A p-value $< 0.05$ is considered a statistically significant difference.....	45
Table 4-1. Lignin fractionation results including molecular weight of each fraction after acetylation measured by gel-permeation chromatography (Mn: Number-average molecular weight; Mw: Weight-average molecular weight, PDI: polydispersity index). .....	64
Table 4-2. Hydroxyl content of kraft lignin fractions by $^{31}\text{P}$ NMR calculated as mmol/g of solid. The polarity of the organic solvent used to dissolve each fraction relative to water is listed as a reference value. C5-substitued-OH can be either 5-5 biphenyl structure or $\alpha$ -5 condensed G-unit. C5-free-OH contains a hydrogen in the C5 position. Finally, H-OH phenolic is the C5 and C3 free phenolic-OH. ....	66
Table 4-3. Critical initial lignin concentration ( $C_0$ ) and resulting average particle diameters measured by DLS for each solvent system. ....	76
Table 5-1. Parameters and goodness of fit for the Weibull release kinetic model. $R_\infty$ is the asymptotic maximum cumulative release, $\tau$ is the scale factor, $\beta$ is the shape factor, and $R^2$ is the coefficient of determination. ....	101
Table 6-1. Reynold's number calculation for the continuous LNP Venturi mixer.....	123

## LIST OF FIGURES

Figure 1-1. Conventional monolignols for lignin biosynthesis .....	1
Figure 1-2. Diagram of the LignoBoost method from Valmet (Hamaguchi et al., 2012; <i>Lignin Extraction Process</i> , n.d.) .....	3
Figure 1-3. Total packaging waste disposal pathways in the U. S. from 1960 to 2018 (US EPA, 2018). .....	5
Figure 1-4. Types of nanostructured encapsulation systems applied for essentials oils with antiviral activity (Marquez et al., 2022). .....	13
Figure 2-1. Gibb’s free energy diagram of the surface free energy and bulk free energy contributions to nucleation events as a function of particle radius (Thanh et al., 2014). .....	19
Figure 2-2. Gibb’s free energy correction factor ( $\beta$ ) for heterogeneous nucleation as a function of particle interface contact angle ( $\Theta$ ). .....	21
Figure 2-3. Free energy of mixing diagram and the solution composition in terms of polymer concentration (Brick et al., 2003; C. Zhao, 2016). .....	23
Figure 2-4. Free energy of mixing and phase diagram of a solute precipitation from solution by the addition of a non-solvent ( $C_{0-3}$ ) (Brick et al., 2003) .....	24
Figure 2-5. Phase diagram of divinylbenzene precipitated from an ethanol water solution (Ganachaud & Katz, 2005; Vitale & Katz, 2003). .....	26
Figure 2-6. The relationship between the particle radius and chemical potential of a molecule at the surface of a particle. ....	29
Figure 2-7. Chemical potential of a molecule at the surface of a particle containing a ripening inhibitor. ....	30
Figure 3-1. Average log CFU/cm <sup>2</sup> of <i>L. innocua</i> and <i>S. Typhimurium</i> on bleached and unbleached paper specimens over a 40-day period. The average log CFU/cm <sup>2</sup> was corrected for the extraction efficiencies ( $\epsilon$ ) as described previously. The error bars are representative of the standard deviation. ....	42
Figure 3-2. Standard least squares regressions for each of the four conditions (two bacteria, two papers). The average log CFU/m <sup>2</sup> was corrected for the extraction efficiencies ( $\epsilon$ ) as described previously. The error bars are representative of the standard deviation. Slopes, y-intercepts, and R <sup>2</sup> values are displayed in Table 2. ....	43
Figure 3-3. Least squares (LS) means of each of the four conditions studied. Error bars are representative of the 95% confidence interval. ....	46

Figure 4-1. Schematic of different solvent shifting methods including a) lignin solution-into-water, b) water-into-lignin solution, and c) dialysis of lignin solution with water. ..	54
Figure 4-2. Flowchart of lignin fractionation, characterization, and particle synthesis. ....	57
Figure 4-3. Methodology of kraft lignin solvent fractionation and description of lignin fractions. ....	59
Figure 4-4. Percentage yield of KL distributed in each fraction by mass percent. The first column (left) represents the completely separated fractions of KL extracted through solvent fractionation. The middle and right columns are representative of combined lignin fractions by dissolving KL in acetone (AE-Frac) and THF (TAE-Frac), respectively. ....	63
Figure 4-5. Molecular weight distribution curves of each lignin fraction with the intensity normalized to 1 as measured by GPC. Higher molecular weight molecules elute first, whereas lower retention time corresponds to higher molecular weight. ....	64
Figure 4-6. Average particle diameter ( $\delta$ ), weight average MW, and phenolic hydroxyl content for 1) E-LPs, 2) AE-LPs, 3) A-LPs, 4) TAE-LPs, and 5) T-LPs at a precursor lignin solution concentration of 5 g/L. Error bars are smaller than the size of the icons. Standard deviation of particle diameters were < 10 nm. ....	68
Figure 4-7. a) TEM images of E-LPs, A-LPs, and T-LPs formed from the three separate lignin fractions, E-Frac, A-Frac, and T-Frac at an initial lignin concentration of 5 g/L. b) TEM images of AE-LPs and TAE-LPs formed from the combined lignin fractions, AE-Frac and TAE-Frac. c) Proposed mechanism of lignin particle nucleation and particle swelling. i) T-LP and A-LP nucleation of higher MW species followed by adsorption particle growth. ii) E-LP nucleation followed by adsorptive growth and particle swelling by means of osmosis. iii) TAE-LP and AE-LP nucleation of high MW lignin followed by particle growth by adsorption of lower MW lignin. Top row of TEM images scale bars = 500 nm and bottom row of TEM images = 100 nm ....	70
Figure 4-8. Average particle diameter as a function of precursor lignin concentration for TAE-LPs, E-LPs, A-LPs, T-LPs, and AE-LPs as determined by DLS. TAE-LPs are plotted alongside the fractionated LP samples for comparison of the average particle diameter over the concentration profiles. Error bars are smaller than the size of the icons. Standard deviation of particle diameters were < 10 nm. ....	75
Figure 4-9. Scattered light intensity weighted particle size distribution of T-LPs approaching the critical concentration, $C_0$ , measured by DLS. ....	77
Figure 4-10. TEM images of T-LPs at an initial lignin concentration of 5 g/L and 1 g/L in THF prior to antisolvent addition. ....	77
Figure 4-11. Energy of interactions between lignin particles following DLVO model including electrostatic and Van der Waals interactions. Input parameters are shown in the	

figure legend. Hamaker constant = $1.7 \times 10^{21}$ J, Ionic strength = 0.001 M, $\epsilon = 78.5$ , $\kappa^{-1} = 10$ nm. ....	79
Figure 4-12. a) Lignin particle suspensions with increasing precursor lignin concentration for each of the separated fractions. All suspensions seemed visibly well-dispersed with the exception of E-LPs at 7.5 and 10 g/L where sedimentation and flocculation is visible. b) TEM images of E-LPs at an initial lignin concentration of 5 g/L and 10 g/L in solution prior to antisolvent addition. ....	80
Figure 5-1. Molecular structure of a) eugenol and isoeugenol, and b) monomeric building blocks of lignin.....	86
Figure 5-2. Particle size distribution as measured by dynamic light scattering and the intensity-weight Z-average particle diameter, $\delta$ . ....	94
Figure 5-3. Kraft lignin, isoeugenol, and LNC characteristics including a) GPC chromatogram of each of the lignin fractions and the starting lignin material, b) the yield of each lignin fraction separated by solvent fractionation relative to the unfractionated kraft lignin, b) the precipitation point of each the neat constituents, c) SEM images of d) LNCs formed from the F1 lignin fraction, e) LNCs formed from the F2 lignin fraction, f) LNCs formed from the F3 lignin fraction, g) LNCs formed from the F4 lignin fraction, h) LNCs formed from the unfractionated kraft lignin sample. The precipitation point was performed in triplicate with no significant standard deviation. ....	96
Figure 5-4. Relative stability of colloidal dispersions of isoeugenol with (LNC) and without (ID) the complexation with kraft lignin. a) Optical density reduction of the ID and LNC suspensions after 12 hours of exposure to a range of NaCl concentrations (1.2 mM to 1.2 M). b) Optical density reduction of the LNC suspensions formed from the fractionated lignins after 12 hours of exposure to varying NaCl concentrations (1.2 mM to 1.2 M). c) Optical density reduction of the ID and LNC suspensions after 12 hours of exposure to elevated temperatures (37°C) in MilliQ water. ....	98
Figure 5-5. Release profile of unfractionated LNCs and IDs reported as cumulative release as a function of time and the fitted Weibull release kinetic model. a) Release profile for LNCs dialyzed with MilliQ water. b) Release profile for IDs dialyzed with MilliQ water. c) Release profile for LNCs dialyzed with phosphate buffer solution. d) Release profile for IDs dialyzed with phosphate buffer solution. This experiment was performed in duplicate and the standard deviation for each sample and time was less than 1%. ....	100
Figure 5-6. Antibacterial activity of the LNCs and IDs. a) Growth curves of <i>S. Typhimurium</i> exposed to varying concentration of IDs measured by optical density as a function of time. b) Growth curves of <i>S. Typhimurium</i> exposed to varying concentration of LNCs measured by optical density as a function of time. c) Growth curves of <i>L. innocua</i> exposed to varying concentration of IDs measured by optical density as a function of time. d) Growth curves of <i>L. innocua</i> exposed to varying concentration of LNCs	

measured by optical density as a function of time. e-g) Transfer of viable *S. Typhimurium* from untreated paper (e), paper treated with IDs (f), and paper treated with LNCs (g) to a human hand. h-j) Transfer of viable *L. innocua* from untreated paper (e), paper treated with IDs (f), and paper treated with LNCs (g) to a human hand. k) Schematic of the transferability of bacteria test from paper to hand. .... 103

Figure 5-7. TEM images of *L. innocua* and *S. Typhimurium* untreated and treated with LNCs. A) Untreated *L. innocua*, B) untreated *S. Typhimurium*, c) treated *L. innocua*, B) treated *S. Typhimurium*. .... 105

Figure 5-8. Proposed LNC formation mechanism. a) ID droplet ripening. b) Low MW lignin LNC formation and drying mechanism. c) High MW lignin LNC formation and drying mechanism. Green is acetone, blue is water, yellow is IE and brown is lignin. d) The interplay of capillary pressure and Laplace pressure between two generic spherical particles (gray) upon evaporation of the solvent (R. Chen et al., 2016). . 109

Figure 6-1. Schematic of the Venturi mixer modified for LNP production at scale. .... 114

Figure 6-2. Diagram of a) the continuous nanoprecipitation mixer (NP<sub>cont</sub>) and b) the batch method of LNP production (NP<sub>batch</sub>). .... 117

Figure 6-3. Saturated solubility of KL in aqueous acetone and aqueous THF. .... 118

Figure 6-4. Average particle size of LNPs produced from fractionated lignins in A90 and THF 90 precursor solvents. .... 120

Figure 6-5. Average particle diameter of LNPs produced from the different precipitation methods: Continuous (NP<sub>cont</sub>), Bench (NP<sub>bench</sub>), and Batch (NP<sub>batch</sub>). .... 122

Figure S10-1: Scanning electron microscope image of bleached (left) and unbleached (right) paper specimens. SEM images were taken of the paper specimens with a JEOL JCM-6000 Benchtop SEM. The paper specimens were coated with gold using a sputter coater directly prior to image acquisition. .... 162

# 1 INTRODUCTION

## 1.1 Lignin description

Lignin exists in almost all forms of biomass and is the second most abundant biopolymer in nature behind cellulose. It acts as a structural component of plant cell walls that provides rigidity and support at the cellular and organismal level. It is a polyphenolic biopolymer with a diverse chemical structure dependent on the biomass source. It is synthesized from three phenylpropanoid subunits, termed monolignols that undergo a polymerization process within the plant cells resulting in a complex structure that is not very well characterized due to chemical changes during extraction (see Figure 1-1). The ratios of these monolignols vary with the biomass source, greatly affecting the chemistry of the polymer. Softwood lignin results from the polymerization, *in vivo*, of predominantly one of the three monolignols, namely coniferyl alcohol, whereas hardwood lignin results from the polymerization of a mixture of coniferyl alcohol and sinapyl alcohol. All three monolignols are prominent during the polymerization of non-wood lignin.

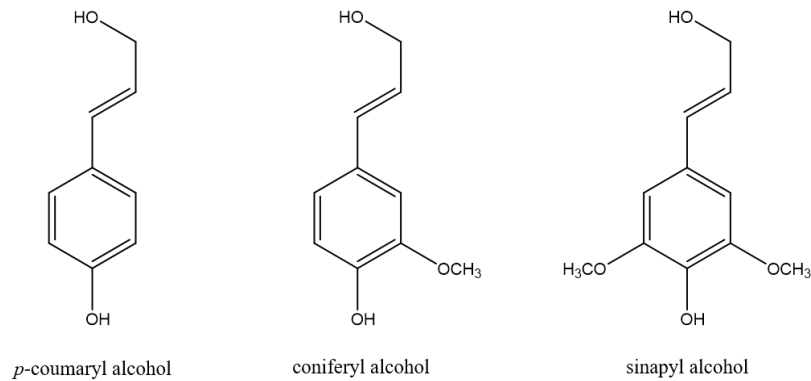


Figure 1-1. Conventional monolignols for lignin biosynthesis

Utilizing lignin as a valuable biomaterial has its challenges given that it must undergo rather intense extraction processes. Most commonly, lignin is extracted during the kraft pulping process in the pulp and paper industry. Kraft pulping involves the extraction of lignin and hemicellulose from biomass through high alkaline conditions, in which the lignin is solubilized and separated from cellulose. The mixture of lignin, hemicellulose and extractives from the pulping process is colloquially referred to as black liquor. Lignin can then be further purified from the black liquor through acid precipitation, in which lignin is no longer soluble. The precipitation and purification of lignin has been implemented at the industrial scale using the LignoBoost process (Valmet).

During the extraction of kraft lignin (KL) from biomass, the macromolecule is broken down by a series of complex thermochemical reactions that, among other products, generate a large number of phenolic hydroxyl groups by the cleavage of ether bonds (Hu et al., 2016). KL thus has a significantly different structure than native lignin. Due to KL's newly formed multi-functional groups, mainly phenolic hydroxyl, carboxyl, and aliphatic hydroxyl groups, it possesses a unique set of properties related to its UV absorption (Qian, Qiu, & Zhu, 2015; Yearla & Padmasree, 2016), emulsion stabilization ability (Nypelö et al., 2015), antioxidant effects (Yearla & Padmasree, 2016), chelation (Guo et al., 2008).

## **1.2 Lignin availability and commercial isolation**

The primary source of lignin readily available for use on a large scale is found in wood pulping liquors, colloquially referred to as black liquors. On a global basis, more than 78 million tons of lignin are generated from Kraft and sulfite pulping operations (Jardim et al., 2020). However, 96% of this lignin is not isolated but instead burned on-site to provide steam for heat and power generation. The heating value of lignin is similar to ethanol (27 KJ/g), and is a

suitable source for bioenergy (Culbertson et al., n.d.; Jardim et al., 2020). For this and other practical reasons, most of the industrial lignins are burned on-site, and only a small fraction is used for materials manufacturing. However, the huge opportunity for securing vast quantities of lignin from the pulp and paper industry, and at large scale, is compatible with developments in biorefineries and bioproduct mills that integrate biomass conversion processes aiming at increasing the value of under-utilized streams such as lignin. As previously mentioned, recent technological developments have made possible the extraction of lignin from pulp and paper operations at a cost less than USD 250/ton (Abbati De Assis et al., 2018; Prasad et al., 2018) with a production volume near the hundreds of tons per day available for further value-added transformation. Examples of industrial lignins, also known as technical lignins that are commercially available include BioChoice Lignin (Domtar) and Indulin (Ingevity). The scalable extraction of lignin from kraft pulping liquors has been implanted at an industrial scale at various pulp mills. One of the more common industrial methods is the LignoBoost method depicted in **Error! Reference source not found.** (Hamaguchi et al., 2012; *Valmet LignoBoost - Lignin Extraction*, n.d.).

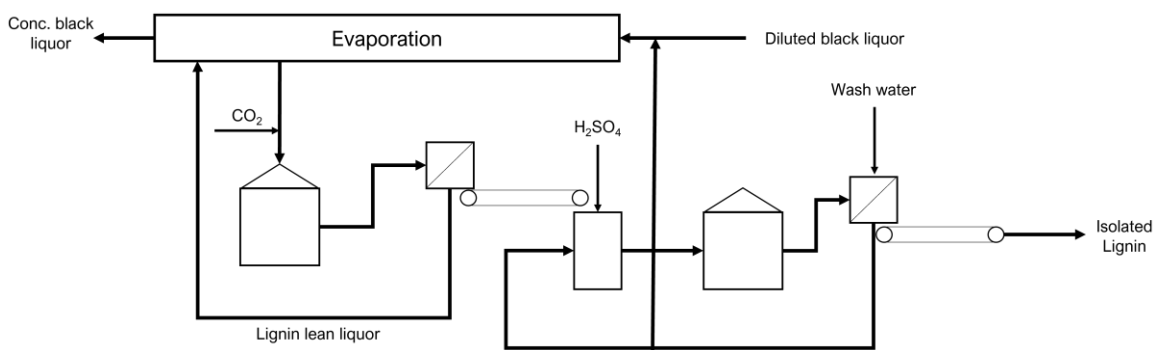


Figure 1-2. Diagram of the LignoBoost method from Valmet (Hamaguchi et al., 2012; *Lignin Extraction Process*, n.d.)

The LignoBoost method involves the precipitation of lignin by acidifying the alkaline black liquor effluent stream. Acidification will protonate phenolic groups of kraft lignin, drastically reducing its solubility in an aqueous medium. The precipitate is washed, pressed, and acid washed to remove hemicellulose and inorganics.

Furthermore, recent environmental life cycle, cradle-to-gate analysis on the impact of adding a commercial-scale lignin extraction process to an existing kraft pulp mill (modeled after the BioChoice Lignin produced at Domtar), indicated a considerable reduction of the estimated global warming potential (Culbertson et al., n.d.).

### **1.3 The rise of paper packaging**

Our society is facing a pivotal moment in the transition to a more sustainable future as a direct result of the global effects of climate change and the rise of more environmentally conscious generations. The initial focus was aimed toward CO<sub>2</sub> reduction and renewable clean energy projects and has since achieved great progress in the development of electric cars, industrial process optimization, and even carbon capture technologies. With the energy sector making such great strides in their fight against an uninhabitable future, the next step is limiting the amount of waste our society produces. While plastics have contributed toward many societal and economic benefits by protecting our food, transporting liquids, and clothing our bodies, their resilient nature poses a potential environmental disaster. The EPA reports that more than 80 million tons of packaging waste were generated in the U.S. in 2018 (US EPA, 2018). Fortunately, the recycling rate of packaging materials has increased from 10% in 1960 to 54% in 2018 (US EPA, 2018), yet the net amount of landfilled mass has been steady during the same time interval (see Fig. 1-3).

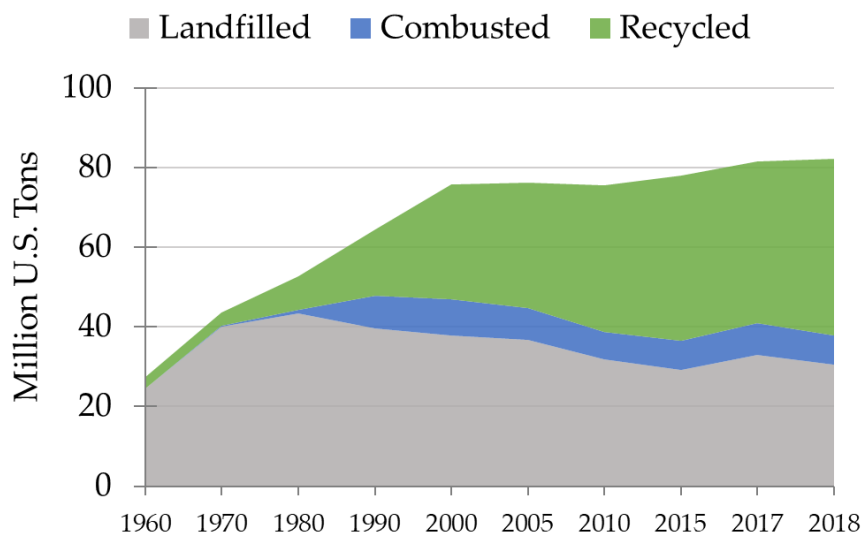


Figure 1-3. Total packaging waste disposal pathways in the U. S. from 1960 to 2018 (US EPA, 2018).

The major packaging materials used for food, drinks, and other goods are primarily paper and plastics, with nearly three times more paper packaging products by mass being generated than plastic packaging (US EPA, 2018). Plastic waste poses major environmental concerns and challenges related to biodegradability and processibility in recycling efforts due to the variability in plastic types (e.g., PET, PLA, polyethylene, etc.). Plastics are highly desirable in their resilience to environmental conditions (e.g., moisture, mechanical stress), high production volume and low-cost (Siracusa, 2016). Conversely, paper and paperboard materials were recycled at a rate of nearly 81% in 2018 (US EPA, 2018) and are considered biodegradable given their natural origin, yielding it a better option for packaging materials from an environmental perspective.

On the other hand, bio-based plastics such as starch and cellulose derived films, are a major research interest due to their natural origin and biodegradability. The demand for products that are eco-friendly, safe, and non-toxic continues to grow, with many consumers willing to pay

more for environmentally certified products (Barbarossa & De Pelsmacker, 2016; Rokka & Uusitalo, 2008; Vlosky et al., 1999). As a result, the market value of paper-derived packaging materials is nearly USD 400 billion with a 6 % annual growth rate (*Food Packaging Market Worth \$456.6 Billion By 2027*, n.d.). Moreover, the recent SARS-CoV-2 pandemic has contributed to a 40% surge in e-commerce, an industry that almost solely utilizes corrugated box for primary and secondary packaging (U.S. Department of Commerce, 2021).

#### **1.4 Foodborne pathogens and their prevalence**

The SARS-CoV-2 pandemic has sparked a global conversation and scientific research relating to the transmission of pathogens through direct human contact and/or inanimate surfaces. Hundreds of thousands of deaths annually are linked to foodborne pathogen-related diseases, and up to 600 million illnesses and 400 thousand deaths worldwide every year (Adley & Ryan, 2016; WHO, n.d.). Additionally, these pathogens generate economic losses in produce transportation and food storage systems due to microbial food spoilage that can be accounted for in the billions of dollars (Agrillo et al., 2019; Pitt & Hocking, 2009a). It is estimated that in the U.S. alone \$10 – \$100 billion is lost each year due to produce losses generated by fungi and mold. Most of these losses are incurred in produce such as strawberries and grapes. In addition to a tremendous amount of food waste, it is estimated an extra \$1 billion is spent on fungicides, profoundly affecting the balance sheet of the berry and wine industries (Dean et al., 2012; Hua et al., 2018; Snyder & Worobo, 2018).

Pathogens can be foodborne and persist on (packaging) surfaces for hours or even days (Chin et al., 2020; Gonçalves et al., 2021; Johnson et al., 2021; Siroli et al., 2017a; Sizun et al., 2000; van Doremalen et al., 2020a). The occurrence of novel viruses and the potential for future pandemics have created an awareness recently in this regard (Chin et al., 2020; Mallakpour et

al., 2021; Marzoli et al., 2021; van Doremalen et al., 2020a). In a new report, SARS-CoV-2 has been detected on surfaces for up to 28 days (Marzoli et al., 2021), which is much longer than other coronaviruses. The FDA has recently reported that the transmission of SARS-CoV-2 from packaging is extremely low due to the limited number of particles that are transferred from surfaces to humans, yet more contagious variants are continuously appearing and may require a much lower viral load to result in illness (B. Li et al., 2021). Given the abundant utilization of paper-based packaging and the growing market for bio-based plastic alternatives, it is necessary to prioritize consumer health and safety by understanding the behavior of pathogens on these surfaces. Once the problem is fully addressed, potential solutions by developing active antimicrobial additives will help mitigate further pandemics, secure supply chains, combat foodborne illnesses, and extend the shelf-life of produce and other perishables.

Packaging of foods are designed currently to have “passive” protection. Passive protection can be defined as having barrier properties to the environment including, but not limited to, moisture, microbial contamination, heat (insulators), animals, and UV light radiation. This passive protection is very effective for non-porous, hydrophobic materials such as plastics, but absorptive and porous materials like paper or bio-based plastics are at an increased risk to microbial contamination via the absorption of aqueous media like contaminated water, blood, or myoglobin.

Foodborne bacterial pathogens account for nearly 3.6 million illnesses annually and make up 64% of the total foodborne pathogen related deaths in the U.S (Scallan et al., 2011). More specifically, the CDC listed *Salmonella spp.*, *Listeria monocytogenes*, and *E. coli* as the most prominent bacteria to cause multistate foodborne illness outbreaks in the U.S. (*List of Selected Multistate Foodborne Outbreak Investigations | Foodborne Outbreaks | Food Safety | CDC*,

n.d.). The USDA actively estimates the total annual cost of the most common foodborne pathogens and bacterial pathogens alone account for nearly 12 billion USD (Table 1-1) (*USDA ERS - Cost Estimates of Foodborne Illnesses*, n.d.).

Table 1-1. Estimated cost of foodborne illness from bacterial pathogens

<b>Bacteria</b>	<b>Cases</b>	<b>Cost</b>
<i>Salmonella</i> (non-typhoidal species)	1,027,561	\$4,142,179,161
<i>Listeria monocytogenes</i>	1,591	\$3,189,686,110
<i>Campylobacter</i> spp. (all species)	845,024	\$2,181,485,783
<i>Clostridium perfringens</i>	965,958	\$384,277,856
<i>Vibrio vulnificus</i>	96	\$359,481,557
<i>Yersinia enterocolitica</i>	97,656	\$313,297,920
Shiga toxin-producing <i>Escherichia coli</i>		
O157 (STEC O157)	63,153	\$311,036,907
<i>Shigella</i> (all species)	131,254	\$159,202,402
<i>Vibrio</i> non-cholera species other than		
<i>V. parahaemolyticus</i> and <i>V. vulnificus</i>	17,564	\$81,749,064
<i>Vibrio parahaemolyticus</i>	34,664	\$45,735,332
non-O157 Shiga toxin-producing		
<i>Escherichia coli</i> (STEC non-O157)	112,752	\$31,701,852
<b>Total</b>	<b>3,297,273</b>	<b>\$11,199,833,944</b>

Natural food preservatives have been used since ancient times due to the appearance of multiple food related illnesses, generated mainly by different types of bacteria (Cruz et al.,

2018), while fungi have been linked to food spoilage and produce losses (Pitt & Hocking, 2009b). Although virus transmission through food is less reported, the main sources are hepatitis A and norovirus related outbreak cases, creating awareness of healthy food safety practices (Koopmans & Duizer, 2004). The appearance of SARS-CoV-2, which is not a foodborne virus but rather a virus that can be transmitted through direct contact with the infected patient, had indirect consequences at an early stage of the pandemic, including heightened awareness of surface cleaning practices in 2020 and 2021 (Barman et al., 2021; Kitz et al., 2021; Zhang et al., 2021). Although surface transmission is not the primary transmission route for SARS-CoV-2, several studies reported surface-survival time (Marzoli et al., 2021), which can reach up to 28 days on metal, polymeric and banknote surfaces, longer than other coronaviruses. The virus was found on different surfaces, e.g., hand sanitizer dispensers, medical equipment, shelves for medical equipment, and door handles (Razzini et al., 2020). Disruptions in supply chains occurred due to the number of illnesses, high contagious rate, and economic uncertainty, indicating the consequences that a virus outbreak can generate on a global scale (Barman et al., 2021; Hayes et al., 2021; Marquez et al., 2021; C.-H. Tang et al., 2021). More direct changes in the packaging industries because of COVID-19 was the drastic increase in e-commerce and direct-delivery related industries (e.g., Uber Eats, Amazon, Hello Fresh), which rely heavily on containerboard and plastic packaging.

#### **1.4.1 Foodborne infections**

Pathogens are defined as microorganisms or biological materials that prompt human disease (Balasubramaniam et al., 2021; Otter et al., 2013; Siroli et al., 2017b; Sirsat, 2020a). The two main categories of pathogens, namely facultative and obligate (Balloux & van Dorp, 2017), have had a massive impact on human history, shaping it through the toll on human life and the

economic and societal upsets which have followed epidemics. The rise of new viruses and their relation to pandemics have created societal awareness recently in this regard (Chin et al., 2020; Mallakpour et al., 2021; Marzoli et al., 2021; van Doremalen et al., 2020b). At present, infectious diseases continue to be significant health threats, with foodborne infections being one of the most frequently reported.

Hundreds of thousands of deaths are linked to foodborne pathogens-related diseases annually, including bacteria and viruses, with up to 600 million illnesses and 400 thousand deaths worldwide every year (Adley & Ryan, 2016; WHO, 2019).

Table 1-2 shows some recent foodborne illness outbreaks in the U.S., *Listeria monocytogenes*, *Salmonella* spp., and *Escherichia coli* are reported to be the leading causes of fresh produce-related outbreaks (Vieira & Boyer, 2015). On the other hand, it is known that in the U.S., meat products are responsible for a significant share of the 500-1500 foodborne outbreaks that have been reported yearly between 2000 and 2021 (Kumar et al., 2020; Siroli et al., 2017c; Upadhyay et al., 2013).

Table 1-2. Examples of recent outbreaks of foodborne illness in the U.S. (FDA, 2020)

<b>Year</b>	<b>Outbreak source</b>	<b>Contaminating pathogen</b>
2016	Beef products and alfalfa sprouts	<i>Escherichia coli</i>
2016	Frozen vegetables and packaged salads	<i>Listeria monocytogenes</i>
2016	Frozen strawberries and scallops	<i>Hepatitis A</i>
2017	Papaya	Multiple <i>Salmonella</i> strains
2018	Precut melon	<i>Salmonella adelaide</i>
2018	Romaine lettuce	<i>Escherichia coli</i>
2018	Packaged vegetable trays	<i>Cyclospora</i>
2019	Fresh papayas and frozen tuna	<i>Salmonella</i>
2019	Fresh blackberries	<i>Hepatitis A</i>

Table 1-2. (Continued)

<b>Year</b>	<b>Outbreak source</b>	<b>Contaminating pathogen</b>
2019	Romaine lettuce, salad mix and flour	<i>Escherichia coli</i>
2019	Hard-boiled eggs	<i>Listeria monocytogenes</i>
2020	Red onions, peaches, and mushrooms	<i>Salmonella</i>
2020	Bagged salad	<i>Cyclospora</i>
2020	Mushrooms	<i>Listeria monocytogenes</i>
2020	Clover sprouts	<i>Escherichia coli</i>
2020	Cheese	<i>Listeria monocytogenes</i>
2020	Alkaline water	<i>Hepatitis</i>
2021	Shrimp	<i>Salmonella</i>
2021	Salad	<i>Salmonella</i>
2021	Onions	<i>Salmonella</i>
2021	Spinach	<i>Escherichia coli</i>
2021	Packaged salad	<i>Listeria monocytogenes</i>
2022	Packaged salad	<i>Escherichia coli</i>
2022	Powdered infant formula	<i>Cronobacter and Salmonella</i>
2019	Romaine lettuce, salad mix and flour	<i>Escherichia coli</i>
2019	Hard-boiled eggs	<i>Listeria monocytogenes</i>

The occurrence of pathogens in produce and food products stems from various sources, and their transmission follows a set of complex surface chemistries, environmental conditions, and inherent viability. It has been found that the long-lasting presence of some microorganisms on the surface of fresh produce packaging can lead to their rapid multiplication and possible biofilm formation in the case of bacteria (Karumathil et al., 2016; Rawdkuen et al., 2016; Yahaya et al., 2019). Regarding viruses, norovirus and hepatitis A are known to be transmitted via surfaces, such as the case of packaged food handled without standard healthy practices. Thus,

several outbreaks have been reported in recent years in the U.S. and other countries (Greening & Cannon, 2016; Lin et al., 2021; Petrović & D'Agostino, 2016).

#### **1.4.2 Essential oils entrapment**

EOs are volatile compounds that can easily evaporate and/or degrade under heat, pressure, light, and oxygen, limiting their use in packaging applications. Furthermore, their relatively non-polar structure makes them practically insoluble in water, and simple aqueous formulations cannot be readily prepared. However, such drawbacks can be ameliorated to enhance the physical stability and bioactivity of such compounds during processing, application and storage by employing nano-/micro-encapsulation technologies, resulting in a practical and efficient approach.

Encapsulation is generally defined as the entrapping of active compounds (solid, liquid, or gas core) in solid or micellar capsules. The capsule or shell material protects the active core from the surrounding environment and may allow, in many cases, controlled release of the core substances (e.g., EO molecules, drugs, biocides, among others). The encapsulation of essential oils can be attained by different methods (Figure 1-4), mainly as solid-lipid nanocarriers, liposomes, and nanoemulsions (Chelliah et al., 2019). The encapsulation material can vary. Surfactant molecules, polymer complexes, phospholipids and biopolymers have been used effectively as encapsulation materials.

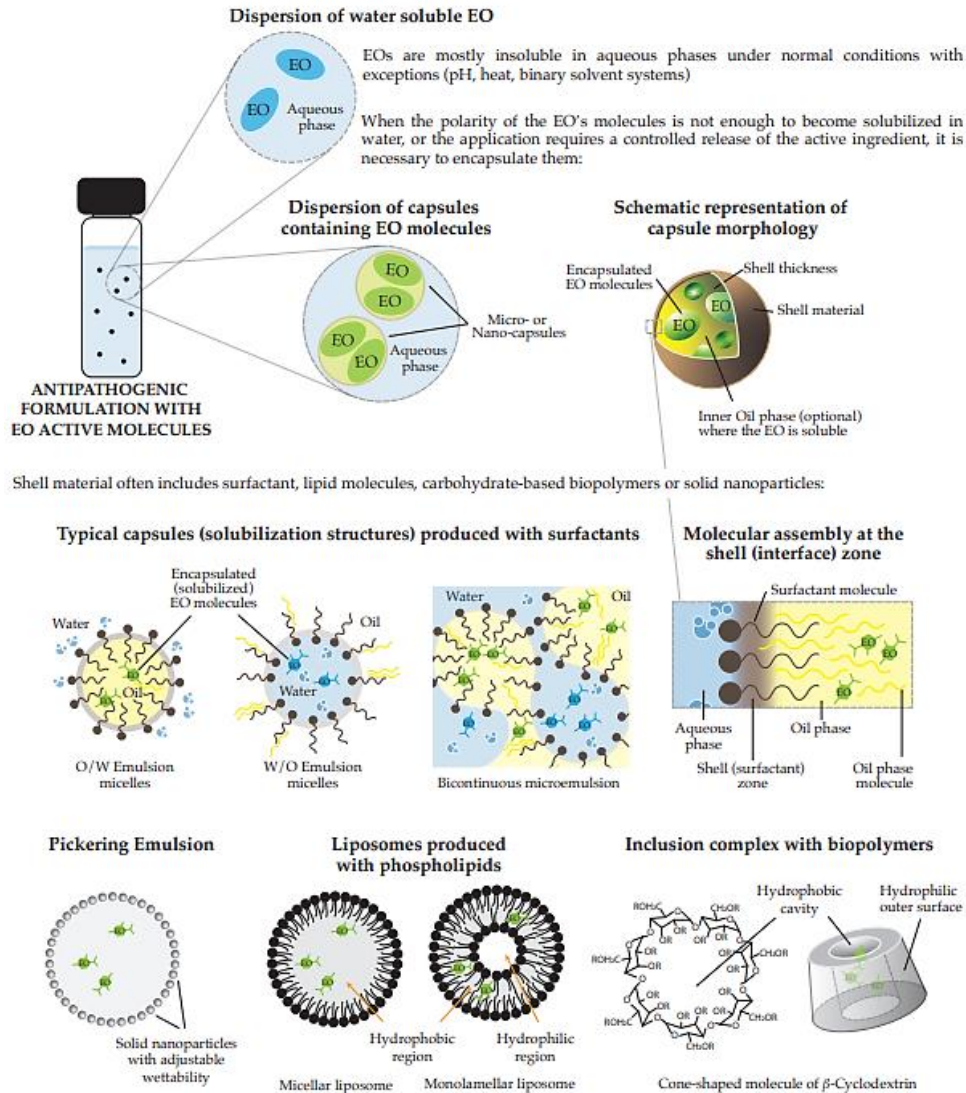


Figure 1-4. Types of nanostructured encapsulation systems applied for essentials oils with antiviral activity (Marquez et al., 2022).

Alternatively, essential oils may also be encapsulated as nanoemulsion using surfactants. Nanoemulsions are the most reported method to encapsulate essential oils. EOs nanoemulsions have been stabilized by using nonionic ethoxylated sorbitan esters surfactants to attain oil-in-water (O/W) emulsions (Prakash et al., 2018). The presence of the surfactant or linker molecules allows a gradual polarity change at the vicinity of the interface (shell of the capsule), and thus more beneficial interactions between surfactant–aqueous phase and surfactant–oil phase where

solubilized EOs bioactive compounds are encountered (Chu et al., 2014; Salager et al., 2005, 2019). This allows the Winsor R relation (Bourrel & Schechter, 2010; Salager et al., 2022; Winsor, 1954) to become  $R < 1$  (i.e., hydrophilic-lipophilic deviation,  $HLD_N < 0$ ) if an O/W emulsion is the target (Forgiarini et al., 2021; Salager et al., 2020). On the other hand,  $R = 1$  or  $R$  slightly lower than 1, would be necessary if a bicontinuous microemulsion ( $HLD_N = 0$ ) or O/W microemulsion are needed, respectively (Ontiveros et al., 2013; Queste et al., 2007; Salager et al., 2020).

The method for nanoemulsion preparation uses spontaneous emulsification if low-energy emulsification methods are preferable (Bullón et al., 2007, 2021; Forgiarini et al., 2001; Komaiko & McClements, 2015) or high-energy emulsification with homogenizers or microfluidizers (McClements & Rao, 2011). The formulation could be applied as a liquid spray solution or placed inside an absorbent pad after generating the O/W emulsion or gel (by using a rheology modifier polymer or a high concentration of surfactants), e.g., in food packaging (Prakash et al., 2018). It has also been found that in cosmetic formulations, lotions, and hand sanitizers, among others, a quantity of encapsulated essential oil has been incorporated to generate a specific antiviral activity (Oliveira et al., 2020; Takeda et al., 2021; Yadav et al., 2017). The maximum concentration limit is usually determined by a toxicity threshold for some essential oils, e.g., clove essential oil or eugenol (Millet et al., 1981). If a homogenous external oil phase is preferable, as is the case with W/O nanoemulsions, EOs compounds have to be solubilized in biocompatible or biobased solvent oils, which has been found to be difficult due to its high hydrogen bonding (H) and polar (P) parameters according to a Hansen Solubility Parameter approach (Benazzouz et al., 2014). A summary of methods to entrap or encapsulate essential oil compounds is listed as the following (Figure 1-4):

1. Encapsulation in inclusion complexes with cyclodextrin biopolymers. Cyclodextrins (CD)-essential oil inclusion complex has been attained with various essential oils (Poulson et al., 2022), (Buendía-Moreno et al., 2019; L. B. Moreno et al., 2020; Suprani et al., 2019). The molecular structure of  $\alpha$ -CD,  $\beta$ -CD, and  $\gamma$ -CD allows tuning the encapsulation of EOs to be applied in a CD vehicle as a coating in packaging materials.
2. Encapsulation in liposomes with phospholipids. Liposomes have been used (although scarcely) for essential oil encapsulation for antimicrobial applications (Varona et al., 2013). Despite its complex fabrication, advantages of this type of encapsulation are the biocompatibility and the possibility of controlled release due to the membrane-like structure given by lecithin, which is used in most formulations reported (Yasuda, 1991).
3. Encapsulation in Pickering emulsions using solid nanoparticles. Thymol, cinnamon and chamomile essential oils have been encapsulated mainly in silica nanoparticles-based pickering emulsions (Das, Horváth, Šafranko, Jokić, Széchenyi, & Kőszegi, 2019; Fasihi et al., 2019; J. Li et al., 2018; Sun et al., 2020; Zhou et al., 2018). Antimicrobial activity has been reported, although certain authors have raised safety concerns regarding nanoparticle-based formulations, suggesting that further studies addressing such concerns might be required (Dickinson, 2010; Espitia et al., 2016; Slavova et al., 2020).

## 2 BACKGROUND

### 2.1 Nanoprecipitation method

A nanoparticle can be considered as a form of matter that has at least one dimension with a length between 1 nm and 1000 nm. Nanomaterials can be synthesized from metal ions, proteins, organic molecules, or polymers and frequently utilized in the food and agriculture, pharmaceutical and technology and communication industries. Reducing the size of materials to the nanoscale greatly enhances the surface-area-volume ratio, allowing for superior functionality compared to macroscale materials.

Nanomaterials from organic matter are commonly involved in the creation of colloidal dispersions in aqueous or lipid mediums. These materials are sometimes referred to as “soft matter.” The nanometric features allow for high dispersibility without sedimentation in stable systems, resulting in molecular characteristics of typically insoluble materials. These can be in the form of nanoparticles, nanoemulsions, micelles, coacervation complexes, nanogels, and many others.

A variety of methods exist to fabricate nanomaterials, with one of the more common methods being solvent exchange or nanoprecipitation. Nanoprecipitation involves changing the physical state of a dissolved system by drastically reducing the strength of interaction between the solute and solvent. This can be achieved by changing the composition of the solvent or chemically altering the solute (e.g., protonation/deprotonation, redox reactions, crosslinking, polymerization, etc.). In the case of polymers or organic small molecules, this most frequently involves the dissolution of the material in an organic solvent followed by the addition of an antisolvent (usually water) that is miscible with the organic solvent. Alternatively, the material can be dissolved in a binary solvent including both a volatile organic solvent and water, followed

by the evaporation of such volatile organic solvent. In both cases, the solvent composition is drastically changed to a point at which the solute is no longer in a dissolved state and a thermodynamically driven process occurs to generate a dispersed state of matter. The molecules will arrange themselves by means of surface energy minimization, in which the surface area-to-volume (S/V) ratio is minimized. Therefore, this process most commonly generates spherical morphologies, in which the S/V ratio is lowest. The thermodynamics of this process will be discussed in later sections.

Common practices of nanoprecipitating polymers, include 1) the injection of a dissolved polymer into water, 2) the injection of water into a polymer solution, or 3) the integration of two streams, one being water and the other being the polymer solution. All of which have proven to be relatively simple and low-energy methods to produce polymeric nanoparticles.

## **2.2 Mechanisms of nanoparticle formation**

### **2.2.1 Classical nucleation and growth**

Nucleation of matter is the phase separation of heterogeneous materials (i.e., solvent and solute) from a single-phase system to a biphasic system, comprised of a dispersed phase and continuous phase. Nucleation is driven by the transition from a metastable state to a stable state by means of self-assembly. Although there is an overall favorable energy change, nucleation and growth cannot proceed without overcoming kinetic and thermodynamic barriers, as discussed further in this section. Nucleation can be segmented into homogeneous and heterogeneous nucleation, with the former being the spontaneous generation of clusters of a single material and the latter requiring a nucleating agent or crystallization surface to initiate nucleation. Both nucleation events can hypothetically occur, but homogenous nucleation is less common due to

the purity requirement. Any impurities in the system (e.g. dust, supramolecular clusters, air, etc.) will lower the energy of nucleation and therefore must be defined as heterogenous nucleation. However, nucleation can be described thermodynamically under the assumption of homogeneous nucleation and heterogenous nucleation can be derived thereafter. In depth descriptions of CNT have been described many times since its initially birth in 1878 by Josiah Willard Gibbs, but will also be reviewed briefly here (Karatutlu et al., 2018; Thanh et al., 2014; C. Zhao, 2016).

The propensity for a particle to form is dependent on whether the seed nucleus will remain stable after phase separation or will redissolve. The reciprocation between nucleation and dissolution will occur many times at early stages of nucleation. This phenomenon can be described mathematically in terms of free energy. According to the classical nucleation and growth model for homogenous nucleation, the total free energy of a particle can be described in terms of surface free energy of a particle and free energy of molecules in the bulk (Eq. 1 and 2),

$$\Delta G = 4\pi r^2 \gamma + \frac{4r^3 \Delta G_v}{3} \quad (1)$$

$$\Delta G_v = \frac{-k_b T \ln(S)}{v_m} \quad (2)$$

where  $\Delta G$  is the total Gibb's free energy,  $r$  is the particle radius,  $\gamma$  is the surface free energy,  $\Delta G_v$  is the free energy difference per unit volume between the nucleating material and the solvent,  $k_b$  is the Boltzman constant,  $T$  is temperature,  $S$  is supersaturation ratio  $C_x/C_{max}$ , and  $v_m$  is the molar volume.

In the case that a cluster of molecules spontaneously aggregate in a supersaturated solution such that  $\Delta G_v$  is negative, and the surface free energy always being positive, the total

free energy of the formed particle scales with  $r$  with a maximum free energy at critical radius  $r^*$  (Figure 2-1)

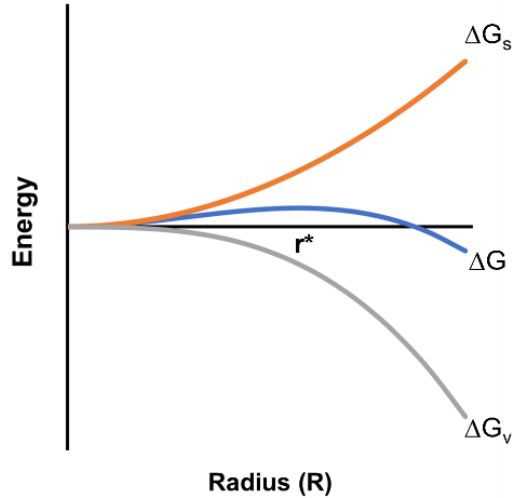


Figure 2-1. Gibb's free energy diagram of the surface free energy and bulk free energy contributions to nucleation events as a function of particle radius (Thanh et al., 2014).

Figure 2-1 shows that as the size of the clustered molecules increases, the surface free energy increases and scales with  $r^2$  and the free energy in the bulk decreases and scales with  $r^3$ . The total free energy of the particle is a sum of the two terms where the supersaturation drives the nucleation, whereas the surface free energy acts as a barrier to the progression of nucleation. The radius of the nuclei at which the change in free energy of the bulk is favorable enough such that the surface free energy barrier is overcome can be defined by Equations 3 and 4.

$$\frac{d\Delta G}{dr} \Big|_{r=r^*} = 0 \quad (3)$$

$$r^* = \frac{2\gamma v_m}{k_b T \ln(S)} \quad (4)$$

The critical radius is therefore the minimum radius at which nuclei can exist without being redissolved into solution. As mentioned previously, the nucleation of particles from a supersaturated solution must overcome an energy barrier to form stable nuclei seeds, thus, by definition, the solution of molecules prior to nucleation is in a metastable state. The derivation of the critical radius is important considering it is a rearrangement of the Ostwald-Freundlich equation which describes the Ostwald ripening phenomenon in which small particles or nuclei redissolve and merge with larger, more stable nuclei. This concept of Ostwald ripening will be revisited in later sections.

The kinetic barrier of CNT is that of a statistical probability that molecules will collide and interact to form initial nuclei for growth to spontaneously occur. This probability is greatly enhanced by supersaturating the local environment. The rate of nucleation ( $dN/dt$ ) can be defined in Equation 5 by the classical nucleation theory and is independent of whether heterogenous or homogenous nucleation occurs, as the pre-exponential term, A, will account for the discrepancy (Thanh et al., 2014).

$$\frac{dN}{dt} = A \exp\left(-\frac{16\pi\gamma^2 v_m^2}{3(k_b T)^3 (\ln(S))^2}\right) \quad (5)$$

Equation 5 states that the rate of nucleation is highly dependent on the degree of supersaturation. Assuming the mixing rate is faster than formation of nuclei and the supersaturation condition is met, a large number of nuclei at radius  $r^*$  will be formed, greatly decreasing the solute concentration, limiting the formation of future nuclei. Thus, the remaining mass of metastable or unstable solute molecules will adsorb onto the surface of preformed nuclei

and the particles will grow. This is essentially the burst nucleation mechanism developed by La Mer (Lamer & Dinegar, 1950).

In the case of heterogeneous nucleation, the nuclei will not form a complete sphere initially, but rather forming an ellipsoid with a contact angle,  $\theta$ , respective of the already-present surface and the bulk solvent (Equation 6).

$$\Delta G_2(r^*) = \beta \Delta G_1(r^*) = \frac{(2 + \cos\theta)(1 - \cos\theta)^2}{4} \Delta G_1(r^*) \quad (6)$$

Since the surface is already present in the solid state, the energy barrier,  $\Delta G(r^*)$ , is less than that of homogenous nucleation (See Figure 2-2).

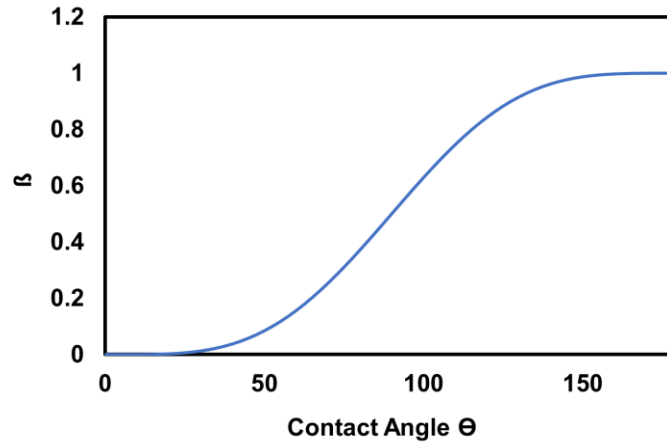


Figure 2-2. Gibb's free energy correction factor ( $\beta$ ) for heterogeneous nucleation as a function of particle interface contact angle ( $\Theta$ ).

Once the conditions are met where the critical radius of the nuclei is achieved, there is kinetic exchange between the formation of new nuclei, redissolution, and the growth of pre-existing nuclei. Energetically, the growth of already formed nuclei is more favorable than the formation of a new surface, but this is spatially constrained and cannot be extrapolated to the bulk. Therefore, let us consider the thermodynamic propensity and growth rate of preformed nuclei. The total flux of molecules,  $J$ , can be described as a function of the diffusion coefficient,

D, particle radius,  $r$ , and distance from the particle surface,  $x$ , the concentration of the particle molecules at the solid-liquid interface,  $C_i$ , and the concentration of the solute molecules in the bulk,  $C_b$  (Equation 7).

$$J = 4\pi Dr(C_b - C_i) \quad (7)$$

### **2.2.2 Solid-liquid phase transitions**

Supersaturated solutions and their relationship with phase transitions of polymers and small molecules can be described in terms of free energy of mixing, where the solution can be in several different energy states including stable, unstable, and metastable (Brick et al., 2003; C. Zhao, 2016). The phenomenon of spinodal decompositions occurs under this description in the unstable regime. In spinodal decomposition, the solute is in a highly supersaturated state where it is inherently unstable in terms of free energy of mixing and the energy barrier for nucleation to occur is non-existent.

Figure 2-3 describes the qualitative relationship between free energy of mixing and the solution composition in terms of polymer concentration (Brick et al., 2003).

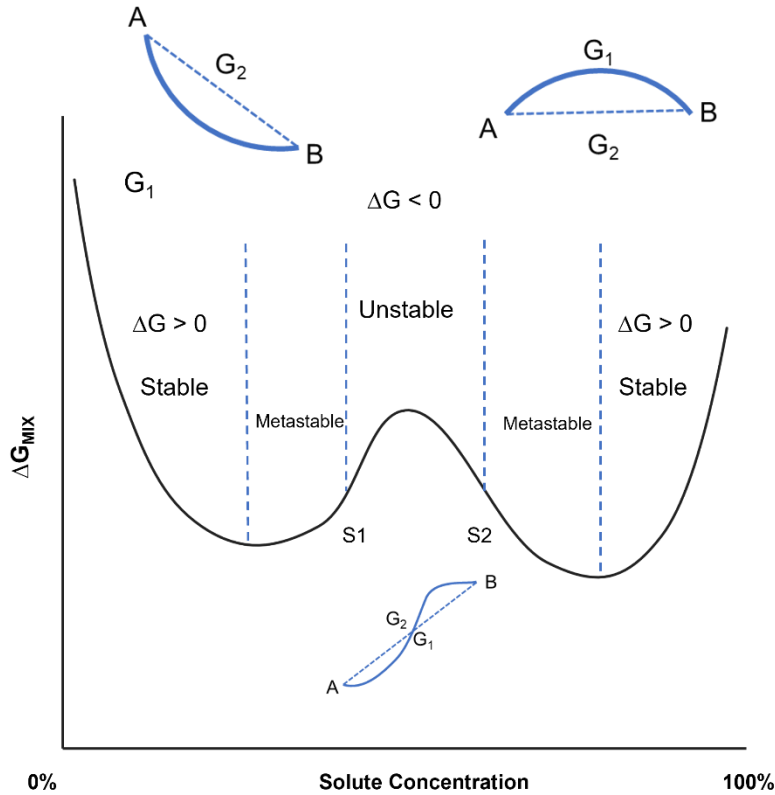


Figure 2-3. Free energy of mixing diagram and the solution composition in terms of polymer concentration (Brick et al., 2003; C. Zhao, 2016).

At low solute concentration, the free energy of mixing is negative and the change in free energy ( $G_2 - G_1$ ) during a phase separation into two phases, A and B, is positive (non-spontaneous), therefore redissolves into the bulk. Similarly, when the “solute” concentration is nearly 100%, the solute will be in a swollen solid state and the phase separation will also be unfavorable energetically due to insufficient solvent. Conversely, when the solute is locally supersaturated,  $S_1 < C_x < S_2$ , where  $C_x$  is the solute concentration, the phase separation is highly energetically favorable due to a negative change in free energy. However, the metastable regions between the local minimum and the spinodal points ( $S_1, S_2$ ) require additional energy for a complete phase separation which can be provided by large fluctuations in solute concentrations.

S1 and S2 are the spinodal points edging the concentration regime of the saddle point, where spinodal decomposition occurs.

Based on the previous description, a solute can undergo a phase separation by either increasing in the solute concentration, decreasing the solvent concentration, or decreasing the solubility of the polymer (pH, temperature, etc.). The nanoprecipitation method through antisolvent precipitation can be described by relating the various points along the  $\Delta G_{\text{mix}}$  vs solute concentration curve over an array of antisolvent concentrations and the binodal (equilibrium) curve and spinodal decomposition curve can be constructed as in Figure 2-4.

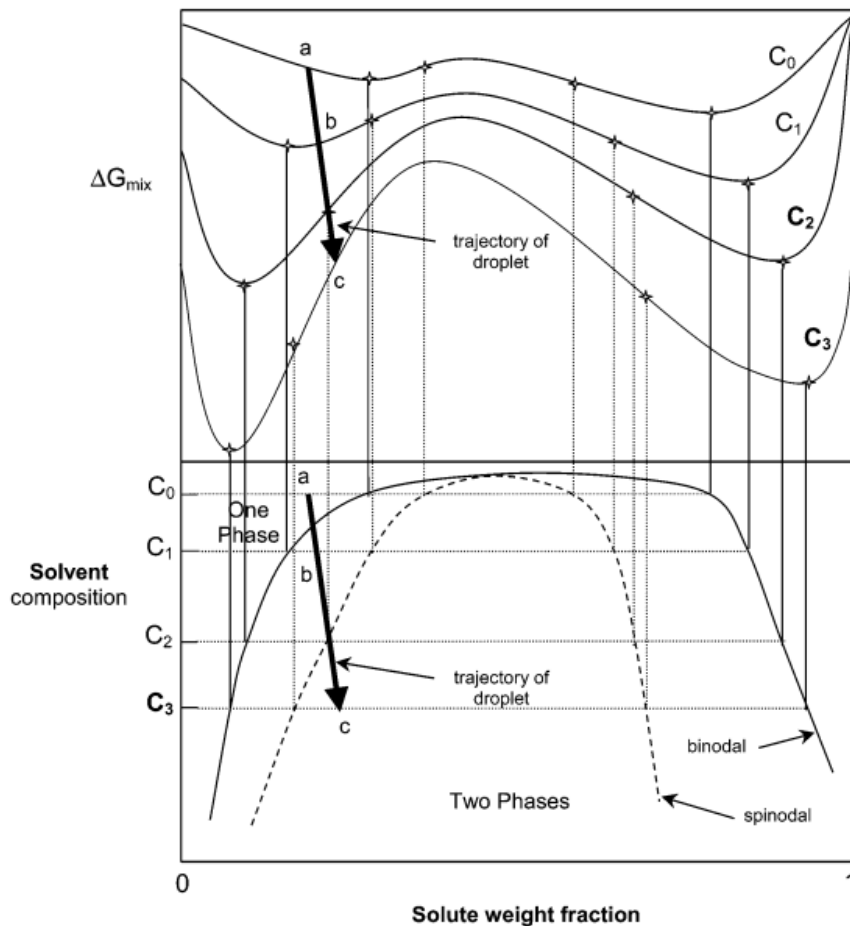


Figure 2-4. Free energy of mixing and phase diagram of a solute precipitation from solution by the addition of a non-solvent ( $C_{0-3}$ ) (Brick et al., 2003)

In Figure 2-4,  $C_0$ - $C_3$  are the increasing concentrations of the antisolvent in the system. The occurrence of spontaneous phase separation (spinodal decomposition) will occur at lower solute concentrations when more antisolvent is added to the solution. The region between the binodal and spinodal curves represents the metastable regions. As previously mentioned, classical nucleation theory requires energy to form stable nuclei and eventually form particles. This energy is provided by the energy release during the statistical fluctuations in the formation of a single stable nuclei, driving more nuclei formation. Both classical nucleation and spinodal decomposition possess the requirement of supersaturation to occur, with spinodal decomposition requiring higher levels of supersaturation due to the statistical independence. Thus, both models can be present in the same system assuming high supersaturation, where there is a distribution of events, especially in systems of heterogeneous nucleation. As the concentration of the solute greatly decreases, the system is pushed into the metastable regions where the statistical formation of nuclei drives further particle growth.

### **2.3 The Ouzo effect**

Ouzo, a popular alcoholic beverage in some Mediterranean countries, is a mixture of ethanol, water and a small amount of anise oil that turns milky-white when diluted with additional water and remains stable for long periods (Ganachaud & Katz, 2005; Vitale & Katz, 2003). It was speculated that the dilute anise oil is precipitated out of solution in a droplet form when the solvent composition becomes less favorable for the hydrophobic compounds. This phenomenon intrigued colloid researchers and prompted a wave of investigations into the mechanism and exploitation of the precipitation of hydrophobic compounds in aqueous systems. This interest was quickly expanded to include the food, material, and pharmaceutical sciences, among others. It was apparent that hydrophobic molecules can be precipitated from hydrophilic

solvents by simply the addition of excess water. Many hydrophilic solvents are also commonly more volatile than water such as ethanol, acetone, and THF, and can be easily recovered via evaporative techniques.

The ouzo effect is a special type of spontaneous emulsification that typically does not require a surfactant to remain stable for a finite amount of time. More specifically, this occurs when two immiscible liquids are in contact with one another and emulsify without agitation (Groves, 1978). The ouzo effect is restricted to a specific range of mixture compositions called the “ouzo region.” The ouzo region is in the metastable regime, between the binodal and spinodal regions (see Figure 2-4). For the nucleation of hydrophobic molecules, this means a low solute-to-solvent ratio and a low solvent-to-antisolvent ratio. Vitale et. al., details the experimental description of the ouzo effect and the many variables that may affect the formation and stability of the colloidal dispersion (Vitale & Katz, 2003). For example, the phase diagram of a divinylbenzene in an ethanol water mixture is depicted in Figure 2-5 (Ganachaud & Katz, 2005; Vitale & Katz, 2003).

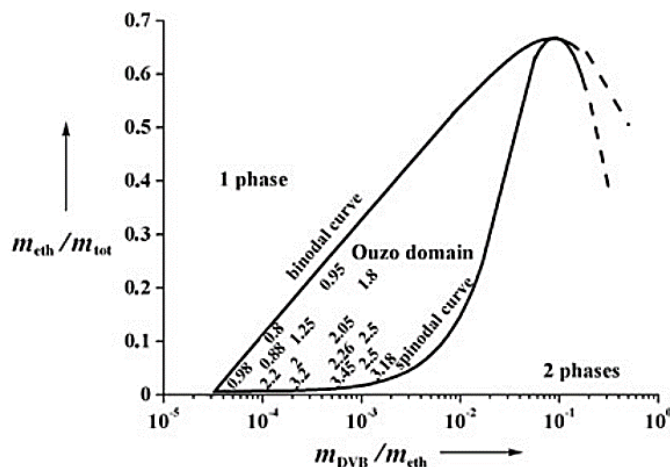


Figure 2-5. Phase diagram of divinylbenzene precipitated from an ethanol water solution (Ganachaud & Katz, 2005; Vitale & Katz, 2003).

As previously mentioned, the spontaneous emulsification of hydrophobic molecules by solvent shifting occurs in the metastable regime between the binodal and spinodal curves. Thus, the ouzo effect is that of a nucleation mechanism rather than a spinodal decomposition mechanism. Energetically, the formation of the hydrophobic droplet dispersions will follow the homogeneous nucleation mechanism described in Section 2.2.1. In Figure 2-5, the region above the binodal line will result in a dissolved state of the hydrophobic compound, whereas below the spinodal line, spinodal decomposition will occur, forming very large droplets that will quickly coalesce and phase separate. At very high solute and solvent concentrations, a reverse ouzo dispersion may form where water, the antisolvent, is the dispersed phase. Mechanistically, when the solubility limit is reached, the hydrophobic compounds will rapidly nucleate creating a local depletion of solute, restricting further nuclei formation. The nucleation will be followed by absorption/adsorption of excess solute molecules by existing nuclei. The small droplets will then grow over time by coalescence through particle collisions or Ostwald ripening, homogenizing the size distribution. The particles will reach a larger enough size where Ostwald ripening is limited, and the dispersion will become stable. However, it must be noted that the destabilizing mechanisms of Ostwald ripening and coalescence will not simply halt but will occur at a lower rate. Thus, many researchers include stabilizers such as surfactants or ripening inhibitors to reduce further destabilization occurrences.

## **2.4 Ostwald ripening**

Classical nucleation theory provides a high-level description of the formation of nanoparticles by nanoprecipitation but has its limitations, much of which can be attributed to the capillary assumption, where the nuclei are considered to have an infinitely flat surface at its interface. However, in cases of low solute concentration or very high mixing rates, nuclei are

likely to be composed of very few molecules, which is better represented by having a sharp, curved surface at small sizes. This, in turn, will generate an increase in the so-called Laplace pressure, in which there is an inverse relationship between the internal pressure of a spherical particle and its radius (Equation 9).

$$\Delta P = \gamma \left( \frac{1}{R_1} - \frac{1}{R_2} \right) = \frac{2\gamma}{R} \text{ (Let } R_1 = R_2 \text{)} \quad (9)$$

The Laplace pressure will increase the energy barrier to form stable nuclei. The Laplace pressure of a particle with radius  $R$  times the molar volume,  $v_b$ , yields the chemical potential,  $\Delta\mu$ , of dissolution of molecules in the bulk,  $\mu_b$ , and phase separation of molecules in a particle,  $\mu_p$ , as in Equation 10 (Kabalnov, 2001; Webster & Cates, 1998).

$$\Delta\mu = \mu_p - \mu_b = \frac{2\gamma v_b}{R} \quad (10)$$

$$\frac{d\Delta\mu}{dR} = -\frac{2\gamma v_b}{R^2} \quad (11)$$

The chemical potential is always positive in the case of a positive surface energy, which agrees with the argument that a particle dispersed in a continuous phase is always dissolving (Kabalnov, 2001). The derivative of the chemical potential difference with respect to particle size is always negative and scales with  $1/R^2$ , so any instances of polydispersity will drive the system to quickly stabilize by dissolution of molecules from metastable small particles and deposit on larger, more stable particles in a saturated solution (Equation 11, Figure 2-6). This is the definition of Ostwald ripening.

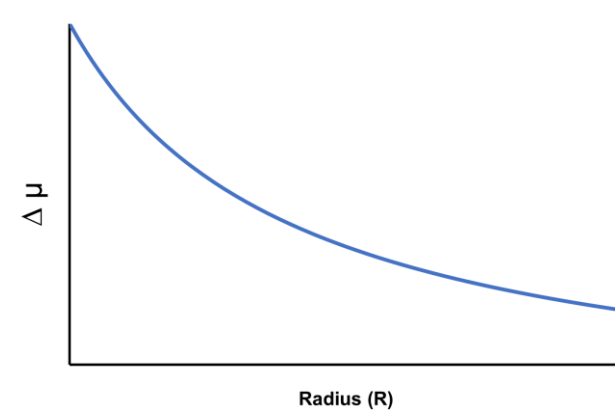


Figure 2-6. The relationship between the particle radius and chemical potential of a molecule at the surface of a particle.

However, there are methods to inhibit Ostwald ripening. One type of ripening inhibitors is the trapped species model. In this case, a third constituent is introduced to the solution that is more soluble in the dispersed phase and highly insoluble in the continuous phase. The introduction of this third entity yields a modification of Equation 10 into Equation 12:

$$\Delta\mu = \left[ \frac{2\gamma}{R} - \frac{Nk_B T}{\frac{4\pi R^3}{3}} \right] v_b \quad (12)$$

In Equation 12, N is the number of molecules of the third component dissolved in the dispersed particle/droplet. The first term is related to the Laplace pressure. However, the Laplace pressure is in constant competition to the osmotic pressure of the trapped species, the second term, due to relatively high local concentrations of the solute in a phase separated particle. Now, at small particle sizes, the change in chemical potential favors the particle state over the dissolved state ( $\Delta\mu < 0$ ). The relationship between particle radius and chemical potential is shown in Figure 2-7.

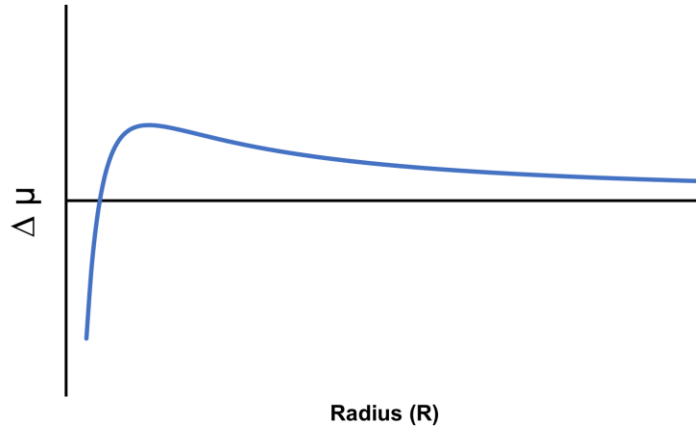


Figure 2-7. Chemical potential of a molecule at the surface of a particle containing a ripening inhibitor.

The critical radius  $r^*$  from classical nucleation theory mentioned in Section 2.2.1 is the radius at which the particle will remain phase separated and grow rather than redissolve. A similar critical radius,  $R^*$ , can be derived from the first derivative of Equation 12 where the osmotic pressure and Laplace pressures are equal:

$$R^* = \sqrt{\frac{3Nk_B T}{8\pi\gamma}} \quad (13)$$

Above this critical radius, the chemical potential is positive, and the particle will dissolve. Below the critical radius, the chemical potential is negative, and the dissolution of the particle will not occur. As the number of trapped species in the droplet,  $N$ , increases, the larger the particle can exist without Ostwald ripening occurring. This type of ripening inhibition is especially effective in the case of the dispersed droplet having partial solubility in the continuous phase and the third component (trapped species) having less solubility in the continuous phase than the dispersed component yet being highly miscible with the dispersed phase.

### **3 SURVIVABILITY OF *SALMONELLA* TYPHIMURIUM (ATCC 14208) AND *LISTERIA INNOCUA* (ATCC 51742) ON LIGNOCELLULOSIC MATERIALS FOR PAPER PACKAGING**

#### **3.1 Abstract**

Lignocellulosics are a major resource for food packaging materials. Given their highly porous and absorptive nature, the uptake and retention of bacteria during food processing, transportation, and storage presents a potential risk for outbreaks of foodborne disease. Thus, a greater understanding of how bacteria proliferate and survive on lignocellulosic surfaces is crucial. The aim of this work was to compare the growth and survivability of *Salmonella* Typhimurium and *Listeria innocua* on bleached and unbleached paper packaging materials. Two different paper materials were fabricated to simulate linerboard from fully bleached and unbleached market pulps and inoculated with each bacterium at high bacterial loads ( $10^7$  CFU). The bacteria propagated during the first 48 hours of incubation and persisted at very high levels ( $> 10^7$  CFU/cm<sup>2</sup>) for 40 days for all paper and bacterium types. Unbleached paper allowed for a greater degree of bacterial growth to occur compared to bleached paper, suspected to be due to the more hydrophobic nature of the lignin-containing fibers. However, there are several other considerations such as storage conditions, nutrient availability, and chemical composition of the fibers that may alter the behavior of the bacteria on lignocellulosic surfaces.

#### **3.2 Introduction**

The transmission of harmful pathogens can occur via multiple pathways (e.g., surfaces, direct human interaction, etc.). Recently, due to the SARS-CoV-2 pandemic, the adaptation of consumer behavior has also had indirect consequences on supply chains including surges of

nearly 40% in e-commerce sales that rely heavily on the use of corrugated boxes to store, transport, and deliver goods and food products (U.S. Department of Commerce, 2021). The EPA reports that 33.3 million tons of corrugated boxes, presumably for mainly packaging purposes, were generated in the U.S. in 2018, while only 14.5 million tons of plastic packaging were generated in the U.S. in 2018 (EPA - United States Environmental Protection Agency, 2020). In that same year, the recycling rate of corrugated boxes was 96.5% while the recycling rate for plastic packaging was only 13.6% in the U.S (EPA - United States Environmental Protection Agency, 2020). Thus, much of our food and other goods are distributed and preserved with lignocellulosic packaging materials and the majority are recycled. As sustainability becomes a growing factor in relation to food packaging, it is likely that paper-based packaging will become even more predominate among consumers and industry.

Foodborne disease caused by bacterial pathogens causes approximately 3.6 million illnesses annually and represent 64% of the foodborne pathogen-related deaths annually in the U.S., with the remaining 36% caused by viruses and parasites (Scallan et al., 2011). Many of these illnesses, including those caused by *Salmonella* spp. and *Listeria monocytogenes*, have been linked to human contact with both raw meats and fresh produce, with the transmission emerging from packaging and processing, contaminated irrigation, handler error, improper storage, and contaminated soil systems (Hanning et al., 2009; Harris et al., 2003; Malhotra et al., 2015; Sung et al., 2013). Unfortunately, to the authors' knowledge, there are no published studies directly relating the number of these illnesses contracted through direct or indirect contact with paper packaging specifically, although some early reports attribute cross-contamination to be a major route of transmission (Buzby et al., 1996; Roberts, 1986). Nevertheless, it is important to understand the factors that may influence the survivability of

foodborne bacterial pathogens on paper-based packaging to guide the development of more advanced technologies aimed at combating foodborne disease.

Several studies have investigated the survivability of common foodborne bacteria on various surfaces and have concluded some general understandings to that regard (Kramer et al., 2006; Kusumaningrum et al., 2003; Patrignani et al., 2016; Siroli et al., 2017a; Sirsat, 2020b; Sirsat et al., 2013; Wilks et al., 2006). For example, Siroli *et al.* studied the survivability of *E. coli* and *L. monocytogenes*, among others, on plastic and paper surfaces and found that the plastic surfaces yield higher survivability rates compared to that of paper surfaces (Siroli et al., 2017a). The authors proposed that the sequestration of the microbes in the porous fiber matrix of paper materials restricts the access of the microorganisms to necessary nutrients, whereas the nutrients remain much more accessible on the surface of non-porous plastic materials (Siroli et al., 2017a). On the other hand, Sirsat *et al.* studied the survivability of *Salmonella* spp., *L. monocytogenes*, and *E. coli* on cardboard coupons and found that the microbes can last more than 30 days, apart from *E. coli*, which maintained viability for only 48 hours, yet not much information was given about the surface material other than it being paper-derived (Sirsat, 2020b). The survivability of similar microorganisms on stainless steel surfaces has also been investigated and it was determined that foodborne bacterial pathogens can survive up to four days on such surfaces (Kusumaningrum et al., 2003; Wilks et al., 2006). In conclusion, the longevity of bacteria on surfaces is highly variable and strain dependent, and access to nutrients seems to be a major contributing factor (Kramer et al., 2006; Patrignani et al., 2016; Siroli et al., 2017a; Sirsat et al., 2013).

Paper packaging materials are produced from pulping lignocellulosic biomass containing cellulose, hemicellulose, and lignin. The amount of lignin and hemicellulose present in the paper

decreases with pulping and bleaching (Zambrano, Marquez, et al., 2021). In addition to delignification, conventional bleaching methods oxidize the cellulose, resulting in a relatively large number of carbonyl groups (Zambrano, Marquez, et al., 2021). However, the presence of carbonyl groups on the surface of a cellulosic fibers will not likely result in a dramatic increase in antibacterial activity. Lignin, the second most abundant biopolymer present in biomass behind cellulose, has been associated with antimicrobial activity due to its polyphenolic substructure, deeming it a potential candidate for use as a biobased antimicrobial agent (Espinoza-Acosta et al., 2016). While many studies have examined the antimicrobial effects of lignin as an extractive from pulp and paper processes, termed technical lignins, much of the more promising results are found with lignin composites containing other known antimicrobial agents, such as chitosan, cationic polymers, and metal ions (Alzagameem et al., 2019; Rai et al., 2017; Richter et al., 2015a; Yang et al., 2016). Lignin's primary role as an antimicrobial agent *in vivo* is a barrier polymer for carbohydrates in plants structures (Bhuiyan et al., 2009; Nicholson & Hammerschmidt, 1992; Vance et al., 1980). To the authors' knowledge, there has not been an investigation comparing the behavior of bacteria on unbleached and bleached paper surfaces. Decoupling the effects of lignin content and oxidation of the cellulosic components during pulp bleaching is conceptually difficult due to the harsh chemical treatment needed to perform such process and was not investigated in this work.

Herein, we examined the microbial growth and survivability of *Salmonella* Typhimurium and *Listeria innocua* on bleached and unbleached paper substrates. *Salmonella* Typhimurium is a known foodborne pathogen and commonly associated with the majority of salmonellosis outbreaks (Anderson & Kendall, 2017; Hanning et al., n.d.; Won & Lee, 2017). *Listeria innocua* has been considered a safe, nonpathogenic surrogate for *Listeria monocytogenes* given their

similar biochemical and growth characteristics (Francis & O'Beirne, 1998; Pradhan et al., 2012). The paper substrates were made to simulate linerboard for paper packaging applications using fully bleached and unbleached southern softwood kraft pulp at a lignin content relevant to common paper packaging materials (e.g., corrugated paperboard). It was expected that paper-based materials with higher lignin content could inhibit the growth and longevity of bacteria due to lignin's suggested bioactive properties. This study adds to the current literature investigating the survivability of microbes on packaging materials and may serve as a foundation for developing antipathogenic additives for such materials.

### **3.3 Materials and Methods**

#### **3.3.1 Materials**

Two market wood pulps, southern bleached softwood kraft (SBSK) and southern unbleached softwood kraft (UBSK) pulp from a paper mill in the Southeast United States were used for the formation of paper samples.

Two microbial strains, *Salmonella enterica* serotype Typhimurium MHM 124 (ATCC 14208) and *Listeria innocua* (ATCC 51742), were received as freeze-dried samples from the American Type Culture Collection (ATCC). Trypticase soy broth (TSB) and trypticase soy agar (TSA) were used for overnight cultures incubated at 37° C for both bacterial strains (Fisher Scientific, Waltham, MA, USA). Additional growth factors including dextrose, ammonium iron (III) citrate and anhydrous magnesium sulfate were acquired as well from Fisher Scientific (Waltham, MA, USA).

### **3.3.2 Fabrication of Paper Samples**

Paper test specimens were cut from pressed paper handsheets to simulate cardboard with different chemical compositions, specifically lignin content. The procedure for making paper handsheets is described by TAPPI standard methods (TAPPI T205 sp-02, 2006). The handsheets were made with a basis weight of 120 g/m<sup>2</sup> and were pressed to simulate a similar structure as linerboard for packaging. These handsheets were set to dry in a humidity-controlled room (23°C, 50 % relative humidity) for 48 hours. Once conditioned, the sheets were cut into 2 cm x 2 cm squares. The paper specimens were wrapped in tin foil and autoclaved at 121°C for 60 minutes before inoculating with the bacteria for sterilization.

### **3.3.3 Characterization of Paper Samples**

The paper samples were characterized for their lignin content and associated relative hydrophobicity. The procedure for determining the lignin content of the pulps used for the fabrication of paper handsheets is described by TAPPI T236 cm-85 (TAPPI Test Methods, 1996). The relative hydrophobicity was determined by the water apparent contact angles that were measured by the sessile drop method using a Phoenix 300 contact angle analyzer (Surface Electro-Optics, Suwon City, Korea). Measurements were performed on the first image captured 20 milliseconds after releasing the water droplet to minimize roughness, swelling, and absorptive effects. The water contact angle was estimated using the tangent line-fitting mode from a minimum of seven measurements at various locations on the sheet surface.

### **3.3.4 Inoculation of Microbes on Paper**

Trypticase soy broth media (TSB) was modified with additional growth factors at the following concentrations: 10 mg/L of ammonium iron (III) citrate and 120 mg/L of anhydrous

magnesium sulfate (TSB+). Trypticase soy agar (TSA) media was modified with the same additional growth factors at the same concentrations, with the addition of 2.5 g/L of dextrose (TSA+). The additional growth factors were added to promote bacterial proliferation in overnight broth cultures and colony formation on agar plates. All broth and agar solutions were autoclaved at 121°C for 60 min. A solution of dextrose was autoclaved separately then added to the agar solution after sterilization to avoid Maillard reaction byproducts (Helou et al., 2014).

Each bacterial strain was cultured overnight in TSB+ media at 37°C. The overnight culture was then transferred to sterile 3 mL vials and frozen overnight at -80°C. The frozen culture was scraped with an inoculation loop, and T-streaked on the TSA+ plates, then incubated at 37°C overnight. The colonies from the overnight plates were transferred to a sterile conical tube containing 10 mL of autoclaved saline solution (8.5 g/L of NaCl) and homogenized using vortex mixing. The colonies were added until the suspension reached an optical density at 600 nm (OD) of 1.0 (~10<sup>9</sup> CFU/mL for both microbes). Each microbial suspension was diluted by a factor of 10 in 27 mL of TSB+ media to make the inoculate suspensions. The paper specimens were inoculated by dropping 0.1 mL of the inoculate suspensions on the paper specimens separately, resulting in a final bacterial load of ~10<sup>7</sup> CFU.

Individual paper specimens were allowed to dry for 10 min then placed into 50 mL sterile conical tubes for storage. The paper specimens were inoculated with the bacteria in a broth suspension to simulate a “worst case” scenario, in which the bacteria have optimum conditions to propagate in the initial stages of the experiment (Pradhan et al., 2012; Suominen et al., 1997). The samples were stored for up to 40 days at ambient conditions. The conical tubes were opened every other day to allow for air regeneration. For comparative purposes, two alternative storage conditions for the inoculated paper specimens were studied including 1) a dry, high nutrient

environment and 2) a dry, low nutrient environment (See APPENDIX A: Supplementary Information for Chapter 3).

The microbes were extracted from the paper specimens by adding 20 mL of a sterile saline solution (8.5 g/L NaCl) to a conical tube with the inoculated paper specimen and agitated using a vortex mixer (MN:12-812, Fisher Scientific, Waltham, MA, USA) at 60% power for 30 seconds. The resulting suspension was diluted with the sterile saline solution to the appropriate concentration then plated on TSA+ plates. Each condition had 3 replicates for each day of extraction and the entire experiment was repeated for experimental replication (n=6 per day per condition).

### **3.3.5 Bacterial Enumeration**

The bacteria were incubated on TSA+ plates for 24 hours for *S. Typhimurium* and 48 hours for *L. innocua* at 37°C. The dilutions were plated over three orders of magnitude to account for major increases or decreases in microbial populations on the paper specimens.

### **3.3.6 Statistical Analysis**

All statistical analyses were performed using JMP v. 15 software (SAS, Cary, NC, USA). The customized least squares regression fit model was utilized for the comparison of mortality rates. The JSL code for the mortality rate comparisons is provided in APPENDIX A: Supplementary Information for Chapter 3. The least squares mean comparison was performed using a two-way ANOVA standard least squares regression model. Tukey's HSD multiple comparisons test was used for determining significant differences between groups at a 95% confidence level. Further information on the individual tests is described in later sections.

## 3.4 Results

### 3.4.1 Survivability of bacteria on lignocellulosic materials

The two bacterial strains (*L. innocua*, *S. Typhimurium*) were inoculated on bleached (SBSK) and unbleached (UBSK) paper specimens separately and were stored in ambient conditions over a 40-day period. The concentration of each bacterial inoculum was quantified prior to inoculation of the paper specimens as a control. The number of bacteria extracted from the paper specimens by vortex mixing was not equal for bleached and unbleached samples, thus an extraction efficiency ( $\varepsilon$ , Eq. 1) was calculated and used to correct for the actual bacterial populations in each sample for each day studied. The corrected bacterial count,  $\hat{y}$ , was calculated using Eq. 2,

$$\varepsilon = \bar{y}_0 / \bar{y}_c \quad (1)$$

$$\hat{y} = y_i / \varepsilon \quad (2)$$

where  $\varepsilon$  is the extraction efficiency on the log scale,  $\bar{y}_0$  is the average log CFU recovered from paper on Day-0,  $\bar{y}_c$  is the average log CFU in the inoculum, and  $y_i$  is log CFU on Day- $i$ . The Day-0 point represents the number of bacteria extracted from the sheet 30 minutes after inoculation. Both papers were characterized by their microbial extraction efficiencies, lignin content, and relative hydrophobicity by contact angle (Table 3-1).

Table 3-1. Paper characteristics and extraction efficiencies ( $\epsilon$ ) of microbes from bleached (SBSK) and unbleached (UBSK) pulps. The arithmetic extraction efficiency is the average CFU extracted from each paper type divided by the average CFU in the inoculum.

<b>Paper Characteristics</b>				
Paper Type	Bleached	Unbleached		
Lignin Content (%)	<1 <sup>a</sup>	13.0 ± 0.1		
Contact angle (°)	20 ± 3	55 ± 5		
<b>Extraction Efficiencies</b>				
Bacteria	<i>L. innocua</i>	<i>L. innocua</i>	<i>S. Typhimurium</i>	<i>S. Typhimurium</i>
Paper	Bleached	Unbleached	Bleached	Unbleached
$\bar{y}_c$ (log CFU)	7.3	7.3	7.28	7.28
$\bar{y}_0$ (log CFU)	7.16	6.81	6.86	6.5
$\epsilon$ (Log Scale)	0.98	0.93	0.94	0.89
$\epsilon$ (arithmetic)	0.77	0.32	0.40	0.17

<sup>a</sup> The lignin content of fully bleached softwood kraft pulp is below the limit of detection by the kappa test used in this experiment but has been determined elsewhere (Zambrano, Wang, et al., 2021).

The lignin content of the bleached paper was less than 1%, whereas the unbleached paper contained 13.0% lignin. Since lignin is a relatively hydrophobic molecule, a higher water contact angle was expected for the unbleached paper (55° vs 20°). The increase in relative hydrophilicity of bleached paper could be due to both the removal of lignin and oxidation of the cellulose during bleaching. The extraction efficiency from the bleached paper was more than twice that of unbleached paper for both microbes, and the extraction efficiency of *L. innocua* was about twice that of *S. Typhimurium* for both paper types (Table 3-1). The results of the extraction efficiencies show that the bleached samples release more bacteria from the fiber matrix than unbleached samples during vortex mixing. It was observed that the bleached samples lost most

of their original structure when vortex mixing (i.e., free suspended fibers), whereas the unbleached samples showed almost no structural change from agitation.

The number of bacteria extracted from the bleached and unbleached paper specimens for each of the microbes was studied over a 40-day period under a worst-case condition (moist, nutrient-dense environment) (Figure 3-1). Both bacteria species seem to not only survive but proliferate ~500-fold after 48 hours on the paper specimens due to the nutrients present in the inoculum (Figure 3-1). After 40 days, the viable microbial populations are still higher than their initial population extracted 30 minutes after inoculation. The growth and survivability of the bacteria was also tested over a three-day period under less favorable conditions, specifically a drier and less nutrient-enriched environment (APPENDIX A: Supplementary Information for Chapter 3). Under drier conditions but a nutrient-dense inoculum, the bacterial growth was shortened by one day compared to the worst-case scenario and a reduction of the overall population to the level of the initial inoculum within three days (APPENDIX A: Supplementary Information for Chapter 3). In contrast, in the absence of excess nutrients (saline inoculation media) and continuous air regeneration, the bacteria were at populations lower than the limit of detection after 24 hours (APPENDIX A: Supplementary Information for Chapter 3).

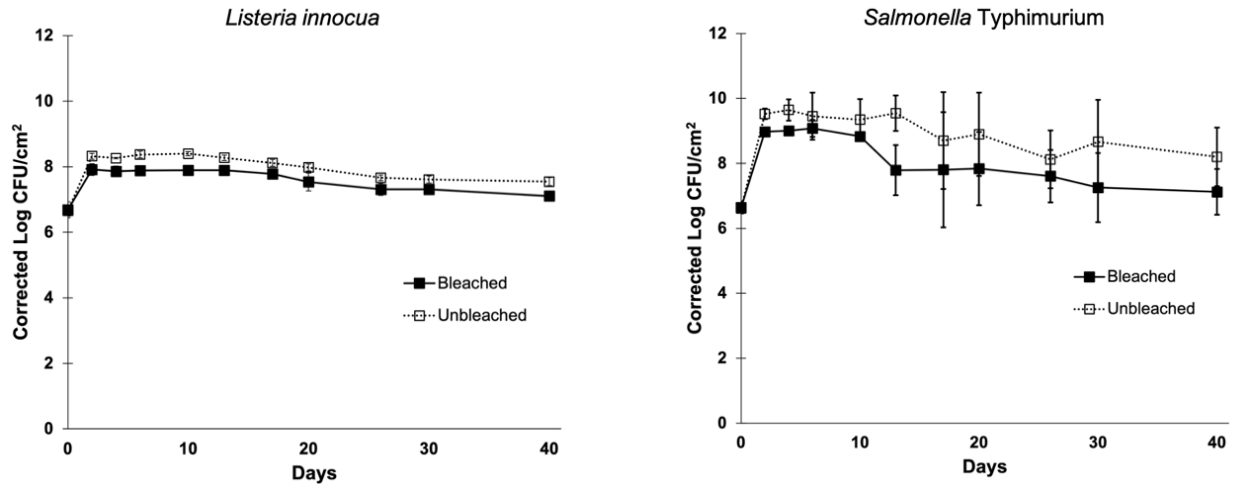


Figure 3-1. Average log CFU/cm<sup>2</sup> of *L. innocua* and *S. Typhimurium* on bleached and unbleached paper specimens over a 40-day period. The average log CFU/cm<sup>2</sup> was corrected for the extraction efficiencies ( $\epsilon$ ) as described previously. The error bars are representative of the standard deviation.

In consideration of the extensive growth of the bacteria in the first 48 hours, followed by a gradual decline thereafter, a non-linear cell growth and decay model was performed on the dataset from day 0 to day 40 (APPENDIX A: Supplementary Information for Chapter 3). This non-linear model fits reasonably well, but the growth parameter is not very accurate due to the limited number of data points taken within the growth stage. Given that the dataset was corrected for the extraction efficiencies and the inoculum concentrations were roughly the same (Table 3-1), the Day-0 data points are therefore trivial for all conditions, and a more representative linear model was applied to the dataset from days 2 through 40 (Figure 3-2).

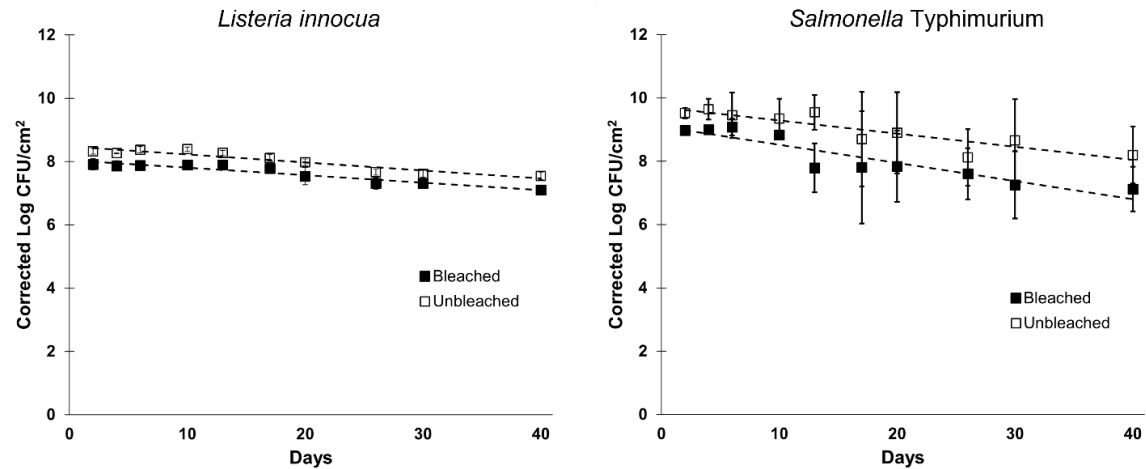


Figure 3-2. Standard least squares regressions for each of the four conditions (two bacteria, two papers). The average log CFU/m<sup>2</sup> was corrected for the extraction efficiencies ( $\epsilon$ ) as described previously. The error bars are representative of the standard deviation. Slopes, y-intercepts, and  $R^2$  values are displayed in Table 2.

From the linear regressions, the mortality rates ( $\beta$ ) are reasonably similar between all four conditions with greater variability present in the *S. Typhimurium* samples (Table 3-2). It should be noted that the *S. Typhimurium* samples exhibited much greater variability between replicates than the *L. innocua* samples, thus explaining the relatively low  $R^2$  -values (Table 3-2). However, the variability reported in this work is comparable to previously reported studies where similar microbial species were examined (Kusumaningrum et al., 2003; Sirsat, 2020b; Sirsat et al., 2013; Wilks et al., 2006). To test the statistical significance of the differences between slopes, a customized least squares comparison model was performed on the dataset from days 2 through 40 (Table 3-2). From the data analysis, there is enough evidence to suggest with 95% confidence that *S. Typhimurium* on bleached paper decays significantly faster than the *L. innocua* samples on either paper type. The samples containing *S. Typhimurium* exhibited considerably higher growth after 48 hours of incubation ( $\bar{y}_{\max}$ ) compared to the samples containing *L. innocua* (Figure 3-2, Table 3-2).

Table 3-2. Fitting parameters for each of the linear regressions displayed in Fig. 3-2. Values for the parameters were calculated using JMP standard least squares fit model with paper and bacteria as fixed effects as well as the interaction term. The comparison of slopes test was computed using a customized least squares regression (see supplementary material, Section 2). A p-value < 0.05 is considered a statistically significant difference.

<i>L. innocua</i>					
Parameter	Bleached	Unbleached			
$\bar{y}_0$	6.686	6.655			
$\bar{y}_{max}$	8.064	8.493	$y = \bar{y}_{max} + \beta t$		
Mortality ( $\beta$ )	-0.024	-0.026			
R <sup>2</sup>	0.73	0.82			
<i>S. Typhimurium</i>					
Parameter	Bleached	Unbleached			
$\bar{y}_0$	6.643	6.607			
$\bar{y}_{max}$	9.092	9.708	$y = \bar{y}_{max} + \beta t$		
Mortality ( $\beta$ )	-0.057	-0.042			
R <sup>2</sup>	0.39	0.24			
<i>Comparison of Slopes (<math>\alpha = 0.05</math>)</i>					
Bacteria	Paper	-Bacteria	-Paper	$\beta_1 - \beta_2$	P-value
<i>L. innocua</i>	Bleached	<i>L. innocua</i>	Unbleached	0.002	0.881
<i>L. innocua</i>	Bleached	<i>S. Typhimurium</i>	Bleached	0.033	0.002
<i>L. innocua</i>	Bleached	<i>S. Typhimurium</i>	Unbleached	0.017	0.095
<i>L. innocua</i>	Unbleached	<i>S. Typhimurium</i>	Bleached	0.031	0.003
<i>L. innocua</i>	Unbleached	<i>S. Typhimurium</i>	Unbleached	0.016	0.129
<i>S. Typhimurium</i>	Bleached	<i>S. Typhimurium</i>	Unbleached	-0.016	0.120

In contrast to the initial hypothesis, the lignin-containing unbleached paper samples yielded higher viable bacterial populations for each day studied, for both types of bacteria (See Figure 3-1, Figure 3-2, Table 3-2). To confirm the significance of these effects (bacteria, paper),

a statistical comparison was performed on the dataset (Table 3-3). The time interval of interest is after the initial growth period between days 2 and 40 for reasons previously stated, therefore, the Day-0 data points for all conditions were omitted. A least squares means plot is included in the analysis for graphical representation of the differences (Figure 3-3).

Table 3-3. Comparison of least squares means for each of the four conditions tested.  
A p-value < 0.05 is considered a statistically significant difference.

<i>L. innocua</i>					
<b>Paper</b>	<b>LS Mean (<math>\mu</math>)</b>	<b>Std. Error</b>			
Bleached	7.64	0.087			
Unbleached	8.04	0.087			
<i>S. Typhimurium</i>					
<b>Parameter</b>	<b>LS Mean (<math>\mu</math>)</b>	<b>Std. Error</b>			
Bleached	8.10	0.083			
Unbleached	8.98	0.083			
<i>Tukey HSD Comparison of Means (<math>\alpha = 0.05</math>)</i>					
<b>Bacteria</b>	<b>Paper</b>	<b>-Bacteria</b>	<b>-Paper</b>	<b><math>\mu_1 - \mu_2</math></b>	<b>P-value</b>
<i>L. innocua</i>	Bleached	<i>L. innocua</i>	Unbleached	-0.402	0.007
<i>L. innocua</i>	Bleached	<i>S. Typhimurium</i>	Bleached	-0.455	0.001
<i>L. innocua</i>	Bleached	<i>S. Typhimurium</i>	Unbleached	-1.343	< 0.001
<i>L. innocua</i>	Unbleached	<i>S. Typhimurium</i>	Bleached	-0.053	0.972
<i>L. innocua</i>	Unbleached	<i>S. Typhimurium</i>	Unbleached	-0.941	< 0.001
<i>S. Typhimurium</i>	Bleached	<i>S. Typhimurium</i>	Unbleached	-0.888	< 0.001

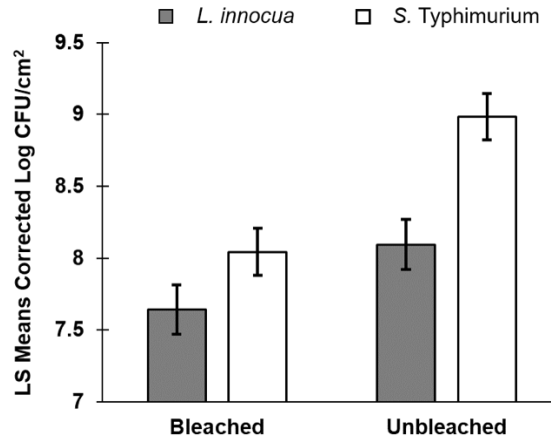


Figure 3-3. Least squares (LS) means of each of the four conditions studied. Error bars are representative of the 95% confidence interval.

The results from Table 3-3 and Figure 3-3 suggest with 95% confidence that unbleached paper yields higher viable bacterial populations than bleached paper for both microbial species studied. When combining these results with the comparison of slopes in Figure 3-2 and Table 3-2, a few conclusions can be made. The microbial growth in the first 48 hours is higher for *S. Typhimurium* on paper surfaces than *L. innocua*. The mortality rates are statistically similar between groups apart from *S. Typhimurium* on bleached paper which decays at a slightly higher rate than the *L. innocua* bleached and unbleached samples. There was no significant difference of mortality rates between the different paper types for *S. Typhimurium*.

### 3.5 Discussion

The aim of this study was to determine if there was a difference in bacterial growth and survivability of bleached and unbleached paper surfaces for both *L. innocua* and *S. Typhimurium* bacterial strains. It was determined that unbleached paper substrates containing a higher lignin content allowed for higher levels of microbial growth compared to bleached paper with minor differences in mortality rates over a 40-day period. This conclusion contradicts the initial

hypothesis that lignin in its lignocellulosic form would have a negative effect on bacterial growth and survivability. The difference in chemical compositions of the two paper materials is more complex than lignin content, such as oxidation of cellulose and hemicellulose during bleaching. Decoupling these components is conceptually difficult given that delignification involves some degree of oxidation of cellulose, such as the case for fully bleached market pulp (Zambrano, Marquez, et al., 2021). This presents a limitation in this study regarding the root causes of the bacterial growth and survivability differences on the two surfaces. Future work could address this limitation by controlling pulping and bleaching conditions and tracking the growth and survivability of bacteria on the resulting materials. Nevertheless, the significance of this work is apparent in identifying the high potential for bacterial contamination and viability on industrially significant paper materials developed for packaging.

One potential reason for unbleached paper favoring microbial growth could be the more hydrophobic nature of the fibers derived from the higher lignin content, as evidenced by a greater water contact angle. Zambrano et al. determined that unbleached pulp has a higher absorption capacity for water than bleached pulp due to the increased interstitial spaces between fibers (APPENDIX A: Supplementary Information for Chapter 3), whereas the bleached pulp retains much more water within the fiber cell wall, as evidenced by a higher wicking rate (Zambrano, Marquez, et al., 2021). The more hydrophobic nature of the fibers may reduce the amount of wicking of broth media from the inoculum, resulting in more nutrients available to the bacteria in the form of droplets in the interstitial space between fibers during the early growth stages. This would explain why the unbleached paper had consistently higher microbial growth after 48 hours of incubation. Since the mortality rates of the microbes were similar, the unbleached paper will have consistently higher bacterial populations since they grew to a much greater number initially.

If the inhibition of bacterial growth was due to bioactivity of either the lignin in unbleached paper or oxidized cellulose in bleached paper, there would likely be more dramatic differences in the mortality rates between the groups overtime. The higher hydrophobicity may also explain the lower extraction efficiency of unbleached samples. The more hydrophilic bleached fibers swell and loosen to a greater extent than unbleached fibers when submerged in the saline solution. The bleached fibers also lack the additional structural rigidity given by the presence of lignin. Both effects result in the disintegration of the bleached fiber network under vortex agitation. The free fibers expose more surface area to the medium and thus release nearly twice as many microbes into the saline solution.

More generally, the results show that these microbes can survive for longer than one month on paper materials at ambient conditions with very low mortality. Both bacterial species studied can form biofilms which may have enhanced their survivability in unfavorable conditions (Andino & Hanning, 2015; Jeon et al., 2018). As previously mentioned, the survivability of *Listeria* spp. and *Salmonella* spp. (among others), on surfaces is highly strain-dependent and can vary from hours to months depending on the experimental conditions (Kramer et al., 2006; Kusumaningrum et al., 2003; Wilks et al., 2006). The survivability of these microbes in this study is much greater than other studies performed on similar microorganisms. As previously referenced, Sirsat *et al.* reported more than 1000-fold decreases in the bacterial populations on cardboard coupons after two days of incubation. The authors also reported *Listeria* spp. having much lower survivability than *Salmonella* spp. on paper (Sirsat, 2020b). Similarly, Siroli *et al.* observed reduction in bacterial populations greater than a 100-fold CFU/cm<sup>2</sup> in 48 hours after inoculation for all species and surfaces, and in some cases below the limit of detection as soon as one hour after inoculation (Siroli et al., 2017a). Differences in the bacterial strains studied as

well as storage humidity, nutrient availability, and temperature likely contribute to the discrepancies in reports (see supplemental material, Section 1). For instance, using saline instead of nutrient broth for the inoculation media will result in an increase in the concentration of NaCl during evaporation, essentially dehydrating the cells. These discrepancies should be evaluated systematically in future work and a standard procedure should be developed in accordance to more realistic conditions.

The high survivability of these foodborne bacterial pathogens poses a problem in the food and agricultural industries with a high chance of cross-contamination when utilizing paper-based packaging materials (Patrignani et al., 2016). Farmers, food transportation, and restaurants should be cautious when reusing and recycling these materials after exposure to dairy products or raw meat and eggs. Also, the generation of biofilms in paper recycling plants pose a threat to production operations and quality control (Brandwein et al., 2016; Carpentier & Cerf, 1993; Shi & Zhu, 2009).

### **3.6 Conclusions**

Foodborne bacterial pathogens pose a great risk to human health and may result in great economic losses in the food and agriculture industries. The survivability of two model organisms for foodborne bacterial pathogens, *L. innocua* and *S. Typhimurium*, on bleached and unbleached paper surfaces was determined. This work showed that the bacteria grow on both bleached and unbleached paper for 48 hours after inoculation and experience very little losses over a 40-day period with sufficient access to nutrients. It was also shown that lignin, which has been generally thought to have antimicrobial properties, did not greatly inhibit the bacterial growth or survivability in paper materials. In fact, the lignin-containing samples (unbleached paper) exhibited higher microbial growth than that of non-lignin containing samples (bleached paper).

This was attributed to the higher hydrophobicity of the fibers that may reduce the wicking of the aqueous nutrient broth, thereby improving the accessibility of nutrients. The results presented in this study further elucidates the necessity of active antimicrobial packaging materials to mitigate microbial growth in even the worst environmental conditions. Lignin may be a potential candidate for a bio-based antimicrobial packaging additive but will require further modification to observe any substantial effect.

## 4 UNDERSTANDING LIGNIN MICRO- AND NANOPARTICLE NUCLEATION AND GROWTH BY SOLVENT FRACTIONATION<sup>1</sup>

### 4.1 Abstract

In recent years, there have been many advances toward developing sustainable, micro- and nanoscale materials from biobased resources such as lignin to further strengthen the bioeconomy. It is critical to study the factors affecting nucleation and growth mechanisms, as well as stability of lignin micro- and nanoparticles (LPs) to further enhance the development of such materials. However, there remains a gap in the literature examining the many interactions present during LP formation. These interactions vary with the chemical composition and molecular weight distribution of different kraft lignin (KL) fractions. To examine the composition of different lignin fractions, KL can be fractionated using water-miscible organic solvents of different polarities such as tetrahydrofuran (THF), acetone, and ethanol. Herein, we show that the micro- and nanoparticles formed from each lignin fraction exhibit significant differences in their size (50-300 nm), particle aggregation and fusion propensity, and spherical morphology in aqueous suspensions. These differences are proposed to be due to the solvent-lignin-water interactions related to molecular weight and functional groups of the lignin fractions and solvent/water polarity. Another factor affecting the nucleation and growth of LPs is the lignin concentration. The LPs formed at low lignin concentrations exhibit a larger average particle size compared to the LPs formed at higher lignin concentrations due to the aggregation and fusion of the small particles. These results will allow for a stronger foundation in understanding the nucleation and growth of LPs when attempting to develop value-added applications for kraft lignin.

## 4.2 Introduction

Lignin micro- and nanoparticles have had heightened interest in the past decade in the attempt to enhance and apply lignin, a by-product of the pulp and paper industry, to more valuable applications. Applications of lignin have been investigated for close to 70 years, and yet the most practical use of this biopolymer is to combust it for energy and steam production. In the present work, softwood lignin was examined. Softwood lignin results from the polymerization, *in vivo*, of predominantly one of three monolignols, namely guaiacyl (G-unit), along with small amounts of *p*-hydroxyphenyl (H-unit) (Duval & Lawoko, 2014; Gellerstedt & Henriksson, n.d.).

Kraft lignin (KL) has a significantly different structure than native lignin due to the harsh alkaline treatment during pulping. This includes the generation of a large number of hydroxyl groups as a result of the cleavage of ether bonds (Chakar & Ragauskas, 2004; Hu et al., 2016). Due to lignin's multi-functional groups, mainly phenolic hydroxyl, carboxyl, and aliphatic hydroxyl groups, a unique set of properties are revealed related to its UV light absorption (Qian, Qiu, & Zhu, 2015; Yearla & Padmasree, 2016), emulsion stabilization ability (Nypelö et al., 2015), antioxidant effects (Yearla & Padmasree, 2016), chelation (Guo et al., 2008) and antimicrobial activity (Richter et al., 2015b; Yang et al., 2016). These properties invoke the potential for the development of eco-friendly, high-value products from lignin. Although KL has great potential for valorization, there has remained a lack of exploitation of such properties due to KL's challenges in product development. Commonly met challenges in the attempt to apply KL to value-added applications include its propensity to form large, amorphous aggregates, its lack of solubility in water, and immiscibility with many thermoplastic and thermosetting polymers (Kun & Pukánszky, 2017).

In order to improve the suitability of kraft lignin for high-value applications, it can be modified chemically (X. Jiang et al., 2018a), fractionated to form more homogeneous samples (X. Jiang et al., 2017), or precipitated into spherical submicron particles for easier dispersion and improved features (C. Jiang et al., 2013; Rahman et al., 2018; Richter et al., 2015b). Unmodified KL tends to form large, irregular-shaped aggregates with a high degree of heterogeneity. Although mechanical treatment can make such aggregates smaller, morphological uniformity remains an issue. Transforming lignin into small, spherical particles has advantages over utilizing KL in solution form (C. Jiang et al., 2013). Smooth, spherical nanoparticles have intrinsic features such as enhanced electrostatic double layer repulsion for higher stability given the smooth surface (Kämäräinen et al., 2018a; Österberg et al., 2020), minimized surface energy from the spherical shape, and a high total surface area per unit mass derived from their small size (Österberg et al., 2020). They may be easily applied in low viscosity suspensions and can be used when extremely small features are desired.

Solvent shifting, or nanoprecipitation, is a common method to synthesize colloidal lignin suspensions by means of supersaturation (Beisl, Miltner, et al., 2017; Leskinen et al., 2017b; Lievonen et al., 2016; Ma et al., 2020; Richter et al., 2016; Sipponen et al., 2018a; Tardy et al., 2018). Various procedures have been developed experimentally including the addition of a lignin solution into excess antisolvent (Leskinen et al., 2017a), the addition of excess antisolvent into a lignin solution (Richter et al., 2016), and dialysis (Lievonen et al., 2016), which are respectively depicted in Figure 4-1a-c. In previous studies, particle formation mechanisms of lignin under various solvent shifting methods have been investigated, but there remains a gap of comparing resulting particle characteristics and behavior in aqueous suspensions formed from kraft lignin fractionated using different organic solvents (Ago et al., 2017; Leskinen et al., 2017a; Lievonen

et al., 2016; Ma et al., 2020; Österberg et al., 2020; Sipponen et al., 2018a; Wang et al., 2020; W. Zhao et al., 2016a).

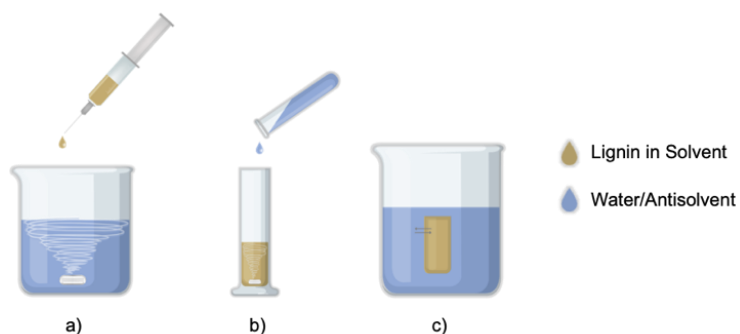


Figure 4-1. Schematic of different solvent shifting methods including a) lignin solution-into-water, b) water-into-lignin solution, and c) dialysis of lignin solution with water.

Sipponen et al. determined that the formation of lignin particles in a common lignin solvent, ethanol, is dependent on solubility and ultimately molecular weight (Sipponen et al., 2018a). It was reported that the formation mechanism of LPs is kinetically limited, where large molecular weight lignin fractions nucleate first and thereafter, smaller lignin molecules adsorb onto the surfaces of the nuclei (Sipponen et al., 2018a). Smaller, metastable soft particles may also form and can eventually fuse with the larger particles through a process called Ostwald ripening, contributing to the overall growth of the particles (Sipponen et al., 2018a). Leskinen et al. discussed a possible micro-emulsification mechanism where lignin molecules become entrapped within a droplet of solvent and as the antisolvent is added, the droplet constricts and eventually phase separates as the solvent concentration greatly decreases (Leskinen et al., 2017a).

Fractionation of KL through solvent extraction is a simple and effective method in homogenizing the lignin sample for LP fabrication (Leskinen et al., 2017a; Ma et al., 2020; Pang et al., 2020a; Pylypchuk et al., 2020). Although, fractionation changes the MW distribution and

chemical composition of the lignin used. Leskinen et al. found that the fractionation of lignin by increasing the concentration of water in THF as the solvating system yields a smaller particle size (Leskinen et al., 2017a). In contrast, Ma et al. showed that fractionating smaller molecular weight lignin molecules by using varying concentrations of ethanol and water prior to particle precipitation led to an inverse relationship between lignin molecular weight and particle size (Ma et al., 2020). The results were attributed to the increase in the hydrophilic character of the lower molecular weight species, where hydrophobic forces tightly compacting the lignin particles are reduced (Ma et al., 2020). It is worth noting that the lowest molecular weight fraction contained 67% of the starting lignin material, relating to a large degree of polydispersity (Ma et al., 2020).

Previously reported studies have shown there are relationships between molecular weight, chemical composition, and resulting particle size by fractionation techniques, but the fractionation techniques used prior to nanoprecipitation did not result in extensive separation of the low and medium molecular weight lignin fractions (Leskinen et al., 2017a; Ma et al., 2020; Pang et al., 2020a; Pylypchuk et al., 2020). Thus, significant aggregation and metastability of lignin particles was not revealed or explored. Additionally, the effect of lignin concentration in solution on particle size has been briefly addressed as a general increasing trend with increasing concentration, but the metastability and aggregation propensity of LPs at low lignin concentrations has not been explored.

Herein, it is shown that fractionating KL with organic solvents of varying polarity (THF, acetone, and ethanol) results in distinct lignin fractions of approximately equal mass yields with significant differences in their molecular weight and chemical composition. The hydroxyl content and molecular weight of lignin fractions were characterized by  $^{31}\text{P}$ -NMR and gel-permeation chromatography (GPC), respectively. The composition differences between the

lignin fractions translates to a variability of colloidal behavior and resulting particle size when precipitated. The LP's size and morphology were determined by dynamic light scattering (DLS) and transmission electron microscopy (TEM), respectively. Using both DLS and TEM particle size analysis techniques concomitantly allows for a greater understanding of the stability and colloidal behavior of the LPs. In addition to studying the effects of solvent fractionation on lignin particle formation, the effects of lignin concentration prior to precipitation are also examined. We propose that lignin particles must contain a high enough hydrophobicity to form discrete, compact, core-shell particles without exceeding a thermodynamically unfavorable surface free energy that may cause aggregation. The novelty of this work is related to describing the connection between the chemical composition of lignin, dissolved lignin concentration, and the colloidal interactions of LPs that result in formation of interparticle aggregates and particle fusion. The contribution of this work includes a deeper understanding of the nucleation and growth of LPs and their colloidal behavior relating to aggregation propensity and/or particle fusion.

## **4.3 Materials and Methods**

### **4.3.1 Materials**

Pine softwood kraft lignin (KL) extracted from black liquor via the LignoBoost method was used for all experiments. KL was acquired as an air-dried powder and the residual moisture was removed by vacuum oven drying for at least 24 hours prior to sampling. Acetone, ethanol, and tetrahydrofuran (1% BHT for stabilization) were acquired from Fisher Scientific (Waltham, MA, USA) and were reported as reagent grade ( $\geq 99\%$  purity). Fractionated samples were centrifuged at 4000 RPM for 5 minutes using 50 mL Falcon centrifuge tubes (Corning, NY,

USA) using an Eppendorf Centrifuge (Model: 5702). The transfer of solutions and solvents was done using Eppendorf volumetric pipettes (500  $\mu$ L-5 mL, 20  $\mu$ L- 200 $\mu$ L). A plastic cuvette was used for dynamic light scattering measurements (Model: ZEN0040, Malvern Panalytical). Dialysis tubing with a molecular weight cut-off (MWCO) of 3500 Da was acquired from Fisher Scientific (Waltham, MA, USA).

### 4.3.2 Methods

To properly examine the effects of solvent fractionation of KL on LP synthesis, each lignin fraction must be analyzed for their chemical structure and molecular weight distribution. This is critical for a better understanding of formed particle morphology, size, and colloidal behavior. Figure 4-2 depicts the overall methodology of this work.

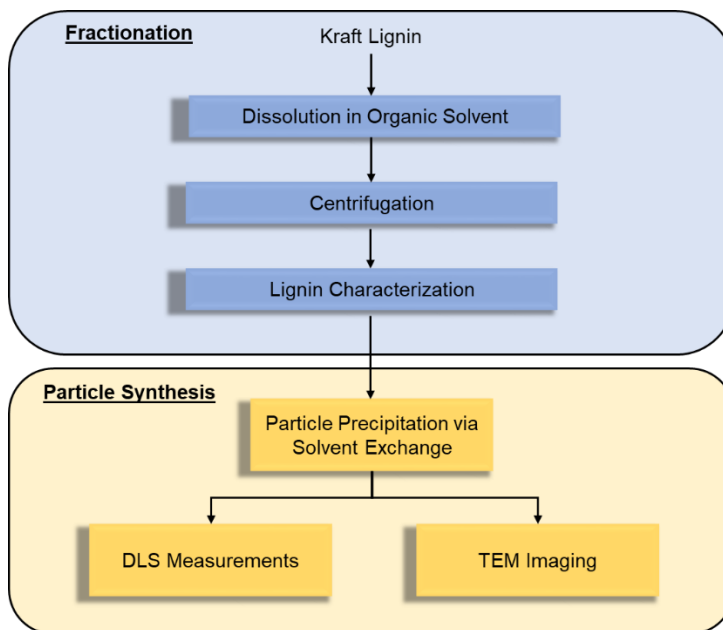


Figure 4-2. Flowchart of lignin fractionation, characterization, and particle synthesis.

### 4.3.3 Fractionation of Kraft Lignin

For preparing the lignin fractions, approximately 1 g of oven-dried KL was added to a 50 mL centrifuge tube along with 40 mL of anhydrous ethanol. The solution was mixed vigorously using a Fisher Scientific Digital Vortex Mixer for 60 seconds at 3,000 RPM to ensure maximum solubility. The mixture was then centrifuged for 5 minutes at 4,000 RPM. The supernatant was decanted and set aside for later use. In the same centrifuge tube, 40 mL of anhydrous acetone was added to the ethanol insoluble fraction and the previous steps were repeated. This process was repeated once more using anhydrous THF as the solvent. The THF insoluble fraction was discarded. This process is depicted schematically in Figure 4-3. Each individual lignin fraction is hereby referred to as E-Frac, A-Frac, and T-Frac for lignin fractions soluble in ethanol, acetone, and THF respectively. Each lignin fraction was then dried by evaporating the solvent using a Büchi Rotovap R-100 followed by vacuum oven drying. Approximately 30 mg OD of each lignin fraction was set aside for GPC and 30 mg OD for NMR analysis. The remaining lignin from each fraction was then re-dissolved in its appropriate solvent to a concentration of 10 g/L. These lignin solutions were then used for LP synthesis

To characterize the KL soluble in acetone and THF without prior fractionation, approximately 1 g of oven-dried KL was added to 40 mL of both anhydrous acetone and THF separately. The solutions were then mixed using a vortex mixer for 60 seconds at 3,000 RPM to ensure maximum solubility. These solutions were centrifuged, and the insoluble portion was oven dried to determine solubility of the lignin in each solvent. The insoluble lignin fractions were discarded and only the soluble fractions were studied. The soluble portions are labelled as the combined acetone and ethanol soluble fractions (AE-Frac), and all three fractions combined, TAE-Frac. The solutions were then used for LP synthesis. The solubility of KL could be

improved with each solvent by adding a portion of water during dissolution, but anhydrous solvents were used to clearly observe the effects of solvent-lignin-antisolvent interactions based on polarity and hydrogen bonding differences. Figure 4-3 illustrates the labelling and description of each fraction.

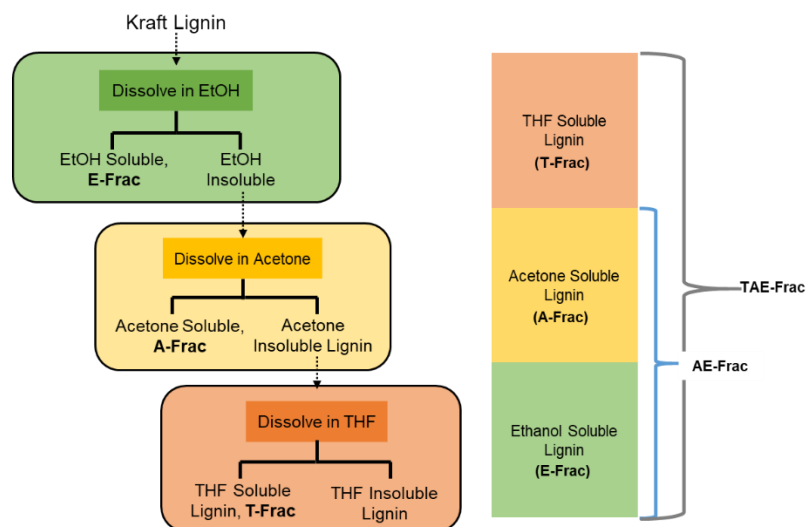


Figure 4-3. Methodology of kraft lignin solvent fractionation and description of lignin fractions.

#### 4.3.4 Molecular Weight Determination of Lignin Fractions by Gel-Permeation

##### Chromatography.

Gel permeation chromatography (GPC) was used to determine the average molecular weights and molecular weight distributions of the kraft lignin fractions. All lignin samples were acetylated prior to analysis to improve solubility in the mobile phase tetrahydrofuran (THF) (Glasser et al., 1993a). The analysis was performed using a Waters GPC instrument equipped with a UV detector (set at 280 nm) using (THF) as the eluent at a flow rate of 0.7 mL/min at 35 °C. A sample concentration of 1 mg/mL and an injection volume of 50  $\mu$ L was used. Two ultra Styragel linear columns linked in series (Styragel HR 1 7.8  $\times$  300 mm and Styragel HR 5E 7.8  $\times$

300 mm) were used. A series of monodispersed polystyrene standards were used as calibration standards.(X. Jiang et al., 2017)

#### 4.3.5 Lignin Hydroxyl Group Content by <sup>31</sup>P-NMR Analysis

<sup>31</sup>P-NMR analysis was performed to identify the various hydroxyl group contents of each lignin fraction. This analysis was performed following the previously reported procedure (Argyropoulos, 1994; Granata & Argyropoulos, 1995). The <sup>31</sup>P-NMR spectra were acquired using a Brüker 500 MHz spectrometer. Each peak was integrated to calculate the hydroxyl contents of each sample.

#### 4.3.6 Derjaguin-Landau-Verwey-Overbeek (DLVO) Model of Lignin Particles

The energy of interaction as a function of interparticle distance was modelled using the DLVO theory of colloidal stability to determine the overall stability of the lignin particles with decreasing particle size. This model excludes non-DLVO forces beyond electrostatic repulsion and Van der Waals attractive forces. The following equations were used for the model derived by Israelachvili (Israelachvili, 2011):

$$V_{rep} = \frac{R}{2} 9.22 \times 10^{-11} \tanh^2 \left( \frac{\zeta_0}{103} \right) \exp(-\kappa D) \quad (1)$$

$$V_{vdw} = -\frac{AR}{12D} \quad (2)$$

$$V_{tot} = V_{rep} + V_{vdw} \quad (3)$$

In Equations 1-3,  $V_{rep}$  is the potential energy of electrostatic repulsion at 25°C in an aqueous medium between two identical spheres with radii R, where  $\zeta_0$  is the surface potential

approximated as the Zeta potential,  $\kappa$  is the Debye length, and  $D$  is the interparticle distance.

$V_{\text{vdw}}$  is the attractive Van der Waals potential energy, where  $A$  is the Hamaker constant of lignin approximated to be  $1.7 \times 10^{-20}$  J by Hollertz et al (Hollertz et al., 2013).

#### **4.3.7 Preparation of Kraft Lignin Particles**

The synthesis of colloidal lignin particles was performed by first transferring 1 mL of the lignin fraction from each solvent solution to a 15 mL scintillation vial. After which, 9 mL of antisolvent (water or dilute NaOH solution) was quickly poured into the solution under rapid magnetic stirring (Figure 4-1 b). The colloidal suspensions are hereby referred to as TAE-LPs, AE-LPs, E-LPs, A-LPs, and T-LPs for particles precipitated from their respective lignin fractions TAE-Frac, AE-Frac, E-Frac, A-Frac, and T-Frac (Figure 4-3). In order to obtain a concentration profile of particle size and morphology for each solvent system, dilutions of each lignin solution with the appropriate organic solvent were performed to obtain concentrations ranging from 0.5 to 10 g/L prior to antisolvent addition. Each suspension was dialyzed with DI water for 24 hours with Fisherbrand dialysis tubing (MWCO: 3500 Da) then further diluted with DI water to a final lignin concentration of 0.01 wt.%.

#### **4.3.8 Dynamic Light Scattering**

A Zetasizer Nano ZS instrument (Malvern Instruments Ltd.) was used for particle size analysis and  $\zeta$ -potential of all samples. For particle size measurements, approximately 2 ml of the colloidal lignin suspension was added to a plastic cuvette (ZEN0040, Malvern, U.K) with lignin concentrations of 0.01 wt.% for each sample, within the concentration range advised by the manufacturer (Malvern Panalytical Ltd.). Particle size measurements were performed in duplicate at 25°C after an equilibration time of 120 seconds. The particle sizes are determined by

an intensity weighted average (Z-average) of scattered light and reported as the average particle diameter,  $\delta$ .

#### **4.3.9 Transmission Electron Microscopy (TEM)**

TEM Images of the lignin particles were taken using a FEI Talos F200X Transmission Electron Microscope (TEM). These samples were prepared by dropping a small amount of each suspension on a TEM grid and dried overnight.

### **4.4 Results and Discussion**

#### **4.4.1 Lignin Fractionation and Molecular Weight Distribution**

It has been previously established that KL has different solubilities in various organic solvents due to the polarity of the solvent and hydrogen-bonding capability between the KL and the solvent (X. Jiang et al., 2017; Schuerch, 1952b). Lignin has been shown to be successfully fractionated either with organic solvent/water mixtures (Leskinen et al., 2017a; Ma et al., 2020; Sipponen et al., 2018a) or using separate anhydrous organic solvents (X. Jiang et al., 2017; Schuerch, 1952b). The characterization of KL fractions separated with three, water-miscible, anhydrous organic solvents directly used for particle precipitation has yet to be completed and is provided herein.

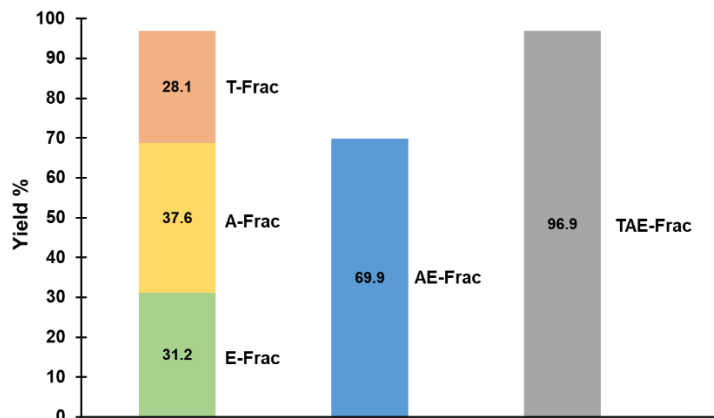


Figure 4-4. Percentage yield of KL distributed in each fraction by mass percent. The first column (left) represents the completely separated fractions of KL extracted through solvent fractionation. The middle and right columns are representative of combined lignin fractions by dissolving KL in acetone (AE-Frac) and THF (TAE-Frac), respectively.

Figure 4-4 includes the yields of KL in each fraction from solvent fractionation. KL was first dissolved in ethanol. The ethanol-insoluble portion was then dissolved in acetone. The remaining acetone-insoluble lignin was then dissolved in THF (see Figure 4-3). Only 31.2% of KL was soluble in ethanol (E-Frac). Acetone was able to dissolve 54.7% of the ethanol-insoluble portion, corresponding to 37.6% of total KL mass (A-Frac). THF was able to dissolve 90.1% of the remaining KL, corresponding to 28.1% of the total KL mass (T-Frac). Directly mixing the original KL in acetone resulted in a solubility yield of 69.9% (AE-Frac). Finally, directly mixing the original KL with THF resulted in the dissolution of 96.9% of the entire KL sample (TAE-Frac).

Table 4-1. Lignin fractionation results including molecular weight of each fraction after acetylation measured by gel-permeation chromatography (M<sub>n</sub>: Number-average molecular weight; M<sub>w</sub>: Weight-average molecular weight, PDI: polydispersity index).

Fraction	M <sub>n</sub> (Da)	M <sub>w</sub> (Da)	M <sub>w</sub> /M <sub>n</sub> (PDI)
TAE-Frac	1200	5600	4.66
AE-Frac	1200	3400	2.83
E-Frac	800	1400	1.75
A-Frac	1600	4000	2.5
T-Frac	5500	13000	2.36

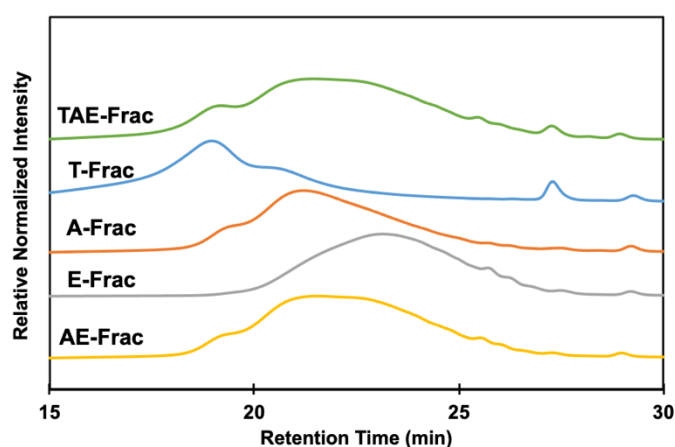


Figure 4-5. Molecular weight distribution curves of each lignin fraction with the intensity normalized to 1 as measured by GPC. Higher molecular weight molecules elute first, whereas lower retention time corresponds to higher molecular weight.

In Figure 4-5, the molecular weight distribution curves of each KL fraction acquired through GPC are shown. Table 4-1 contains the calculated number average (M<sub>n</sub>) and weight average (M<sub>w</sub>) molecular weight of each fraction from the distribution curves. In GPC, higher molecular weight (MW) species are too large to become entrapped within the pores of the column and elute first while the smaller MW species are entrapped within the small pores of the column and elute last (Figure 4-5). When KL was fractionated, the low MW fractions reside in the ethanol solution (E-Frac), the intermediate MW fractions reside in the acetone solution (A-

Frac), and only highest MW fractions of KL were solubilized in the THF solution (T-Frac), as evidenced in Figure 4-5 and Table 4-1.

The combined KL fractions, TAE-Frac and AE-Frac, have much broader MW distributions compared to the individual fractions, as evidenced by Figure 4-5 and Table 4-1. The AE-Frac MW distribution curve is representative of a mixture of the A-Frac and E-Frac, as expected. The TAE-Frac MW distribution contains all three of the individual lignin fractions (see Figure 4-5). Solvents that result in a lower solubility of the KL sample, such as ethanol, can dissolve only the lower MW fractions, whereas the solvents that can dissolve higher MW fractions, such as THF and acetone, can also dissolve lower MW fractions. Reasons for this phenomenon are related to the chemical structure of the lignin fractions and will be discussed in the next section.

#### **4.4.2 NMR Analysis of Solvent Fractionated Kraft Lignin**

The solubility of KL fractions in organic solvents is dependent on the strength of interactions between the solute and solvent. For this reason, it was necessary to understand the chemical structure of the lignin fractions.  $^{31}\text{P}$  NMR is a useful technique for identifying the hydroxyl content of lignins, which can then be related to the overall hydrophilicity or hydrophobicity of the sample. Table 4-2 describes the breakdown of hydroxyl groups present in each KL fraction.

Table 4-2. Hydroxyl content of kraft lignin fractions by  $^{31}\text{P}$  NMR calculated as mmol/g of solid. The polarity of the organic solvent used to dissolve each fraction relative to water is listed as a reference value. C5-substituted-OH can be either 5-5 biphenyl structure or  $\alpha$ -5 condensed G-unit. C5-free-OH contains a hydrogen in the C5 position. Finally, H-OH phenolic is the C5 and C3 free phenolic-OH.

Hydroxyl Group	TAE-Frac	AE-Frac	E-Frac	A-Frac	T-Frac
<b>Aliphatic OH</b>	1.93	1.41	1.41	1.51	2.04
<b>Total Phenolic OH</b>	<b>4.47</b>	<b>4.54</b>	<b>4.98</b>	<b>4.45</b>	<b>3.01</b>
C5-substituted-OH	1.98	1.93	2.03	2.08	1.48
C5-Free-OH	2.14	2.25	2.57	2.03	1.27
H-OH	0.36	0.35	0.38	0.34	0.26
<b>COOH</b>	0.62	0.62	0.60	0.51	0.37
<b>Total OH</b>	<b>7.03</b>	<b>6.30</b>	<b>6.99</b>	<b>6.47</b>	<b>5.42</b>
<b>Solvent</b>	THF	Acetone	Ethanol	Acetone	THF
Rel. Polarity of Solvent <sup>a</sup>	0.225	0.355	0.654	0.355	0.225
Boiling Point (°C)	66 <sup>b</sup>	56 <sup>c</sup>	78 <sup>d</sup>	56 <sup>c</sup>	66 <sup>b</sup>

<sup>a</sup> (Reichardt & Welton, 2010)

<sup>b</sup> (National Center for Biotechnology Information, 2020c)

<sup>c</sup> (National Center for Biotechnology Information, 2020a)

<sup>d</sup> (National Center for Biotechnology Information, 2020b)

In lignin, a higher hydroxyl content, notably phenolic hydroxyls, corresponds to higher hydrophilicity of the lignin molecule (Wang et al., 2020). Due to their more acidic nature, the phenolic hydroxyl content (pKa~10) and carboxyl group (pKa~4) content will contribute more to the overall hydrophilicity of KL than the aliphatic hydroxyl groups (pKa~17) (Ragnar et al., 2000). Table 4-2 illustrates that ethanol is only able to dissolve the most hydrophilic lignin species (E-Frac), as evidenced by the higher total hydroxyl content, whereas acetone soluble lignin fractions contain intermediate hydrophilicity (A-Frac) as well as high hydrophilic fractions (AE-Frac). THF can dissolve all KL species (TAE-Frac), including the most hydrophobic fractions (T-Frac) present in the sample (see Table 4-2). The higher polarity of the solvent precludes the dissolution of only more hydrophobic KL fractions, whereas lower polarity solvents (THF) are less selective in which KL fractions they may dissolve. This is due to the

overall hydrophobic nature of KL, derived from its aromatic character (Wang et al., 2020). While KL contains hydrophilic moieties, such as hydroxyl or carboxyl groups, the non-polarity of the KL remains significant.

Combining the results from both GPC and NMR analysis, a few conclusions can be made. First, KL can be fractionated using different organic solvents of varying polarity. More importantly, a smaller MW KL fraction, such as E-Frac, is related to a more hydrophilic character. In contrast, a larger molecular weight fraction, such as T-Frac, is related to a more hydrophobic character, (see Figure 4-5 and Table 4-1). High polarity water-miscible solvents limits dissolution to lower MW, more hydrophilic lignin fractions, whereas lower polarity water-miscible solvents are less selective. These results are important when precipitating KL in a highly polar antisolvent such as water. In support of green chemistry principles and commercial scale-up of LP synthesis, acetone has the advantages for processing lignin due to the lower boiling point compared to ethanol and relatively low toxicity compared to THF.

#### **4.4.3 Fractionation Effects on Lignin Particle Formation**

The precursor soluble lignin fractions can be precipitated quickly into colloidal suspensions using water as an excess antisolvent. The effect of the KL fraction's chemical structure and molecular weight distribution on particle formation and colloidal behavior in aqueous suspensions is described here.

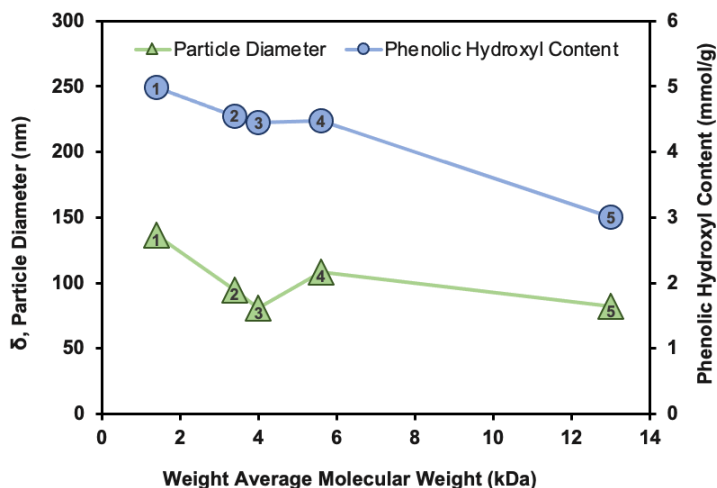


Figure 4-6. Average particle diameter ( $\delta$ ), weight average MW, and phenolic hydroxyl content for 1) E-LPs, 2) AE-LPs, 3) A-LPs, 4) TAE-LPs, and 5) T-LPs at a precursor lignin solution concentration of 5 g/L. Error bars are smaller than the size of the icons. Standard deviation of particle diameters were < 10 nm.

The relationship between the average particle diameters ( $\delta$ ) measured using DLS, MW, and phenolic hydroxyl content for each lignin fraction is presented in Figure 4-6. The LPs were precipitated from a precursor lignin concentration of 5 g/L. The phenolic hydroxyl content is reported in Figure 4-6 rather than the total hydroxyl content because it is more likely representative of the overall hydrophilicity/hydrophobicity of the lignin fractions (Wang et al., 2020).

Comparing the DLS results for fractionated KL samples, E-LPs have the largest  $\delta$  (136 nm) and lowest average MW, whereas A-LPs (81 nm) and T-LPs (82 nm) are significantly smaller at a given lignin concentration despite having a higher average MW (Figure 4-6). The LPs formed from the combined lignin fractions, TAE-LPs (108 nm) and AE-LPS (95 nm), exhibit an intermediate  $\delta$  and phenolic hydroxyl contents relative to the particles formed from the individual lignin fractions that constitute them. The phenolic hydroxyl content and  $\delta$  follow very similar trends with increasing weight-average MW of the KL fractions, indicating both the

chemical composition/hydrophilicity and the MW of lignin molecules contribute to the nucleation and growth of the LPs.

Since DLS measures the hydrodynamic radius of particles in an aqueous medium, the particle diameters reported do not reflect particle shape. Thus, it was necessary to image the particle shape/morphologies using TEM. The TEM images for the individual lignin fractions and combined lignin fractions are shown in Figure 4-7a-b. The TEM images can help explain the discrepancies in  $\delta$  between each lignin fraction.

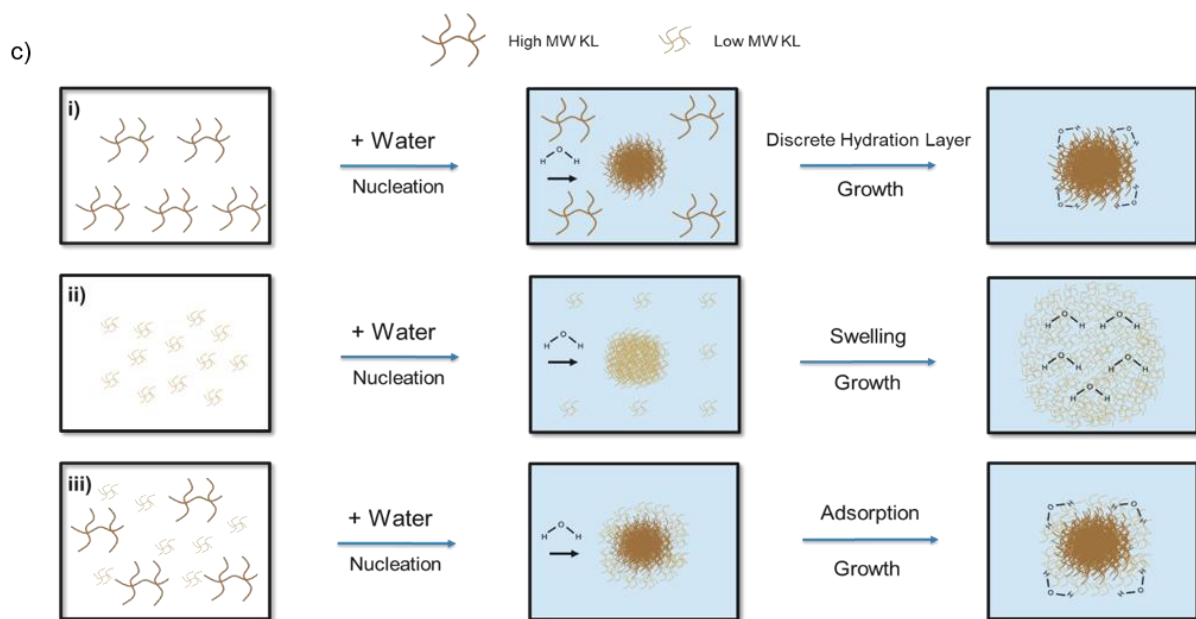
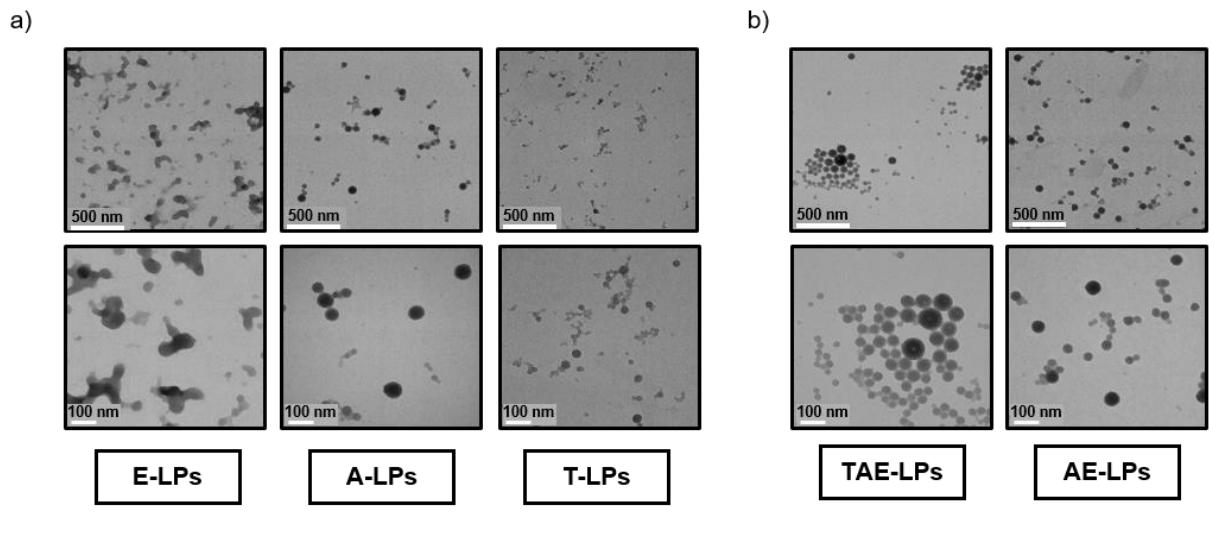


Figure 4-7. a) TEM images of E-LPs, A-LPs, and T-LPs formed from the three separate lignin fractions, E-Frac, A-Frac, and T-Frac at an initial lignin concentration of 5 g/L. b) TEM images of AE-LPs and TAE-LPs formed from the combined lignin fractions, AE-Frac and TAE-Frac. c)

Proposed mechanism of lignin particle nucleation and particle swelling. i) T-LP and A-LP nucleation of higher MW species followed by adsorption particle growth. ii) E-LP nucleation followed by adsorptive growth and particle swelling by means of osmosis. iii) TAE-LP and AE-LP nucleation of high MW lignin followed by particle growth by adsorption of lower MW lignin.

Top row of TEM images scale bars = 500 nm and bottom row of TEM images = 100 nm

The terminology related to the interactions and destabilization of colloidal particles is often misused and should be properly defined in the context of this work. Particle aggregation (or agglomeration) is the adherence of individual particles with discrete particle boundaries and is typically a reversible process (Slomkowski et al., 2011). Conversely, coalescence and Ostwald ripening are irreversible processes that result in the disappearance of particle boundaries for the purpose of minimizing surface free energies, stabilizing otherwise unstable lyophobic particles (“Coalescence in Colloid Chemistry,” 2008; “Ostwald Ripening,” 2008). However, coalescence and Ostwald ripening differ in their mass transfer mechanism. Coalescence occurs once unstable particles have collided, whereas Ostwald ripening involves the dissolution of surface-present molecules of smaller particles and the subsequent adsorption of such molecules on larger particles (“Coalescence in Colloid Chemistry,” 2008; “Ostwald Ripening,” 2008). It is worth noting a more hydrophilic particle favors Ostwald ripening in aqueous systems, due to greater solubility (Lepeltier et al., 2014a). In the case of LPs, it is difficult to distinguish for certain whether Ostwald ripening or coalescence is the mode of action, therefore the two terms will be hereby referred to as particle fusion.

As shown in Figure 4-7a, A-LPs have a well-developed spherical morphology, with similar homogeneity and size as reported elsewhere (Ma et al., 2020; Richter et al., 2016; Setälä et al., 2019). In the case of T-LPs, the particles appear to be much smaller than A-LPs as evidenced by TEM imaging (Figure 4-7a), yet the DLS results report very similar  $\delta$ 's, 82 nm and 81 nm respectively (see Figure 4-6). This could likely be due to the increased degree of aggregation and particle fusion present in the T-LP sample compared to A-LPs. These larger aggregates resemble diameters similar to the A-LPs (see Figure 4-7a).

The smaller individual particle sizes of T-LPs depicted in Figure 4-7a is perhaps due to the more hydrophobic character. The higher hydrophobicity leads to a lower supersaturation concentration, thus favoring nucleation over growth, yielding a large number of smaller particles (Destrée & B.Nagy, 2006; Saad & Prud'Homme, 2016). The increased propensity for T-LPs to fuse and aggregate can be attributed to the higher hydrophobicity. Hydrophobicity at the nanoscale increases the degree of entropic aggregation, as described by the hydrophobic effect, as well as the tendency to reduce the overall surface free energy in aqueous suspensions (Dagtepe & Chikan, 2010; Israelachvili, 2011). The reduction of surface free energy by particle fusion will be discussed further in the next section.

In the case of E-LPs, the TEM images suggest the more hydrophilic lignin fractions form soft, metastable, semi-solid particles in the aqueous medium (see Figure 4-7a). These particles will readily deform and fuse upon collisions with other particles. The lack of hydrophobic forces necessary for phase separation can lead to diffusion of water into the particle structure (particle swelling) and deformation of the LP.

The LPs formed from the combined lignin fractions, TAE-LPs and AE-LPS, may elucidate the effect of MW and MW distribution on particle size. The TEM images in Figure 4-7b suggest the TAE-LPs have a larger particle size distribution and  $\delta$  than AE-LPs. This can be attributed to the higher polydispersity of TAE-Frac compared to AE-Frac. Kinetically, since nucleation is highly dependent on the supersaturation condition, the nucleation of hydrophobic, high MW lignin molecules rapidly reduces the concentration of supersaturated lignin molecules. This results in a larger population of lower MW lignin molecules involved in particle growth (Destrée & B.Nagy, 2006; Lamer & Dinegar, 1950). This rationale is consistent when comparing the  $\delta$  and TEM images of A-LPs and AE-LPs. In this comparison, the lignin molecules that form

the initial nuclei are composed of the same MW and chemical composition, following the aforementioned nucleation mechanism. Therefore, given the same lignin mass, the AE-LPs will contain less lignin molecules that can participate in a nucleation and more lignin molecules that will participate in growth. Thus, greater polydispersity in the lignin sample will lead to less nucleation and more growth.

Figure 4-7c illustrates the proposed particle swelling mechanism of LPs. Two cases are depicted in Figure 4-7c: i) the more hydrophobic, high MW fractions of KL, represented by T-Frac and A-Frac, nucleate and grow into compact hydrophobic particles, ii) the particles formed from the more hydrophilic, low MW fractions of KL swell by osmosis through the particle's surface, driven by stronger interactions of the lignin species with water, representative of E- LPs, and iii) the particles formed from the combined lignin fractions, TAE-Frac and AE-Frac, first nucleate the high MW lignin species, followed by the adsorption of lower MW lignin species on the particle surface, resulting in a compact hydrophobic core, surrounded by a more hydrophilic shell. This swelling mechanism can be supported by previous studies in which the porosity of lignin was investigated indirectly, where LPs were found to be penetrable by water and water-soluble molecules (Dai et al., 2017; Qian et al., 2016; Sipponen et al., 2018a).

Overall, there seems to be a trade-off between the MW distribution and chemical composition of the lignin fractions with respect to resulting particle size and aggregation/fusion propensity. The chemical composition of the lignin fractions used for nanoprecipitation affects the hydrophobicity of the LPs. This hydrophobicity can be related to differences in the nucleation and growth kinetics, particle aggregation/fusion, and particle metastability through partial dissolution in aqueous suspensions upon particle collision and/or close proximities. Previous studies have found aromatic interactions to be a significant contributor to particle

formation (Mishra & Ekielski, 2019; Pylypchuk et al., 2020). These non-DLVO interactions between particles are possible but the steric strain present between spherical structures will likely prevent these close-range interactions from becoming significant. Although, it is possible  $\pi$ - $\pi$  interactions will contribute to the particle growth via coalescence/ripening once particles come into contact. The average particle size reported from DLS is less useful than TEM when comparing the actual morphologies of resulting lignin particles from nanoprecipitation. TEM imaging suggests that particle aggregation/fusion, hydrophobic forces, and surface free energies of lignin particles must be considered.

#### **4.4.4 Concentration Effects on Lignin Particle Formation**

The size of the LPs measured with DLS was investigated as a function of the dissolved lignin concentration (i.e, initial lignin concentration) for each of the lignin fractions. In general, as the initial lignin concentration decreases, the particle diameter decreases as well in the linear region (see Figure 4-8). The general trend can be attributed to fewer lignin molecules present per unit volume participating in nucleation and growth. The lignin particles likely follow the nucleation and growth mechanism proposed by La Mer et al. (Lamer & Dinegar, 1950). This mechanism involves the burst nucleation of supersaturated hydrophobic molecules yielding a constant number of nuclei at a minimum particle size (Destrée & B.Nagy, 2006; Lamer & Dinegar, 1950; Lievonen et al., 2016). The supersaturation condition necessary for burst nucleation quickly subsides after the precipitation of suspended particles. The excess lignin molecules not involved in nucleation possess a very high surface energy in the aqueous medium from their overall hydrophobic character, and readily adsorb to the formed lignin nuclei (Destrée & B.Nagy, 2006; Lamer & Dinegar, 1950). The increase in size with increasing lignin

concentration is due to the growth of the particles via adsorption of lignin molecules to the initially formed nuclei.

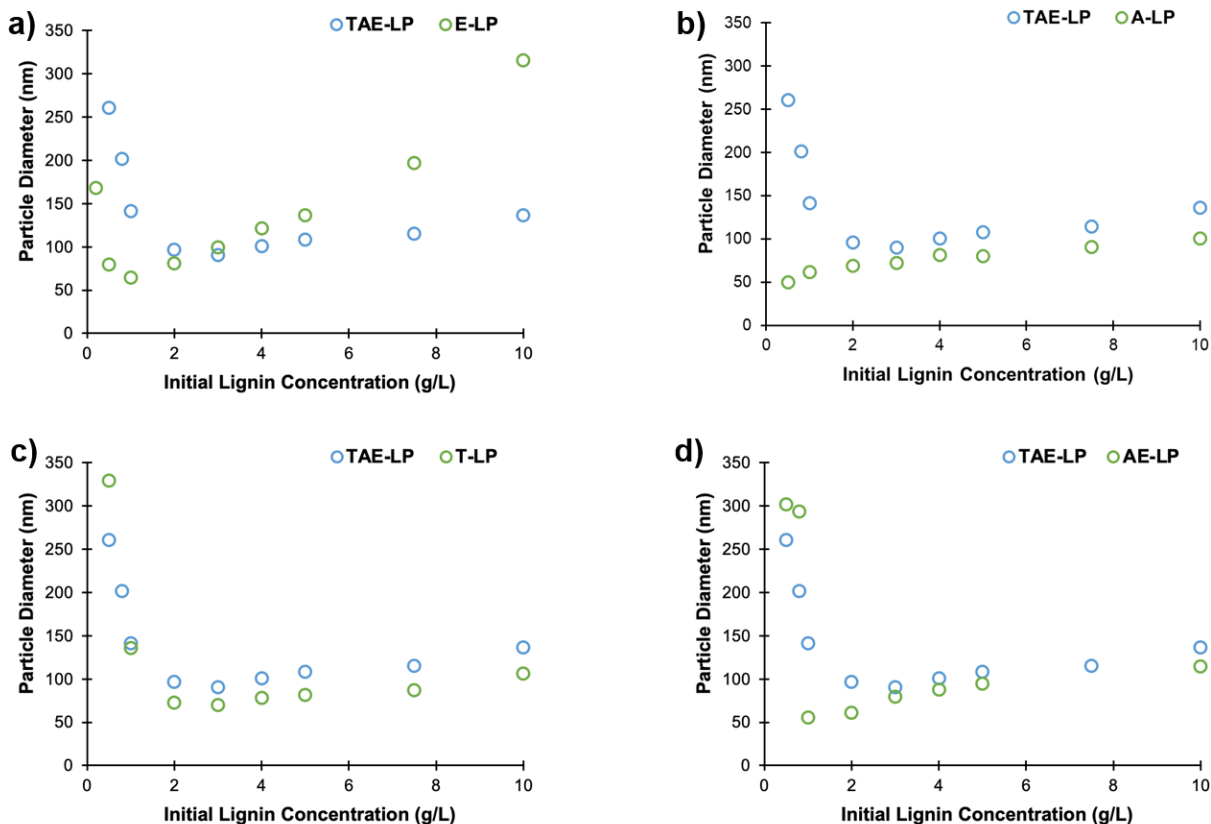


Figure 4-8. Average particle diameter as a function of precursor lignin concentration for TAE-LPs, E-LPs, A-LPs, T-LPs, and AE-LPs as determined by DLS. TAE-LPs are plotted alongside the fractionated LP samples for comparison of the average particle diameter over the concentration profiles. Error bars are smaller than the size of the icons. Standard deviation of particle diameters were < 10 nm.

However, when the initial lignin concentration is reduced significantly, the apparent particle diameters measured via DLS are much larger after precipitation, as evidenced by Figure 4-8. This phenomenon has also been observed in similar studies (Destrée & B.Nagy, 2006; Lievonen et al., 2016; Richter et al., 2016). The concentration at which this occurs can be referred to as the critical concentration,  $C_0$ . This phenomenon is consistent for each lignin

fraction in the concentration ranges studied, with the exception of A-LPs, but occurs at different concentrations of lignin in solution. The  $C_0$  is the highest in T-LPs and TAE-LPs and lowest with E-LPs and AE-LPs (Table 4-3). A-LPs did not exhibit a  $C_0$  from the concentrations measured (0.5 – 10 g/L).

Table 4-3. Critical initial lignin concentration ( $C_0$ ) and resulting average particle diameters measured by DLS for each solvent system.

KL Fraction	$C_0$ (g/L)	Particle Diameter (nm)
TAE-LP	3.0	90
E-LP	1.0	65
A-LP	N/A	50
T-LP	3.0	70
AE-LP	1.0	56

This phenomenon can be further exemplified by Figure 4-9, where the particle size distribution of T-LPs, measured by DLS, above and below  $C_0$  is depicted. For T-LPs,  $C_0$  was 3 g/L, where initial lignin concentrations below  $C_0$  result in the appearance of a peak at much larger particle sizes (~10x). As the precursor lignin concentration is reduced below  $C_0$ , the first peak (left), representative of dispersed individual particles, decreases in intensity and shifts left, indicating smaller particle sizes, but at a lower abundance. The second peak (right) increases in intensity dramatically as the first peak is reduced, indicating the presence of either fusion or aggregation of individual particles.

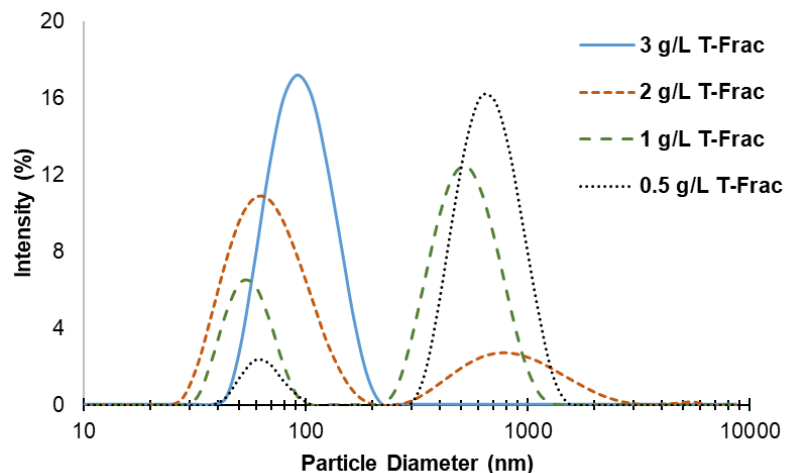


Figure 4-9. Scattered light intensity weighted particle size distribution of T-LPs approaching the critical concentration,  $C_0$ , measured by DLS.

TEM images were taken for T-LPs fabricated at initial lignin concentrations above and below  $C_0$  (5 g/L and 1 g/L, respectively). The TEM images are reported in Figure 4-10.

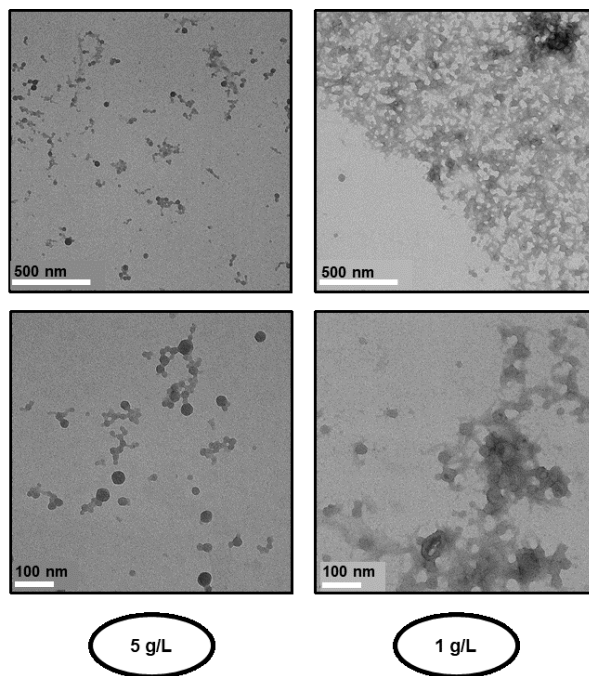


Figure 4-10. TEM images of T-LPs at an initial lignin concentration of 5 g/L and 1 g/L in THF prior to antisolvent addition.

The TEM images suggest extensive aggregation and fusion of the particles at lower lignin concentrations in order to maximize their thermodynamic stability (Ratke & Voorhees, 2002; Thanh et al., 2014). When the lignin concentration is reduced significantly, the particles formed are much smaller, resulting in a very large surface area to volume ratio (S/V, Eq. 4), where R is the particle radius.

$$\frac{\text{Surface Area}}{\text{Volume}} = \frac{4\pi R^2}{\left(\frac{4}{3}\right)\pi R^3} = \frac{3}{R} \quad (4)$$

Smaller, charged particles, will have a favorable charge-to-mass ratio over larger particles, normally improving colloidal stability. Although, when surface charge remains constant and particle size decreases, DLVO theory dictates a lower electrostatic repulsive barrier (Figure 4-11) (Liz-Marzán et al., 2001). The high S/V ratio in a lyophobic suspension can give rise to a high overall surface free energy, eventually leading to particle aggregation and fusion, as determined by the Lifshitz-Slyozov-Wagner (LSW) theory (Dagtepe & Chikan, 2010; Lifshitz & Slyozov, 1961; Marqusee & Ross, 1984; Ratke & Voorhees, 2002; Talapin et al., 2001). In theory, given enough time, all particles of like materials will eventually form one large particle containing the entire mass of the sample. Although, repulsive forces help resist this tendency for all particles to completely fuse. Therefore, the stability of the LPs is determined by the trade-off between electrostatic repulsive forces and surface free energy. The lignin particles formed below  $C_0$  will be highly unstable and quickly aggregate and fuse upon collisions with nearby larger particles (see Figure 4-10). This process enhances the overall thermodynamic stability of the suspension, where the surface free energy is more favorable for larger particles (Ratke & Voorhees, 2002; Ribeiro et al., 2005).

A kinetic reasoning for larger particle size can also be proposed following the previously described mechanism proposed by La Mer et al. (Lamer & Dinegar, 1950). As the lignin concentration drops below  $C_0$ , the supersaturation condition is reduced as well. Thus, the amount of lignin that is involved in nucleation is much less given that the nucleation rate is mostly dependent on the degree of supersaturation (Destrée & B.Nagy, 2006; Saad & Prud'Homme, 2016; Thanh et al., 2014). Therefore, growth or nucleation is favored. Although this may contribute to an overall larger particle size, the TEM images suggest interparticle attraction and particle fusion are the dominating factors driving the sudden gain in apparent particle diameter measured by DLS (see Figure 4-10).

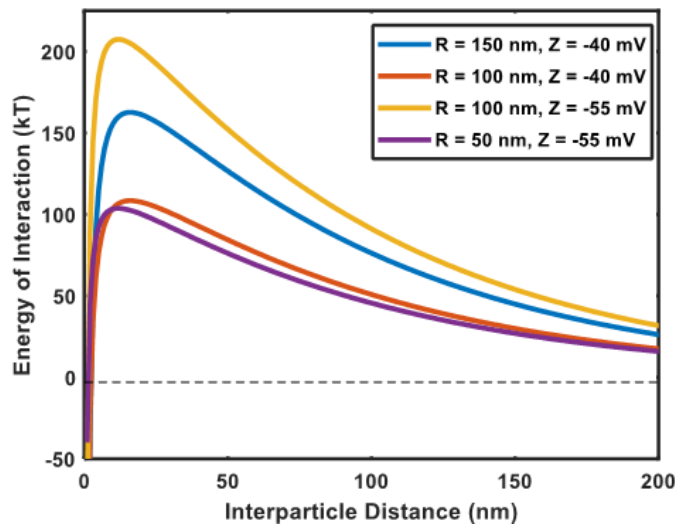


Figure 4-11. Energy of interactions between lignin particles following DLVO model including electrostatic and Van der Waals interactions. Input parameters are shown in the figure legend.

Hamaker constant =  $1.7 \times 10^{21}$  J, Ionic strength = 0.001 M,  $\epsilon = 78.5$ ,  $\kappa^{-1} = 10$  nm.

The proposed LP aggregation/fusion mechanism at low lignin concentration would also explain why the more hydrophobic particles (T-LP, TAE-LPs) have a higher  $C_0$  than the other more hydrophilic particles (see Table 4-3). The more hydrophilic particles will likely have a

lower surface free energy due to the increased content of hydroxyl groups present on the surface of the particles (Table 4-2). Interestingly, A-LPs did not exhibit a significant increase in particle size from a reduction of lignin concentration while the more hydrophilic E-LPs exhibited extensive particle size increases (~150%). This could be the result of the E-LPs “soft” particle morphology due to particle swelling, where there is a lack of a discrete repulsive electrostatic double layer (Leskinen et al., 2017a). The A-LPs exhibited the best overall particle characteristics with respect to small size, morphology, stability and homogeneity, derived from the ability to form a discrete, compact hydrophobic core while still containing enough hydrophilic groups to minimize surface energy.

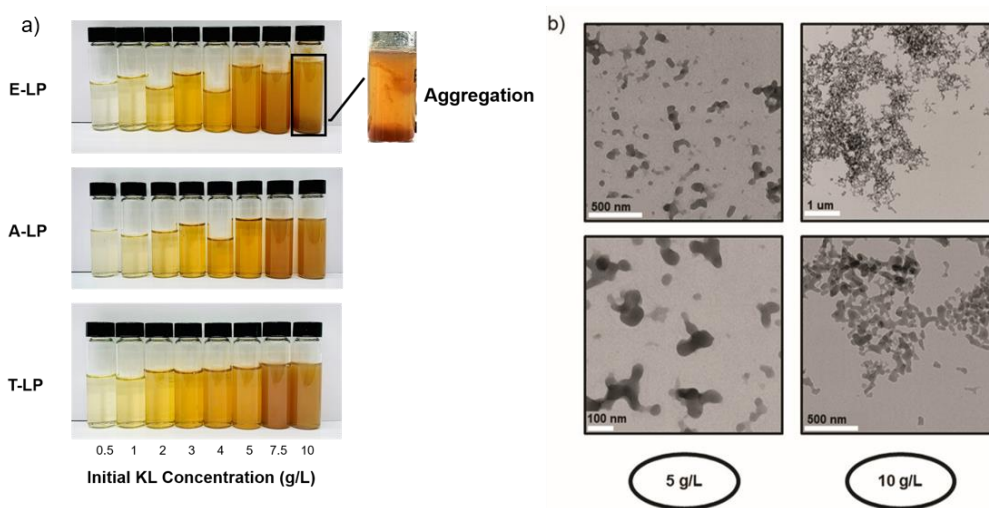


Figure 4-12. a) Lignin particle suspensions with increasing precursor lignin concentration for each of the separated fractions. All suspensions seemed visibly well-dispersed with the exception of E-LPs at 7.5 and 10 g/L where sedimentation and flocculation are visible. b) TEM images of E-LPs at an initial lignin concentration of 5 g/L and 10 g/L in solution prior to antisolvent addition.

It appears that the LPs are well dispersed at higher concentrations for samples including T-LPs and A-LPs but aggregate to the point of visible sedimentation at initial lignin concentrations above 5 g/L for E-LPs (see Figure 4-12a). The extensive aggregation was also

observed by TEM imaging (Figure 4-12b). As already mentioned, as the content of hydrophilic groups present in the lignin fraction is higher, such that as the case for E-LPs, possible particle swelling could lead to the formation of soft, metastable particles (X. Jiang et al., 2017; Ma et al., 2020). This metastability could stem from the reduction of the hydrophobic forces necessary for complete particle phase separation and stability. As the concentration becomes greater, the interparticle distances will decrease significantly, where the metastability can lead to aggregation. Conversely, the LPs with a more hydrophobic behavior remain stable at higher lignin concentrations.

#### **4.5 Conclusions**

Synthesis of lignin particles via nanoprecipitation has improved significantly in the past years with respect to the spherical morphology, homogeneity, and colloidal stability. The results shown in this work suggest more is to be understood about the effects of chemical composition, MW, particle aggregation/fusion propensity, and metastability of LPs.

It was determined that water-miscible organic solvents can be used to effectively fractionate KL into three distinct fractions, each with a unique set of chemical and physical properties. Each of the separate lignin fractions contained roughly 30% of the total KL sample, resulting in an even distribution of the starting KL molecules. It was determined that as the polarity of the solvent increases, the soluble lignin fraction is more hydrophilic. The hydrophilic character of the lignin fraction used likely attributes to particle swelling with water and colloidal metastability. Increased hydrophobicity of lignin also exhibited higher degrees of aggregation of individual particles. Additionally, a mechanism was proposed relating to particle aggregation/fusion and metastability of LPs at low precursor lignin concentrations (< 3 g/L).

These results enable a deeper understanding of the factors contributing to lignin particle synthesis via a solvent shifting method, further elucidating the effect of solvent-lignin-antisolvent interactions, and lignin concentration. With regards to the application or scale-up of colloidal lignin particle synthesis, the effects of organic solvents may become significant with respect to green chemistry principles, cost, particle stability, and biocompatibility. It was concluded that the particle formed from A-Frac is most likely the best option from the solvents studied for the solvent shifting process, when homogeneity, small size, and morphology are of interest. This is due to the favorable equilibrium between the hydrophobicity and hydrophilicity of the lignin fraction leading to a relatively low surface free energy but also a compact hydrophobic core when transformed into a spherical nanoparticle. Additionally, when considering green chemistry principles, acetone will allow for a lower energy demand during solvent removal compared to ethanol, as well as lower toxicity and hazards typically associated with THF.

## 5 ANTISOLVENT PRECIPITATION OF SURFACTANT-FREE ISOEUGENOL LIGNIN NANOCOMPLEXES FOR ANTIMICROBIAL APPLICATIONS

### 5.1 Abstract

Development of active antimicrobial food packaging to prevent foodborne disease and improve the shelf life of food products has become increasingly popular. A greater awareness in the importance of such packaging has emerged due to the COVID-19 pandemic. Technologies that enable active packaging solutions are commonly associated with a unique set of challenges such as achieving low toxicity, low cost, recyclability, and antimicrobial efficacy. Creating a safe and effective biobased alternative to synthetically derived active packaging solutions may remedy such challenges. Herein, we report a method to fabricate a completely biobased antimicrobial suspension of submicron particles comprised of an essential oil component, isoeugenol, and lignin. These lignin nanocomplexes (LNCs) were determined to have double the antimicrobial activity against *Salmonella Typhimurium* and *Listeria innocua* compared to isoeugenol alone. The gain in antimicrobial activity was determined to be due to the improved stability, sustained release, decreased vapor pressure, and smaller droplet size of isoeugenol. We also proposed that this colloidal system is the result of the unique case of “trapped species in a droplet” emulsion, where lignin acts as a ripening inhibitor to isoeugenol droplets. This allows for enhanced stability and bioavailability at a high oil/biopolymer ratio, without the need of traditional surfactants.

### 5.2 Introduction

Active packaging is a growing field in academic research and industry that is focused on developing a new generation of materials to transport, store, protect and preserve our commercial

and consumer products. This new generation of materials extend beyond the traditional barrier properties of standard packaging products and actively changes the products' environment to achieve a specific outcome (Biji et al., 2015). The outcomes that may be achieved through active packaging solutions including gas barriers, antimicrobial activity, water vapor permeability, and radical scavenging, among others, have been extensively reviewed elsewhere (Bastarrachea et al., 2015; Biji et al., 2015; C. B. Contreras et al., 2018; Fuciños et al., 2016; Halonen et al., 2020; Lim, 2019; Yildirim et al., 2018). The current massive global effort to encourage bio-based, recyclable and/or compostable alternatives to petroleum products creates an opportunity to exploit nature's offerings as greener alternatives.

Lignin, a biopolymer present in nearly all plant life, has been under investigation for its chemical structure, modification and potential applications for many decades and could be a viable contributor to utilizing biobased compounds. However, lignin has been associated with several challenges in its commercialization efforts. These challenges are mainly associated with the polydispersity and water insolubility of lignins. Most of the available lignin exists in a heavily modified and degraded form as a byproduct of the kraft pulping of biomass, namely kraft lignin (KL). During kraft pulping, the native lignin is subject to highly alkaline conditions that cleave many chemical bonds such as the  $\beta$ -O-4 ether linkage, resulting in smaller polymer units with greater polydispersity and a high phenolic hydroxyl content (X. Jiang et al., 2017; Zwilling et al., 2021). The phenolic content of lignin is the major functional group that has been targeted for exploitation in applications such as emulsifiers, UV absorbers, resin precursors, antioxidants, and in some cases antimicrobials (X. Jiang et al., 2018b; Lam et al., 2014; Qian, Qiu, Zhong, et al., 2015; Sipponen et al., 2017; Tian et al., 2017; Wei et al., 2012). However, KL often requires significant modification for its effectiveness in the mentioned applications.

One of the more studied and simple modifications to KL is the transformation to spherical nanoparticles (LNPs). Transforming lignin into nanoparticles allows the polymer to be stably dispersed in aqueous media while maintaining a high surface area-to-volume ratio. Unmodified LNPs have shown to be effective in various applications such as sunblock additives and UV-absorbers in polymer composites, but the more impressive applications are those that utilize LNPs as nanocarriers and as a Pickering emulsion stabilizer (Ago et al., 2016; N. Chen et al., 2016; Figueiredo et al., 2018; Iravani, 2020; Lizundia et al., 2021; Österberg et al., 2020; Peng et al., 2020; Sipponen et al., 2019, 2020; Q. Tang et al., 2020; W. Zhao et al., 2016b) .

Another plant-based material, essential oils, are organic compounds that possess a set of unique and potent properties. These plant extracts can be composed of several compounds, many of which are polyphenols, aromatic and aliphatic hydrocarbons, and carbonyl-containing small molecules. Essential oils have been used for centuries in applications of holistic medicine, antimicrobial agents, analgesics, antioxidants, perfumes, among others. As mentioned, many essential oil components have been associated with antimicrobial effects, but some of the more notable molecules are eugenol and its isomer, isoeugenol (Figure 5-1) (Calo et al., 2015; Das, Horváth, Šafranko, Jokić, Széchenyi, & Koszegi, 2019; Froiio et al., 2019; Guimarães et al., 2019; Hyltdgaard et al., 2015; Ju et al., 2019; Krogsgård Nielsen et al., 2016; Marchese et al., 2017; Maurya et al., 2021; Pattnaik et al., 1997).

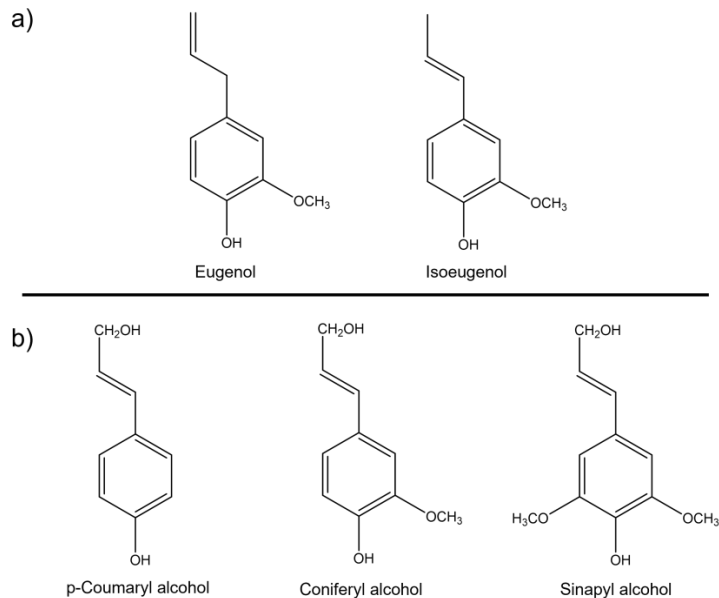


Figure 5-1. Molecular structure of a) eugenol and isoeugenol, and b) monomeric building blocks of lignin.

These phenolic compounds have very similar chemical structures to that of the building blocks of lignin during biosynthesis, especially when compared to coniferyl alcohol (G-Unit), which is the major monomer for softwood lignin. Between the two isomers, eugenol (E) is used much more frequently than isoeugenol (IE) in industry, notably for its widespread historic use in dental cements. However, isoeugenol has been gaining more attention for its greater efficacy as an antimicrobial agent (Hyldgaard et al., 2015; Krogsgård Nielsen et al., 2016).

Herein, a simple process to incorporate antimicrobial essential oil components with lignin nanoparticles (LNPs) through a one-step nanoprecipitation method to produce lignin nanocomplexes (LNCs) is presented. The nanoprecipitation method has been shown to be an effective, low-energy fabrication method for polymeric materials such as lignin and can be used in concert with other hydrophobic small molecules utilizing the “Ouzo effect” (Ganachaud & Katz, 2005; Groves, 1978; Lepeltier et al., 2014b; Vitale & Katz, 2003). The stability, release

rate, and antibacterial activity of the isoeugenol is greatly improved with the inclusion of lignin into the matrix. It is proposed that the mechanism of particle formation and morphology is rather complex and can be further understood through lignin fractionation, isolating specific chemical and physical characteristics of the polymer that translate to LNC properties. It will be suggested that the most probable particle model is that of a trapped species in a droplet model, where lignin is dissolved in isoeugenol droplets at the submicron scale. This presents a several novel notions in colloid research related to biopolymers in that lignin can stabilize partially water-soluble hydrophobic compounds from within the particle by acting as a ripening inhibitor. This proposed mechanism has its advantages over traditional encapsulation methods such as high oil-to-lignin ratios, increased release rates, and enhanced surface exposure of the hydrophobic compound.

### **5.3 Materials and Methods**

#### **5.3.1 Materials**

Two microbial strains, *Salmonella enterica* serotype Typhimurium MHM 124 (ATCC 14208) and *Listeria innocua* (ATCC 51742), were received as freeze-dried samples from the American Type Culture Collection (ATCC). Mueller-Hinton broth (MHB), Trypticase soy broth (TSB) and trypticase soy agar (TSA) were used for overnight cultures (Fisher Scientific, Waltham, MA, USA).

Pine softwood kraft lignin (KL) extracted from black liquor via the LignoBoost method was used for all experiments. KL was acquired as an air-dried powder, and the residual moisture was removed by vacuum oven drying for at least 24 hours prior to sampling. The chemical composition of this lignin was fully characterized in previous work (X. Jiang et al., 2017).

Acetone and ethanol were acquired from Fisher Scientific (Waltham, MA, USA). Isoeugenol

(98%, mixture of cis and trans) was acquired from Sigma Aldrich (Burlington, MA, USA).

Southern unbleached softwood kraft wood pulp was acquired from a paper mill in the Southeast United States and used for the fabrication of paper samples.

### **5.3.2 Solvent fractionation of kraft lignin**

KL was separated into four fractions by solvent fractionation. One gram of KL was dissolved in 40 ml of pure ethanol or acetone and mixed for 3 hours. Each solution was centrifuged to remove insoluble lignin. The soluble lignin in the supernatant was removed and the insoluble portion was dried at 65°C overnight. A small amount of water was added to the supernatant from the pure acetone/lignin solution to a final acetone concentration of 90% v/v. The dried insoluble lignin was then dissolved in 90% v/v acetone/water (A90). The supernatant from the ethanol/lignin solution was evaporated by rotary evaporation and redissolved in A90. The process diagram and fraction labeling can be found in the Supplemental information.

The molecular weight distribution of each KL fraction was determined by gel-permeation chromatography (GPC). All lignin samples were acetylated prior to analysis with pyridine and acetic anhydride (1:1) for 48 hours at room temperature to improve solubility in the mobile phase tetrahydrofuran (THF) (Glasser et al., 1993b; Zwilling et al., 2021). The analysis was performed using an Agilent GPC instrument equipped with a UV detector (set at 280 nm) using THF as the eluent at a flow rate of 0.7 ml/min at 30 °C. A sample concentration of 1 mg/ml and an injection volume of 50 µl was used. Two ultra Styragel linear columns linked in series (Styragel HR 1 7.8 × 300 mm and Styragel HR 4E 7.8 × 300 mm) were used for separation. A series of monodispersed polystyrene standards were used as calibration standards (X. Jiang et al., 2017).

### 5.3.3 Essential oil loaded lignin nanocomplex synthesis

KL was dissolved in A90 for 30 minutes and then centrifuged to remove insoluble components. The insoluble mass was less than 1%. Two milliliters of the KL solution (5 mg/ml) and 50  $\mu$ l of pure isoeugenol were transferred to 20 mL glass vials. The mixture was magnetically stirred at 1000 rpm and 5 ml of MilliQ water was rapidly injected into the solution. The residual acetone in the suspension was removed via rotary evaporation at 35°C. For comparison, IE was dissolved in A90 to form IE nanodroplets (IDs) in the same way, but in the absence of KL.

### 5.3.4 Particle Size Distribution

The particle size distribution (PSD) was measured by dynamic light scattering (DLS) using a Zetasizer Nano ZS (Malvern). The average particle diameter (MPD) is reported as the intensity-weighted Z-average particle diameter.

### 5.3.5 Stability

The stability of the suspensions was determined by measuring the optical density (OD) of the suspension (600 nm wavelength) using a BioTek 96-well plate reader. The suspensions were diluted to a concentration of 5.12 mg/ml in NaCl aqueous solutions of varying concentrations (1.2 mM – 1.2 M NaCl). The OD reduction was also tracked in MilliQ water at elevated temperatures (37°C). The relative absorbance (RA) was calculated by Eq. 1.

$$RA = \frac{OD \text{ after 12 hours}}{Initial OD} \quad (1)$$

### 5.3.6 Isoeugenol release profile

Two milliliters of ID and LNC suspensions were transferred to dialysis tubing (3-4 kDa MWCO) separately and placed in a closed glass jar with 98 ml of MilliQ water or phosphate

buffer solution (pH 7.4). One milliliter of the filtrate was removed and the mass of the isoeugenol in the aliquot was determined by UV absorption at 260 nm. The volume removed was replaced thereafter. The calibration curve of absorbance versus isoeugenol concentration can be seen in the supplemental information. The cumulative release was calculated by Eq. 2-4 (Corsaro et al., 2021; Ravindran Chandrasekaran et al., n.d.).

$$M_t = \text{Measured Concentration} * \text{Total Volume} * \text{Dilution factor} \quad (2)$$

$$P_t = \frac{M_t}{M_i} \quad (3)$$

$$R(t) = V_{aliq} * P_{t-1} + P_t \quad (4)$$

In Eqs. 2-4,  $M_t$  is the total mass of isoeugenol in the solution at time  $t$ ,  $M_i$  is the initial isoeugenol mass in the dialysis tubing at  $t = 0$ ,  $P_t$  is the percentage of isoeugenol diffused through the dialysis tubing,  $R(t)$  is the cumulative release of isoeugenol,  $V_{aliq}$  is the aliquot volume withdrawn from the dialysis solution.

The release data was fitted with a Weibull release kinetics model for a more descriptive analysis for the release of isoeugenol (Eq. 5).

$$R(t) = R_{\infty} \left( 1 - e^{-\left(\frac{t}{\tau}\right)^{\beta}} \right) \quad (5)$$

In Eq. 5,  $R_{\infty}$  is the asymptotic maximum of isoeugenol released,  $\tau$  is the scale factor in units of hours, and  $\beta$  is the shape factor. The data was fitted in using a non-linear regression tool (JMP pro 16.1).

The solubility of isoeugenol was determined by adding an excess (10 ml) of isoeugenol to 90 ml of MilliQ water. The solution was wrapped in aluminum foil and magnetically stirred at 20°C for 48 hours. The concentration was determined by UV spectroscopy.

### 5.3.7 Antibacterial activity

*Salmonella* Typhimurium was grown in Mueller-Hinton broth (MHB). Typically, MHB is the suggested media for antibacterial assays, but it was determined in preliminary work that *L. innocua* required a more nutrient-rich media for overnight growth studies. Therefore, *L. innocua* was grown in Trypticase soy broth media (TSB). Culture plates were made from trypticase soy agar (TSA) with the addition of 2.5 mg/ml of dextrose. All broth and agar solutions were autoclaved at 121°C for 60 min. A solution of dextrose was autoclaved separately then added to the agar solution after sterilization to avoid Maillard reaction byproducts (Helou et al., 2014).

Each bacterial strain was cultured overnight in its appropriate media at 37°C. The overnight culture was then transferred to sterile 3 ml vials and frozen overnight at -80°C. The frozen culture was scraped with an inoculation loop, and T-streaked on the TSA plates, then incubated at 37°C overnight. The colonies from the overnight plates were stored at 4°C and a single colony was transferred to a sterile conical tube containing 20 ml of TSB and homogenized using vortex mixing. The inoculated media was incubated at 37°C for 12 hours and used for further testing.

The MIC was determined using the microdilution 96-well plate assay using standard methods (Balouiri et al., 2016). Briefly, either ID or LNC suspensions were diluted with appropriate bacterial media to an IE concentration of either 5120 µg/ml or 3840 µg/ml, followed by nine, 2-fold dilutions. Ten microliters of each bacterial culture, with a predetermined concentration of  $2 \times 10^6$  CFU/ml was added to each well. The final volume in each well was 100 µl. The OD at 600 nm was measured every ten minutes for 18 hours using a Biotek plate reader. The MBC was determined by transferring 100 µl from the MIC well and the adjacent wells then

plated on TSA plates. The plates were incubated for 48 hours. No dilution was necessary as a 3-fold reduction (-99.9%) of bacterial populations was targeted.

### **5.3.8 Transmission electron microscopy of Bacteria**

An overnight culture of each bacterial strain in TSB was diluted to a concentration of  $2 \times 10^6$  CFU in 10 ml of TSB along with the LNC suspension at a concentration of 1000 ppm. The conical flask was vortex mixed for 1 hour, and the mixture was centrifuged at 4700 rpm for 30 minutes. The resulting pellet was washed three times with sterile DI water and centrifuged to remove any excess broth.

The samples were then fixed overnight in modified Karnovsky's fixative consisting of a mixture of 4% paraformaldehyde and 1% glutaraldehyde, buffered with 0.1 M sodium cacodylate (pH 7.2). After three-10 min buffer washes with sodium cacodylate, the samples were post-stained with 2% osmium tetroxide for 1 hour followed by three-10 min buffer washes with sodium cacodylate. Samples were subsequently dehydrated in an increasing ethanol series. Finally, the samples were infiltrated and embedded in Epon 812 resin and polymerized in an oven at 70 °C for 24 h. Microtomy was performed on a Leica EM UC7 and sections were post-stained with saturated aqueous uranyl acetate for 20 min followed by lead citrate for 5 min. The sections were imaged using a Hitachi 7800 TEM.

### **5.3.9 Antibacterial activity on surfaces**

Paper handsheets were fabricated following the TAPPI standard methods (TAPPI T205 sp-02, 2006) from unbleached southern softwood kraft pulp at a basis weight of 120 g/m<sup>2</sup> and pressed to simulate linerboard for food packaging. The handsheets were cut into 2 cm x 2 cm square pieces and autoclaved at 121°C for 45 minutes. Each paper sample was placed into a

sterile petri dish and 100  $\mu$ l of either the ID or LNC suspension was transferred to the paper. The final isoeugenol concentration on a dry basis was 2.25% w/w. The paper samples were allowed to dry for 24 hours at ambient conditions. The paper was then inoculated with  $10^6$  CFU of *L. innocua* and *S. Typhimurium* in TSB. The samples were allowed to dry in ambient conditions overnight.

After 16 hours, the paper samples were re-wetted with 100  $\mu$ l of sterile DI water. The paper was then gently pressed with the researcher's thumb inside a sterile glove. The thumb was then stamped onto an agar plate (TSA). The agar plate was incubated at 37°C for 48 hours.

## **5.4 Results**

### **5.4.1 Particle Characteristics**

#### **5.4.1.1 Nanoprecipitation of Isoeugenol and KL**

Isoeugenol is a relatively simple molecule, but it has a rather unique behavior in aqueous systems due to its amphiphilic moieties (See Figure 5-1). Isoeugenol is an oily substance with low solubility in water (0.57 g/l), and can self-assemble via spontaneous emulsification, otherwise known as the ouzo effect (Vitale & Katz, 2003). The particle size distribution (PSD) of isoeugenol nanoparticles (IDs) measured by dynamic light scattering shows a polydisperse, yet sub-micron scale droplet distribution of IE in water (Figure 5-2). The PSD and average particle size of KL nanoparticles (LNP) and the combination of KL and IE (LNC) is also depicted in Figure 5-2.

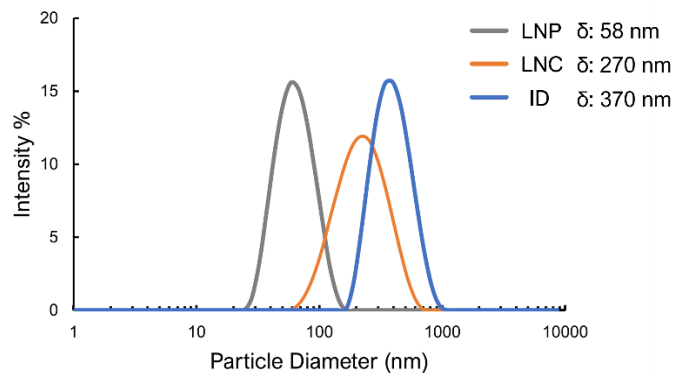


Figure 5-2. Particle size distribution as measured by dynamic light scattering and the intensity-weight Z-average particle diameter,  $\delta$ .

The average particle diameters of the suspensions from ID, LNP and both LNC were 370 nm, 58 nm, and 270 nm, respectively. All PSDs were monomodal, including LNC's, indicating a single colloidal system.

#### 5.4.1.2 Lignin fractionation effects

Due to the complexity of the lignin composition and its hydrogen bonding potential with IE and water, it was necessary to determine the formation events during nanoprecipitation. Lignin is a highly heterogeneous polymer with a broad molecular weight (MW) distribution. In previous work, we showed the chemical compositions within the fractions of high MW and low MW lignins differ greatly (X. Jiang et al., 2017; Zwilling et al., 2021). It has been well understood that the lower MW lignin fractions contain a higher hydroxyl content and is therefore more hydrophilic than its higher MW counterparts (X. Jiang et al., 2017; Ma et al., 2020; Zwilling et al., 2021). Dissolving KL in a relatively poor, polar solvent such as ethanol, can selectively separate lower MW lignin fractions, whereas better lignin solvents such as acetone and acetone/water binary solvents can dissolve higher MW KL fractions (Zwilling et al., 2021).

The solvent fractionation yields and MW distributions of each of the lignin fractions can be seen in Figure 5-3a-b.

Ethanol soluble KL (F1) had the lowest weight-average molecular weight (Mw) of 1,594 Da followed by the acetone soluble fraction (F2) of 2,786 Da. The ethanol and acetone insoluble fractions (F3, F4) had a Mw of 7,075 and 10,960 Da respectively (see Figure 5-3a). Previous work showed that low Mw lignin fractions contain a higher number of phenolic hydroxyl groups relating to a greater hydrophilicity compared to high Mw lignin (X. Jiang et al., 2017; Ma et al., 2020; Pang et al., 2020b; Zwilling et al., 2021).

The fractionated and unfractionated lignins were used to nanoprecipitate the LNCs with IE. The precipitation points of each of the lignin fractions and IE separately was determined by water titration (Figure 5-3c).

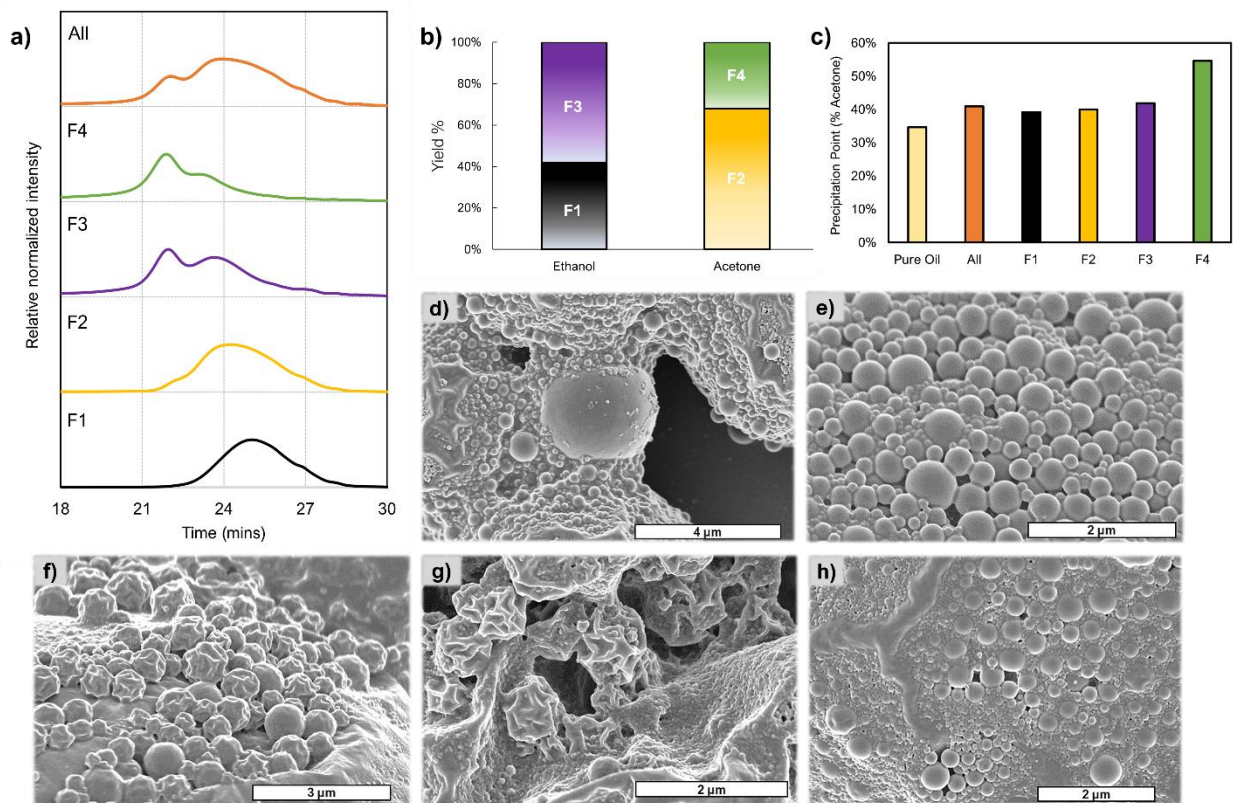


Figure 5-3. Kraft lignin, isoeugenol, and LNC characteristics including a) GPC chromatogram of each of the lignin fractions and the starting lignin material, b) the yield of each lignin fraction separated by solvent fractionation relative to the unfractionated kraft lignin, b) the precipitation point of each the neat constituents, c) SEM images of d) LNCs formed from the F1 lignin fraction, e) LNCs formed from the F2 lignin fraction, f) LNCs formed from the F3 lignin fraction, g) LNCs formed from the F4 lignin fraction, h) LNCs formed from the unfractionated kraft lignin sample. The precipitation point was performed in triplicate with no significant standard deviation.

The precipitation point of lower MW lignin fractions was lower than higher MW lignin fractions, which agrees with the greater hydrophilic character. IE had the lowest precipitation point (35% v/v). These results suggests that lignin is more hydrophobic than isoeugenol and lignin will precipitate shortly before isoeugenol. However, it should be noted that during the formation of LNCs, water is rapidly added to the acetone solution under high mixing conditions.

Therefore, the differences in precipitation point likely contribute to the formation mechanism of LNCs in a very minor way.

The morphologies of the LNCs formed from different lignin fractions was characterized by SEM imaging. The samples were drop casted onto carbon tape and allowed to dry in a vacuum oven at 35°C. During the drying process, the water is removed along with the majority of IE, especially when exposed to the high vacuum during SEM imaging ( $< 5 \times 10^{-6}$  torr). This is much lower than the vapor pressure of IE ( $1.35 \times 10^{-2}$  torr (Stull, 1947)). Nevertheless, the residual particles under vacuum show considerable difference with respect to the MW of lignin (Figure 5-3d-h). More specifically, the LNCs formed from low MW lignins (F1, F2) show smooth surfaces with film-like bridging between particles, indicative of residual or bound IE (Figure 5-3d-e). LNCs formed from high MW lignins (F3, F4) show a polydisperse sample with smaller spheres bridged together and larger spheres with a crumpled surface structure (Figure 5-3f-g). This crumpled surface structure is formed from the capillary pressure upon drying. More specifically, larger particles with a hollow core or less compact structure will collapse due to the capillary pressure exceeding the Laplace pressure (Kämäräinen et al., 2018b; Tirumkudulu, 2018). Further explanation of the LNC formation mechanism will be described in the discussion section.

#### **5.4.1.3 Stability**

The stability of the various LNC formulations was determined by their independent methods: 1) loss of turbidity as a function of changes in the ionic strength of the media, 2) loss of turbidity as a function of time at elevated temperatures (37°C) (Figure 5-4).

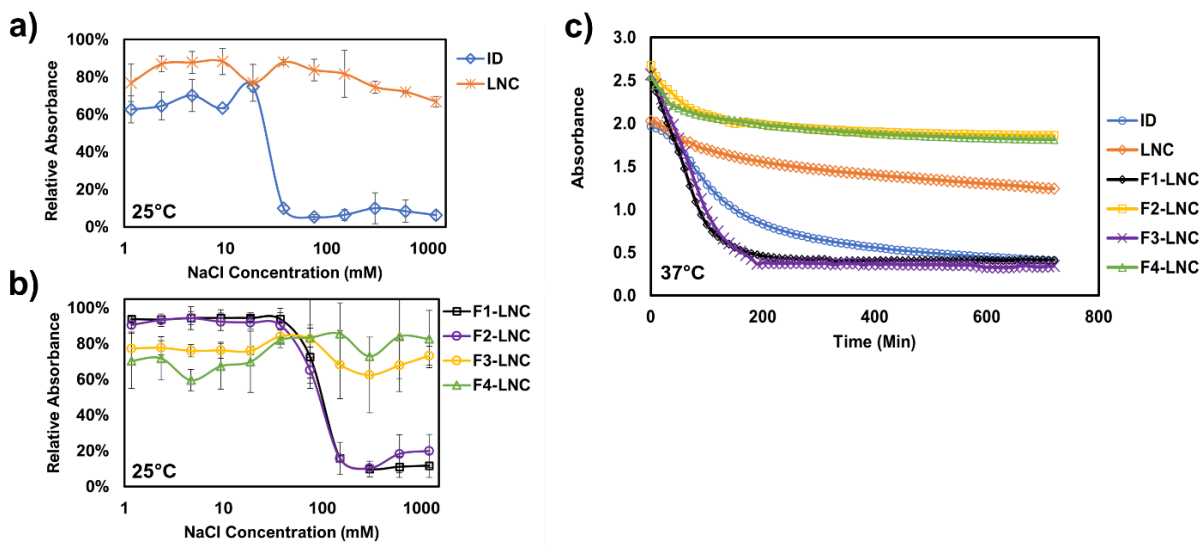


Figure 5-4. Relative stability of colloidal dispersions of isoeugenol with (LNC) and without (ID) the complexation with kraft lignin. a) Optical density reduction of the ID and LNC suspensions after 12 hours of exposure to a range of NaCl concentrations (1.2 mM to 1.2 M). b) Optical density reduction of the LNC suspensions formed from the fractionated lignins after 12 hours of exposure to varying NaCl concentrations (1.2 mM to 1.2 M). c) Optical density reduction of the ID and LNC suspensions after 12 hours of exposure to elevated temperatures (37°C) in MilliQ water.

In Figure 5-4a, the optical density as a function of NaCl concentration of an isoeugenol suspension with and without KL after 12 hours is depicted. Firstly, the ID suspension has a 37% reduction of OD after 12 hours at low NaCl concentrations (1.2 mM), whereas the LNC suspension showed only a 24% reduction in OD. Furthermore, there is a drastic reduction in OD (-67%) at a NaCl concentration of 37.5 mM for IDs. In contrast, LNCs had a minimal OD reduction at higher NaCl concentrations.

The stability of the fractionated LNC suspensions was also examined. In Figure 5-4b, the LNCs formed with low MW KL (F1-LNC and F2-LNC) show similar behavior to IDs at increasing NaCl concentrations, whereas LNCs formed with high MW KL (F3-LNC and F4-LNC) show little changes in the OD at higher NaCl concentrations. This suggests that the LNCs

containing high MW KL remain suspended, whereas the suspensions containing no KL (IDs) or low MW KL fully destabilize at high ionic strengths.

Similarly, the reduction in OD at higher temperatures as a function of time is greatest for suspensions containing no KL or low MW KL (Figure 5-4c). The LNCs containing all KL fractions (LNC) has a reduction of OD less than that of low MW LNCs but greater than high MW LNCs. These results suggest the final suspension is comprised of droplets containing either low MW KL or high MW KL, indicating a highly complex, yet intelligent self-assembly. To summarize, isoeugenol can be stabilized by the addition of KL during precipitation, especially with high MW KL fractions.

#### **5.4.1.4 Isoeugenol release kinetics**

The release of isoeugenol from LNCs in solution state by dialysis in MilliQ water or a phosphate buffer solution (PBS) was measured by UV absorption of isoeugenol over time. The release profiles are provided by Figure 5-5.

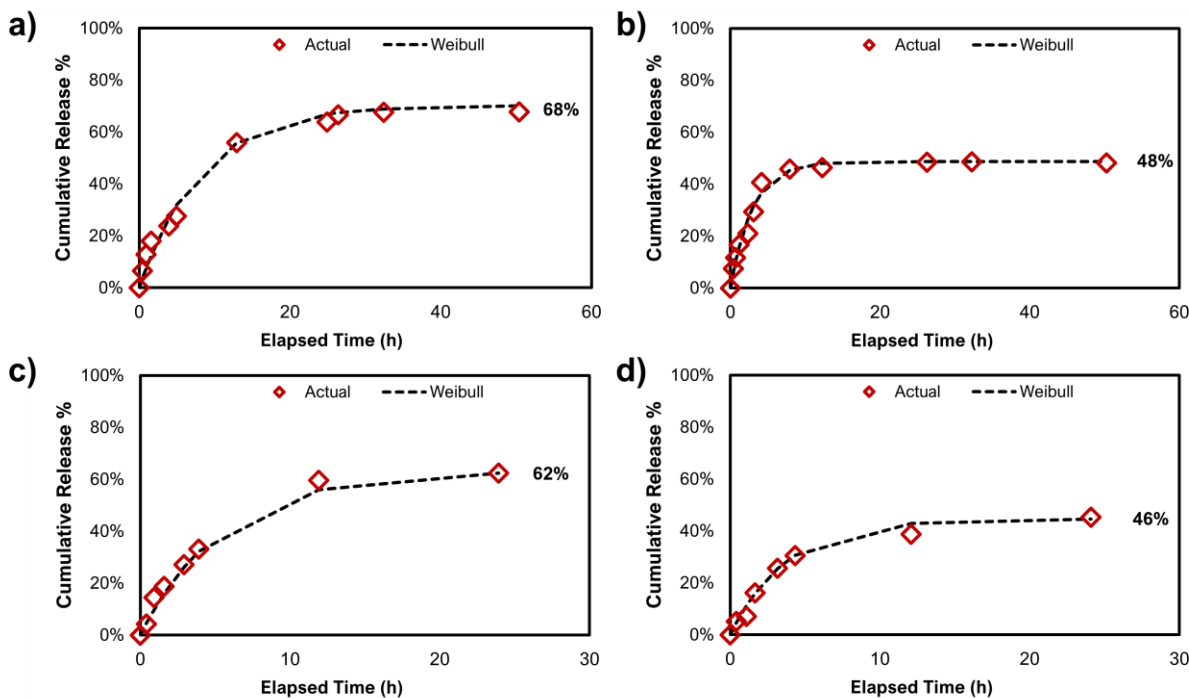


Figure 5-5. Release profile of unfractionated LNCs and IDs reported as cumulative release as a function of time and the fitted Weibull release kinetic model. a) Release profile for LNCs dialyzed with MilliQ water. b) Release profile for IDs dialyzed with MilliQ water. c) Release profile for LNCs dialyzed with phosphate buffer solution. d) Release profile for IDs dialyzed with phosphate buffer solution. This experiment was performed in duplicate and the standard deviation for each sample and time was less than 1%.

The pH of the dialysis solutions was measured after 24 hours for each of the samples in their respective media. The release of IDs and LNCs both resulted in a pH of 5.80 for water and 7.41 for PBS. This was expected due to the similar chemistry between IE and KL and the buffering nature of PBS. The release of IE was enhanced by the complexation with KL, likely due to the reduced particle size and enhanced stability at high bulk surface area-to-volume ratios. The release curves in all samples had a Weibull-like shape with a high rate of release at early time points followed by a plateau at  $t \sim 12$  hours (Figure 5-5). The plateau was more gradual in PBS than in MilliQ water likely due to the increase in the osmotic pressure in the outer solution.

The data was fitted to a Weibull release kinetic model described in the experimental section and the resulting parameters are listed in Table 5-1.

Table 5-1. Parameters and goodness of fit for the Weibull release kinetic model.  $R_{\infty}$  is the asymptotic maximum cumulative release,  $\tau$  is the scale factor,  $\beta$  is the shape factor, and  $R^2$  is the coefficient of determination.

Compound	Medium	$R_{\infty}$ (Max %)	$\tau$ (hrs)	$\beta$	$R^2$
LNC	Water	70%	6.91	0.84	0.988
	PBS	63%	5.17	0.94	0.994
ID	Water	49%	2.94	0.99	0.984
	PBS	45%	3.81	1.02	0.987

The Weibull model has a high correlation with each of the samples ( $R^2 > 0.98$ ). The maximum IE release for LNC was 21% higher than IDs in water and 18% higher in PBS. The characteristic scale factor,  $\tau$ , for LNC was more than double that of IDs in water and 1.36 hrs longer in PBS. The scale factor describes the time point at which 63.2% of the compound would have been released ( $t = \tau$ ). Therefore, the majority of IE with potential to be released is diffused from IDs in a much shorter time than from LNCs. Moreover, the higher scale factor of LNCs is representative of the stability gain. The shape factor,  $\beta$ , is the slope of the curve and can give information of the diffusion mechanism and particle behavior in the medium. Specifically, values of  $\beta$  between 0.75 and 1 are representative of both Fickian diffusion and case II transport (Papadopoulou et al., 2006). This suggest that all samples involved some degree of particle swelling, especially at higher pH's (PBS). The degree of swelling and diffusion was mitigated by the inclusion of KL. This is reasonable considering the partial solubility of IE in water.

## 5.4.2 Antimicrobial activity of LNCs

### 5.4.2.1 Microdilution plate assay

Foodborne bacterial pathogens account for nearly 3.6 million illnesses annually and make up 64% of the total foodborne pathogen related deaths in the U.S. (Scallan et al., 2011). More specifically, the CDC listed *Salmonella spp.*, *Listeria monocytogenes*, and *E. coli* as the most prominent bacteria to cause multistate foodborne illness outbreaks in the U.S. (*List of Selected Multistate Foodborne Outbreak Investigations / Foodborne Outbreaks / Food Safety / CDC*, n.d.). The USDA actively estimates the total annual cost of the most common foodborne pathogens and bacterial pathogens alone account for nearly 12 billion USD (*USDA ERS - Cost Estimates of Foodborne Illnesses*, n.d.). Thus, *Salmonella enterica* Typhimurium and *Listeria innocua* were chosen as foodborne pathogen model organisms for this work. The antibacterial activity of the ID suspension and LNC suspension were determined through microdilution assays, surface extraction, and TEM image analysis. The minimum inhibitory concentration (MIC) defined as the lowest concentration of the compound that prevents visible bacterial growth was determined by the microdilution assay through visual interpretation as well as by OD measurements (See Figure 5-6a-d). The minimum bactericidal concentration (MBC) defined as the lowest concentration of the antibacterial causing 99.9% of the bacteria to be killed is also reported (See Figure 5-6a-d).

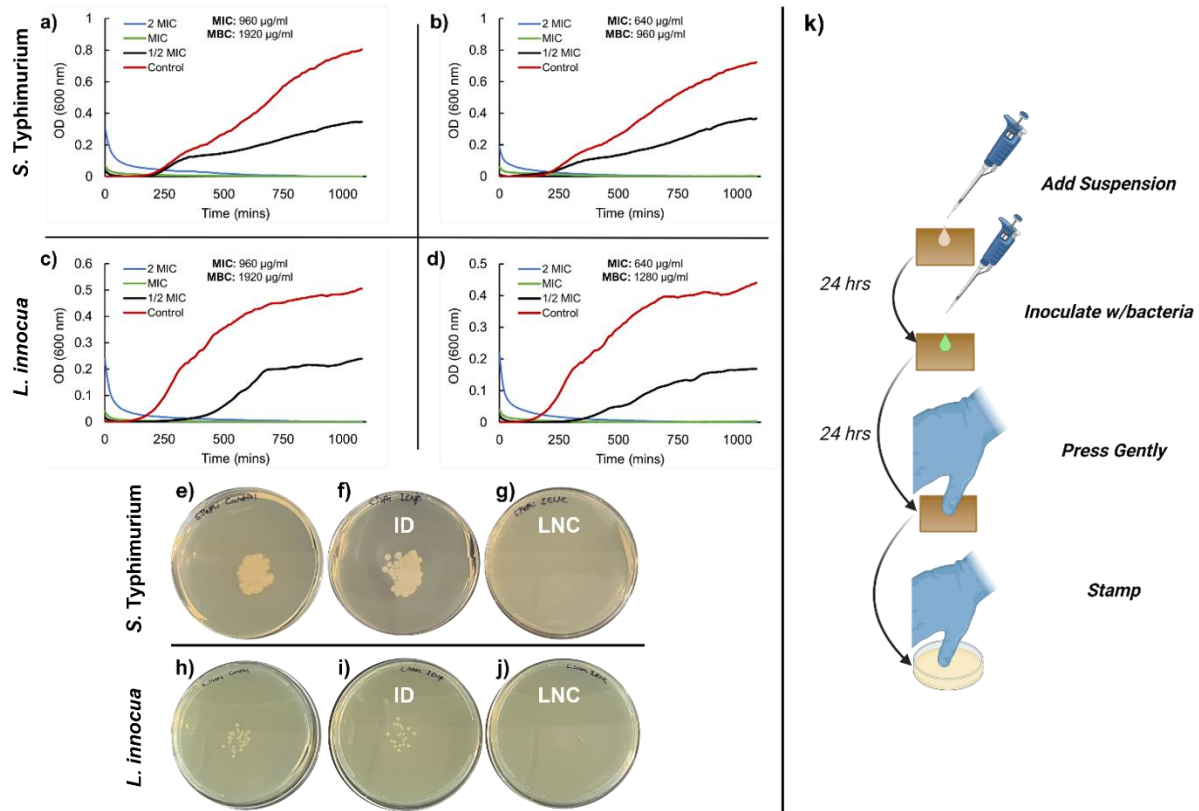


Figure 5-6. Antibacterial activity of the LNCs and IDs. a) Growth curves of *S. Typhimurium* exposed to varying concentration of IDs measured by optical density as a function of time. b) Growth curves of *S. Typhimurium* exposed to varying concentration of LNCs measured by optical density as a function of time. c) Growth curves of *L. innocua* exposed to varying concentration of IDs measured by optical density as a function of time. d) Growth curves of *L. innocua* exposed to varying concentration of LNCs measured by optical density as a function of time. e-g) Transfer of viable *S. Typhimurium* from untreated paper (e), paper treated with IDs (f), and paper treated with LNCs (g) to a human hand. h-j) Transfer of viable *L. innocua* from untreated paper (e), paper treated with IDs (f), and paper treated with LNCs (g) to a human hand. k) Schematic of the transferability of bacteria test from paper to hand.

The inclusion of KL in the IE suspensions resulted in an improvement in both the MIC, and MBC for both the Gram-positive (*L. innocua*) and Gram-negative (*S. Typhimurium*) bacteria (Figure 5-6a-d). The antibacterial activity nearly doubled in all cases. This is an additional

improvement to the initial reduction in the MIC and MBC of IE from its free form to droplet form (Supplemental). This improvement can be attributed to the smaller particle size (higher S/V) and greater stability of LNCs throughout the incubation period (Figure 5-2, Figure 5-3, Figure 5-5). This is especially important considering the incubation conditions including bacterial media containing a fairly high ionic strength (174 mM) and elevated temperatures (37°C).

For practical reasons, the antibacterial activity of the ID and LNC suspensions was investigated in a dry state on paper packaging surfaces. Additionally, the transferability of the bacteria to a human hand was simulated (Figure 5-6k). As mentioned in experimental section 5.3.9, the bacteria transfer from surface-to-hand was simulated by gently pressing the paper surface and then touching the contaminated finger to an agar plate (Figure 5-6k). The resulting agar plates after 24 hours of incubation at 37 °C are shown in Figure 5-6e-j. The paper surface containing IDs exhibited similar growth to the control sample whereas the paper coated with LNCs showed no visible growth.

#### **5.4.2.2 Antimicrobial mechanism of LNCs**

In the previous section, there seemed to be an improvement of the antibacterial activity of isoeugenol when complexed with KL. However, many studies investigating the antibacterial activity of essential oil compounds have suggested rather broad explanations of the antibacterial mechanisms. For that reason, TEM micrographs were taken of the cross section of both bacteria before and after treatment with LNCs (See Figure 5-7).

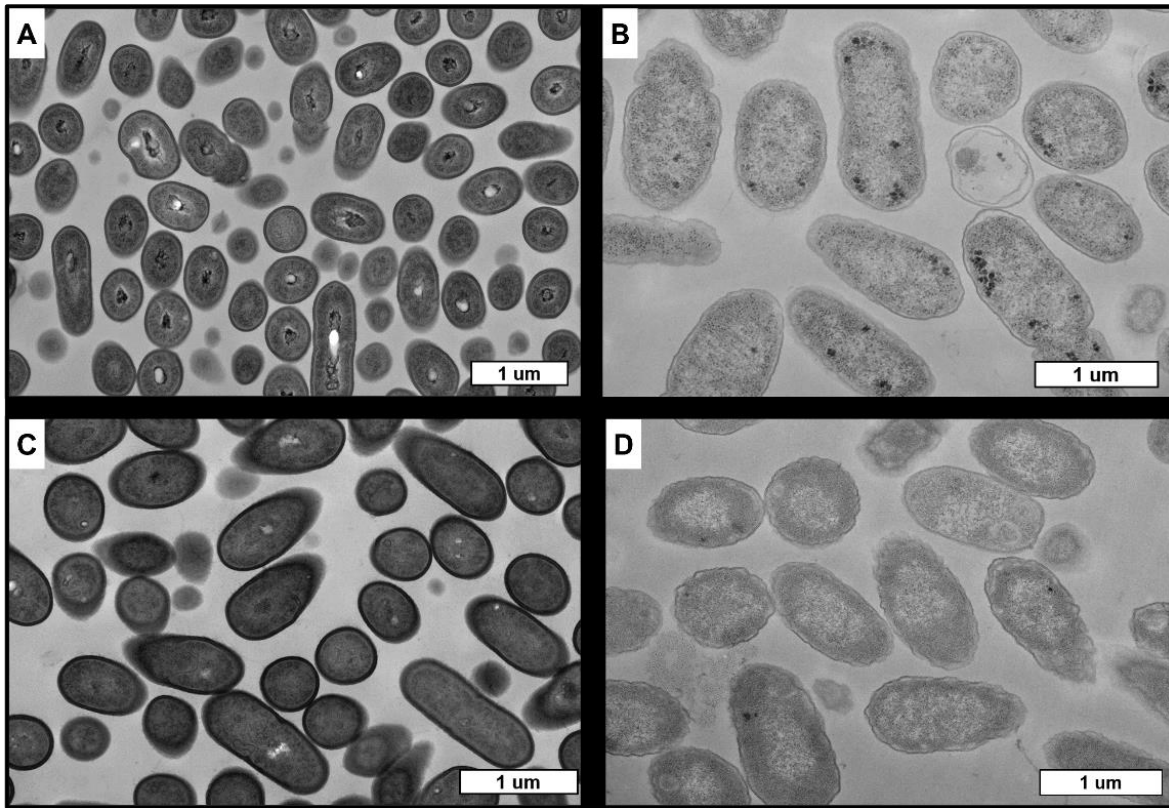


Figure 5-7. TEM images of *L. innocua* and *S. Typhimurium* untreated and treated with LNCs. A) Untreated *L. innocua*, B) untreated *S. Typhimurium*, c) treated *L. innocua*, B) treated *S. Typhimurium*.

In the untreated sample of *L. innocua*, the thick cell wall is clearly visible, which is characteristic of Gram-positive bacteria. In addition, there appears to be a very clear nucleoid contained in a defined space for the untreated *L. innocua* (see Figure 5-7a). However, upon treatment with LNCs, the cell wall and cell membrane are greatly damaged as evidenced by the fuzzy partition between the bacterial cells and the extracellular space (see Figure 5-7c). The cells also show a darkening of the interior of the cell, indicating increased dye uptake, representative of membrane permeabilization (Figure 5-7c). Furthermore, the well-defined nucleoid region is no longer present after treatment with LNCs. Mechanistically, this suggests that IE can penetrate

the cell and may take part in protein denaturation, and other damaging reactions to the nuclear material.

For *S. Typhimurium*, the untreated sample shows a thin, intact outer membrane, as well as aggregates of either inclusion bodies or ribosomes/proteins dispersed within the cytoplasm (Figure 5-7b). Upon treatment with LNCs, a fuzzy characteristic of the cell membrane appears, similar to the treatment of *L. innocua* (Figure 5-7d). Moreover, the membrane permeability is also apparent by the increased dye uptake (Figure 5-7d). The IE also seems to eliminate the presence of inclusions that are visible in the untreated sample, suggesting that IE is disrupting the stability of the inclusions (Figure 5-7d).

## 5.5 Discussion

Nanoprecipitation is a common method to quickly produce colloids by rapidly decreasing the solubility of a substance, thus forcing a phase separation. Fabricating lignin nanoparticles from this method has been done extensively in the past by using the solvent exchange method, where lignin is dissolved in a water miscible, organic solvent and quickly precipitated by the addition of an antisolvent, commonly water. The variables controlling the particle properties of lignin nanoparticles (LNPs) produced by the nanoprecipitation method has been studied elsewhere (Leskinen et al., n.d.; Österberg et al., 2020; Sipponen et al., 2018b; Zwillling et al., 2021). However, the particle formation mechanisms and characteristics upon adding hydrophobic small molecules into the precursor polymer solution prior to nanoprecipitation, had not yet been fully understood.

The Ouzo effect is a special type of nanoprecipitation that has been used to explain the formation of sub-micron, spherical particles, or droplets in water from water-miscible solvent solutions. The ouzo effect was initially discovered during the dilution of ouzo, an alcoholic

beverage containing aromatic oils, with water resulting in a cloudy appearance. More generally, the ouzo effect is the spontaneous emulsification of hydrophobic compounds from solution in the metastable regime (i.e., thermodynamically unstable but kinetically stable). This effect has been extensively studied elsewhere but is likely related to the mechanism of particle formation occurring in this research (Ganachaud & Katz, 2005; Vitale & Katz, 2003). Previous research has shown that lignin can effectively encapsulate essential oil compound, but the oil/lignin ratio must be very low ( $< 0.5$  w/w) (Alqahtani et al., 2020; N. Chen et al., 2016; Piombino et al., 2020; Sipponen et al., 2020; Zikeli et al., 2020). In this research, it was shown that the improvement of stability and antibacterial activity can be achieved at relatively high oil/lignin ratios (5 w/w). Many other works commonly add a water-soluble surfactant to the system to stabilize the capsules/emulsion (Lammari et al., 2020), whereas the LNCs are a surfactant-free system.

### **5.5.1 Trapped Species in a Droplet Hypothesis**

The partial solubility of IE yields a high propensity for Ostwald ripening to occur at small particle sizes. Ostwald ripening is the growth of dispersed particles at the expense of smaller ones driven by the thermodynamic instability. Mechanistically, small molecules on the surface of dispersed particles are redissolved into the continuous phase and diffuse to larger droplets/particles. IE was shown to be slightly more hydrophilic than KL, as evidenced by the larger amount of water necessary for a phase transition to occur (Figure 5-3c). Thus, it would be unlikely that KL would prefer the interface, such as a Pickering emulsion or encapsulation model. More likely is the case of a special type of ripening inhibitor, which has been termed *trapped species in a droplet* (TSID) (Kabalnov, 1998, 2001; Webster & Cates, 1998). The trapping of species in a droplet occurs when a dispersed phase is stabilized in a continuous phase

by the addition of a third component, typically polymeric. TSID is valid provided the following requirements are met (Kabalnov, 2001; Webster & Cates, 1998):

- 1) The oil droplet has low but finite solubility in water.
- 2) The oil/water ratio must be sufficiently low (ouzo region).
- 3) The third component (KL) must be completely immiscible with the continuous phase.
- 4) The third component must be miscible with the dispersed phase.

In the case of LNCs, all four conditions are met given that 1) IE has a solubility of 0.57 mg/mL, 2) IE is suspended at a concentration of 1% v/v, 3) KL is completely immiscible with water at room temperature and 4) KL is miscible with IE.

The TSID model can explain the release phenomena of IE depicted in such that KL enhances, rather than inhibits, the diffusion of IE by dialysis. If KL was at the interface, there would likely be a slower release mechanism as it would be limited to the porosity of the shell material. Instead, KL resides in the core of the droplet where it restricts droplet growth at early stages of particle formation by Ostwald ripening which is attributed to the increase in the osmotic pressure within the droplet. Thus, the tighter particle size distribution offers a larger surface area-to-volume ratio for diffusion to take place. One of the characteristics of TSID is the inhibition of molecular diffusion of the dispersed molecules at sufficiently low droplet sizes by offering a greater osmotic pressure to combat the high Laplace pressure at small particle sizes

Eq. 6

$$\Delta\mu = \mu_d - \mu_s = \left[ \frac{2\gamma}{R} - \frac{Nk_B T}{\frac{4\pi R^3}{3}} \right] \nu_b \quad (6)$$

In Eq. 6,  $\Delta\mu$  is the chemical potential difference between a molecule of IE remaining in particle form ( $\mu_d$ ) or dissolved in the bulk ( $\mu_s$ ),  $\gamma$  is the surface free energy of the particle,  $R$  is the particle radius,  $N$  is the number of molecules trapped in the droplet,  $k_B T$  is the thermal energy, and  $v_b$  is the molar volume. As  $R \rightarrow \infty$ , the second term diverges and  $\Delta\mu$  becomes infinitely negative (i.e., thermodynamically stable). Essentially, this second term is related to Raoult's law, where solute molecules prevent the evaporation, or in this case diffusion, of the solvent molecules (Kabalnov, 2001; Webster & Cates, 1998). Furthermore, the TSID model would agree with the particle morphologies after drying give the film-like appearance (see Figure 5-3d-h). Figure 5-8 below gives a more descriptive schematic of the particle formation events before and after drying as a function of lignin MW fractions.

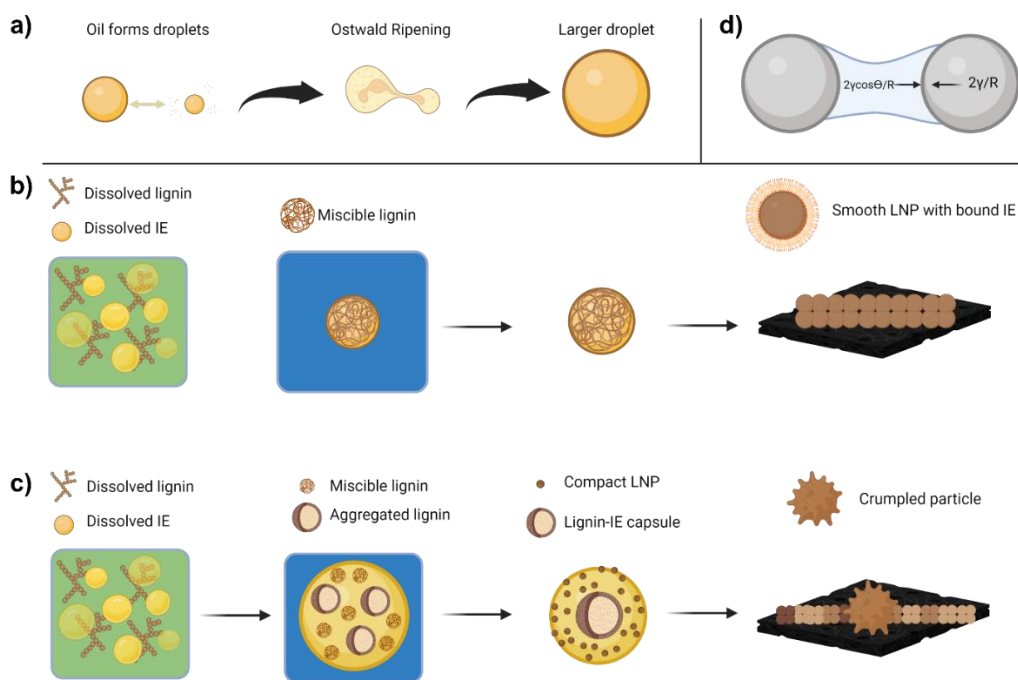


Figure 5-8. Proposed LNC formation mechanism. a) ID droplet ripening. b) Low MW lignin LNC formation and drying mechanism. c) High MW lignin LNC formation and drying mechanism. Green is acetone, blue is water, yellow is IE and brown is lignin. d) The interplay of capillary pressure and Laplace pressure between two generic spherical particles (gray) upon evaporation of the solvent (R. Chen et al., 2016).

In the simplest case of IDs, droplets are formed by ouzo type nucleation and growth, followed by gradual destabilization through Ostwald ripening, driven by perturbations in the homogeneity of radii. We can consider the more complex case of TSID with low MW lignin that is highly miscible in IE (i.e., ideal case) (Figure 5-8b). Lignin molecules and IE are randomly dispersed and well dissolved in A90 prior to water addition. Upon solvent displacement and high mixing, the IE droplets can form, dissolving or swelling the lignin. Since the lignin is highly miscible in IE, it is evenly distributed in the droplet. During the drying process, water is removed, leaving an ID containing dissolved lignin. Further drying by reduced pressure results in the evaporation of IE and the lignin within the droplet contracts to form a solid particle. The particles are bridged by a film of IE between the particles (Figure 5-8b).

Conversely, when high MW lignin is used to form LNCs, an even more complex mechanism can be suggested Figure 5-8c . Given the condensed structure and lower hydrogen bonding capacity of high MW lignins, the miscibility with IE is likely to be lower than with low MW lignin. Thus, there is likely a supramolecular aggregation of high MW lignins that can form a double emulsion-like system within the IE droplet. However, one must consider the polydispersity of the fractionated lignin, such that very small aggregates may form as well as large ones. The resulting dried particle under high vacuum is a mixture of small, compact LNPs bridged by a layer of IE and core-shell particles that collapse due to the exceedingly high capillary pressure and mechanical stress during the drying process (R. Chen et al., 2016; Kämäräinen et al., 2018b; Tirumkudulu, 2018).

### **5.5.2 Antibacterial activity**

As previously mentioned, the solubility of IE in water is low but near the concentrations necessary for bacterial inhibition. However, the IE in water exists not as a free molecule but as

an aggregated droplet. Thus, the additive exposed surface area is greatly reduced. In the presence of additional compounds (salts, proteins, sugars), as is the case for biotic media, the solubility for the IE is expected to decrease. Therefore, IE is the major component involved with enhancing the antibacterial activity, being resistant to ripening, aggregation, and sedimentation. The stability is enhanced by the addition of lignin as a ripening inhibitor.

## **5.6 Conclusions**

In this work, we demonstrated that kraft lignin and isoeugenol can be precipitated out of solution to form submicron particles/droplets in a simple, one-step process. It was shown that while isoeugenol can spontaneously emulsify to form semi-stable colloidal suspensions, the stability can be greatly enhanced with the inclusion of kraft lignin. This enhanced stability translated to twice as effective antibacterial activity in aqueous systems. Furthermore, it was shown that the complexation of isoeugenol with lignin can enhance the antibacterial activity of isoeugenol in the dehydrated state on paper surfaces fabricated to simulate paper packaging materials. In this regard, it appears that kraft lignin reduces the evaporation of isoeugenol in the absence of water. A mechanism of particle characteristics was proposed to explain these results further using the trapped species in a droplet model (TSID). The TSID fundamentally restricts the complete evaporation in the dry state and complete molecular diffusion in the droplet state. This work adds to the rapidly expanding progression of high value lignin-based material developments with a real-world application in antimicrobials.

## **6 HIGH-THROUGHPUT CONTINUOUS NANOPRECIPITATION DESIGN FOR LIGNIN NANOPARTICLE PRODUCTION UTILIZING THE VENTURI EFFECT**

### **6.1 Abstract**

Lignin nanoparticles have gained an immense level of attention from industry and academia for their potential in high-value applications. Much of the work-related to the fundamental understanding of lignin nanoparticle formation has already been performed, yet scalable technologies are scarce to produce this material. Here, we describe a simple low-energy design to produce LNPs at scale that are substantially smaller than LNPs produced at the bench scale or in a batch mixing design. This design involves the adaptation of the Venturi effect to generate a flow of dissolved lignin by passing an orthogonal flow of water through a confined space. This allows for LNPs to be produced at a rate of 225 g/hour. Additionally, a solubility investigation of lignin in aqueous THF and acetone was performed. It was determined that 90% v/v acetone produced LNPs with the smallest average size compared to other concentrations of aqueous acetone and aqueous THF.

### **6.2 Introduction**

Lignin is a biopolymer present in all plant life at varying amounts and has been investigated for potential high value applications including, but not limited to, polymer composites, antioxidants, anticorrosion, cement additive, UV absorber, among others (Beisl, Friedl, et al., 2017; Duval & Lawoko, 2014; Österberg et al., 2020; Rahman et al., 2018; Q. Tang et al., 2020). However, the valorization of lignin has been greatly hindered by its amorphous configuration and heterogeneous chemical and molecular weight distribution (Zwilling et al., 2021). This fact, has propelled a global research effort to chemically modify, homogenize, or

physically transform lignin for enhanced applications. A recent push towards the modification of lignin is aimed at the transformation of the polymer into micro- and nanoparticles. This transformation allows lignin to self-assemble into spherical particles with a distribution of its various functional groups according to the affinity to the external environment. One of the more simple and common methods for transforming lignin into nanoparticles is the nanoprecipitation, or solvent exchange method. This method involves the dissolution of KL in water-miscible organic solvents followed by the rapid addition of a non-solvent phase, usually water. Mechanistically, the rapid mixing generates a series of small droplets of dissolved lignin and the solvent is eventually fully diffused in the water (Beisl, Miltner, et al., 2017; Österberg et al., 2020). The hydrophobic character of KL results in a rapid aggregation of the lignin into nuclei. The spherical shape is characteristic of a surface energy minimization phenomenon. Other additive properties of LNPs are their high surface area-to-volume ratio and dispersibility in various media. The transformation of lignin to a colloidal form allows for molecular-like reactivity in aqueous environments (A. Moreno & Sipponen, 2020).

Kraft lignin has a particularly complex chemistry and molecular weight distribution due to the degradative extraction during biomass pulping. During pulping, lignin undergoes a vast array of reactions that result in a high polydispersity. In previous work, it was shown that the molecular weight of lignin has an inverse correlation with the phenolic hydroxyl content and a positive correlation to its aliphatic character (X. Jiang et al., 2017; Zwillling et al., 2021). Due to the lower pKa, phenolic hydroxyls in lignin relate to the hydrophilicity of the fraction. Thus, each fraction of lignin has a solubility limit in organic solvents that can be related to their polarity. More specifically, more relatively more polar organic solvents are more selective towards more hydrophilic, low MW lignin fractions, whereas solvents that are more non-polar,

such as acetone and THF, are less selective (Ma et al., 2020; Pylypchuk et al., 2021; Zwilling et al., 2021).

The behavior of polymers in solution is a complicated topic, especially for a heterogeneous polymer such as lignin. The degree of solvation will vary greatly among the different lignin fractions. Generally speaking, high MW polymers are more difficult to dissolve than low MW polymers due to entropic considerations. Therefore, it has been proposed that lignin can aggregate into supramolecular structures in a single-phase system (S. Contreras et al., 2008; Guerra et al., 2007). The molecular weight of these supramolecular structures can be on the order of  $10^6$  Da as measured by multi-angle light scattering, whereas GPC of acetylated kraft lignin estimates molecular weights  $< 10$  kDa. Therefore, it is of interest to investigate how the nature of the solvent can affect the formation of LNPs during nanoprecipitation.

The nanoprecipitation method is typically performed by adding a small volume of dilute dissolved lignin to an excess of water under magnetic stirring. At the bench-scale, this method produces high-quality, monodispersed nanoparticles. However, for nanoprecipitation to occur, a high degree of supersaturation must be achieved. This is only possible with exceptional mixing at a larger scale. Therefore, proposals of batch LNP nanoprecipitation processes will likely result in heterogeneous and aggregated colloidal dispersions.

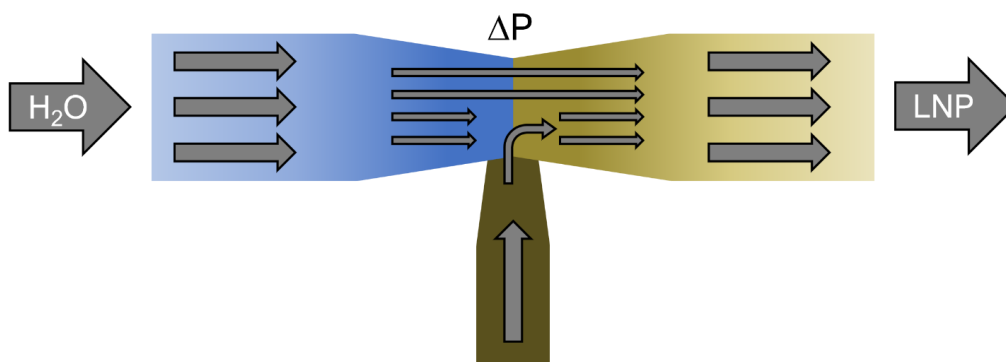


Figure 6-1. Schematic of the Venturi mixer modified for LNP production at scale.

In this research, a high-throughput continuous mixer for the generation of LNPs. The mixer utilizes the Venturi effect was developed (Figure 6-1) to create a self-generated flow of lignin solution to a continuous flow of water in a confined space. The Venturi effect is the decrease in static pressure due to the velocity gain of a fluid passing through a confined volume.

## **6.3 Materials and Methods**

### **6.3.1 Materials**

Pine softwood kraft lignin (KL) extracted from black liquor via the LignoBoost method was used for all experiments. KL was acquired as an air-dried powder, and the residual moisture was removed by vacuum oven drying for at least 24 hours prior to sampling. The chemical composition of this lignin was fully characterized in previous work (X. Jiang et al., 2017; Zwilling et al., 2021). Acetone and tetrahydrofuran (THF) were acquired from Fisher Scientific (Waltham, MA, USA).

### **6.3.2 Methods**

#### **6.3.2.1 Kraft lignin solubility**

Five grams of KL was dissolved in 10 ml of either aqueous THF or aqueous acetone and mixed for 48 hours in the dark. The solution was centrifuged at 10,000 rpm for 30 min and filtered. The filtrate was diluted until an absorbance value between 0.1 and 1.5. A calibration curve of absorbance versus KL concentration was created for each of the solvent systems. The saturated solubility of KL was determined by UV-Vis spectroscopy.

### **6.3.2.2 Fractionation**

For preparing the lignin fractions, approximately 1 g of oven-dried KL was added to a 50 mL centrifuge tube along with 40 mL of anhydrous ethanol. The solution was mixed vigorously using a Fisher Scientific Digital Vortex Mixer for 60 seconds at 3,000 RPM to ensure maximum solubility. The mixture was then centrifuged for 5 minutes at 4,000 RPM. The supernatant was decanted and set aside for later use. In the same centrifuge tube, 40 mL of anhydrous acetone was added to the ethanol insoluble fraction and the previous steps were repeated. This process was repeated once more using anhydrous THF as the solvent. The THF insoluble fraction was discarded. The characterization of these lignin fractions is found in Chapter 4. The ethanol soluble, acetone soluble, and THF soluble fractions will be referred to as F1, F2, and F3. Each of the lignin fractions were redissolved in binary solvent mixture of acetone and THF in water at various compositions.

### **6.3.2.3 Bench-scale production of LNPs**

The synthesis of colloidal lignin particles was performed by first transferring 1 mL of the lignin fraction solution to a 20 mL scintillation vial. After which, 9 mL of antisolvent (DI water) was quickly injected into the solution under rapid magnetic stirring. The colloidal suspensions are hereby referred to as F1-LNPs, F2-LNPs, F3-LNPs, F4-LNPs, and for particles precipitated from their respective lignin fractions.

### **6.3.2.4 Nanoprecipitation mixer design**

A customized nanoprecipitation mixer was designed using the principles of Bernoulli and Venturi. Briefly, a flow of liquid passing through a confined space can create a pressure drop that can act on a path orthogonal to the initial flow stream (Figure 6-1). In this regard, the mixer was

equipped with a Venturi jet mixing adapter with an internal diameter of 1.5 centimeters. Both ends of the adapter were connected to Tygon laboratory tubing with the inlet stream connected to a pressurized DI water reservoir and the other end being the outlet stream. The orthogonal inlet was connected to solvent resistant rubber tubing. The internal diameter was reduced from 10 mm to 5 mm by attaching a glass Pasteur pipette. The capillary end of the Pasteur pipette was connected to solvent resistant peristaltic tubing (Masterflex L/S 14) with an internal diameter of 1.6 mm.

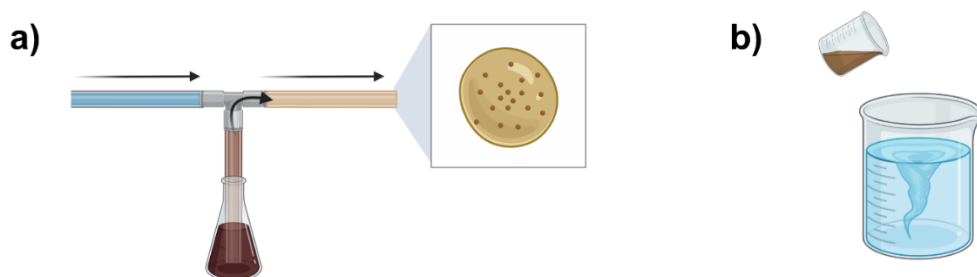


Figure 6-2. Diagram of a) the continuous nanoprecipitation mixer ( $NP_{cont}$ ) and b) the batch method of LNP production ( $NP_{batch}$ ).

For LNP production, KL was dissolved in a binary solvent of acetone and water (90% v/v) overnight. The resulting solution was centrifuged at 4,400 RPM for 10 minutes. The peristaltic tubing was submerged in the lignin solution, and the mixing was propagated by opening the valve to the DI water allowing water to flow through the junction. The flow was allowed to reach steady state at a rate of 3 L/min and velocity of 0.63 m/s. The outlet stream was collected in a volumetric cylinder. The volume of lignin solution was monitored concurrently. The acetone was removed by rotary evaporation at 40°C. The final suspension was stored for particle size analysis.

For comparison, a batch method of LNP synthesis was performed by quickly pouring a lignin solution in A90 into excess water. The lignin/solvent/water ratio was equal to the continuous method. The acetone was removed by evaporation under the same conditions as previously mentioned.

### 6.3.3 Particle size analysis

The particle size distribution (PSD) was measured by dynamic light scattering (DLS) using a Zetasizer Nano ZS (Malvern). The average particle diameter (MPD) is reported as the intensity-weighted Z-average particle diameter.

## 6.4 Results and discussion

### 6.4.1 Solvent effects on LNP formation

It is well established that the solubility of kraft lignin is drastically improved upon the hydration of water-miscible solvents such as acetone. Therefore, the saturated solubility of kraft lignin was estimated in various binary solvents of water and THF or acetone (Figure 6-3).

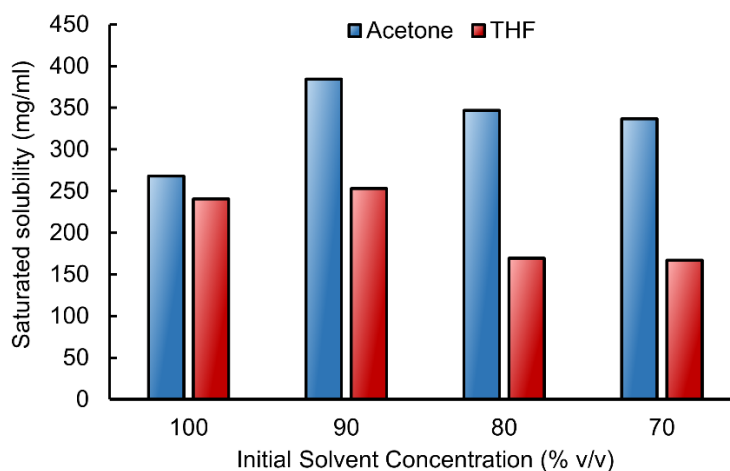


Figure 6-3. Saturated solubility of KL in aqueous acetone and aqueous THF.

In Figure 6-3, the saturated solubility of KL was determined for pure acetone and acetone/water mixtures. There is a substantial increase in the solubility of KL in 90% v/v acetone/water (A90) solvent compared to pure acetone. Additional water causes a slight decrease in the saturated solubility of KL. When KL is dissolved in aqueous acetone well below the saturated limit (10 mg/ml), a single dissolved phase of KL is visible for 90-70% v/v acetone. Pure acetone shows a high degree of sedimentation indicating a fractionation event.

In previous work, we showed that pure acetone is unable to dissolve the highest 33% MW fraction of KL (Zwilling et al., 2021). Therefore, the saturated solubility limit is skewed due to the selectivity of pure acetone. Thus, the fraction of lignin that pure acetone can dissolve is relatively high (~270 mg/ml) considering the maximum availability of pure acetone soluble lignin is 335 mg/ml.

For THF/water mixtures, the maximum solubility was substantially lower than for acetone/water mixtures Figure 6-3. This solubility is slightly improved by the addition of 10% water but gradual declines with added volumes of water. These results propagate an interesting insight into the solubility of KL in organic solvents. Firstly, the increase in solubility with the addition of a small volume of water is contradictory to standard polymer solubility relationships such as Hansen and Hildebrand models (Schuerch, 1952a) . The addition of water should move the solubility parameter further from that of lignin, yet the fraction solubilization and saturated solubility increase significantly. It may be that the potential for a temporary dipole moment exchange between the organic solvent molecule and water. Acetone for instance may form a temporary dipole upon its interaction with water, which may lead to an orientation of the methyl groups toward the hydrophobic moieties of KL. Additional water will eventually reduce the interactions of acetone with lignin leading to a decrease in the saturated solubility limit.

Contrary to acetone, pure THF can solubilize all lignin fractions, but the saturated solubility limit is lower than for acetone. In Chapter 4, it was suggested that the lower polarity of THF allows for the solubilization of more hydrophobic, higher MW lignin molecules. However, this does not necessarily contribute to the quality of the solvent for lignin at high concentrations. The interaction strength of lignin with aqueous THF and aqueous acetone was estimated through molecular dynamics modeling and came to the same conclusion (Zou et al., 2021).

The particle size of the various lignin fractions was determined by DLS precipitated from either aqueous THF (90% v/v) or aqueous acetone (90% v/v) to gather a better understanding of the polymer interactions in solution (Figure 6-4)

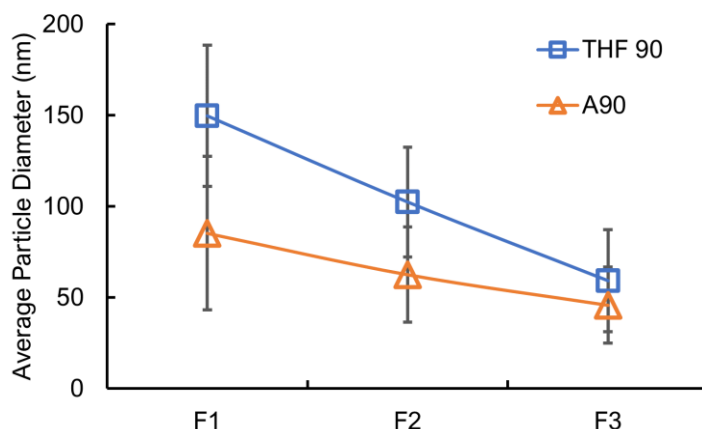


Figure 6-4. Average particle size of LNPs produced from fractionated lignins in A90 and THF 90 precursor solvents.

In Figure 6-4, the LNPs precipitated from acetone were smaller than those precipitated from THF, regardless of the lignin fraction precipitated. There is an inverse relationship between the molecular weight of the lignin and the particle size for both solvents.

The larger particle size for the LNPs precipitated from THF is likely due to the weaker solvent-lignin interactions. During solvent displacement, solvent droplet containing lignin will form at early stages and the strength of interaction will determine the longevity of this droplet's existence. As mentioned in the work of Schubert *et. al.*, the slow diffusion of solvent to the non-solvent will allow for a more complete particle formation, whereas a sudden release of solvent from the supersaturated droplet will result in voids within the particle (Schubert et al., 2011; Zou et al., 2021). In summary, aqueous acetone is a better solvent for KL than THF and will form smaller, more compact nanoparticles. For this reason, aqueous acetone (90% v/v) was the chosen solvent for scalability experiments.

#### **6.4.2 Scalability of LNP production**

In Chapter 4, it was established that the particle size and stability is highly dependent on the concentration of the precursor lignin solution. For that reason, three concentrations of KL in A90, 10 mg/ml and 25mg/ml were used in the scale-up experiments. Considering the method of particle precipitation for the continuous mixer differs greatly compared to the bench-scale method, it was necessary to compare the resulting particle characteristics. The average particle sizes for each of the KL solution concentrations are reported in Figure 6-5 along with the bench-scale and batch method resulting suspensions.

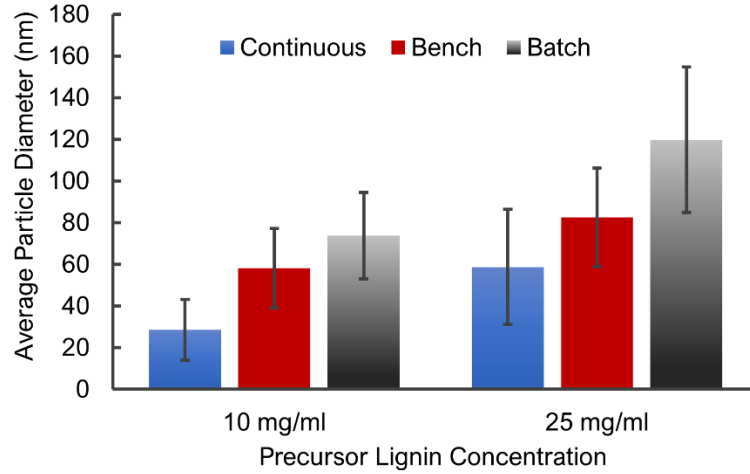


Figure 6-5. Average particle diameter of LNPs produced from the different precipitation methods: Continuous (NP<sub>cont</sub>), Bench (NP<sub>bench</sub>), and Batch (NP<sub>batch</sub>).

The particles formed from the NP<sub>cont</sub> method had smaller average particle size than from either the NP<sub>bench</sub> or NP<sub>batch</sub> methods (see Figure 6-5). The NP<sub>bench</sub> and NP<sub>batch</sub> were much larger likely due to the rate of mixing. According to classical nucleation and growth, the rate of nucleation is strongly dependent on the supersaturation (Eq. 1).

$$\frac{dN}{dt} \propto \exp\left(-\frac{1}{(\ln(S))^2}\right) \quad (1)$$

In Eq. 1, N is the number of particles, t is time, and S is the degree of supersaturation. For the NP<sub>cont</sub>, the degree of local supersaturation at the nanoscale will be much higher than the pour-over methods. This is due to the confined volume in which mixing occurs. The total mixing volume for the NP<sub>batch</sub> method is 100 ml whereas the mixing volume for NP<sub>cont</sub> is approximately 10 ml.

The Reynold's number (*Re*) and for the NP<sub>cont</sub> was calculated using Equation 2 to describe the mixing regime.

$$Re = \frac{QDh}{Av} \quad (2)$$

In Equation 2,  $Q$  is the volumetric flow rate,  $D_h$  is the hydraulic diameter,  $A$  is the cross-sectional area, and  $\nu$  is the kinematic viscosity. Table 6-1 includes the input values and the corresponding  $Re$ .

Table 6-1. Reynold's number calculation for the continuous LNP Venturi mixer.

<b>Variable</b>	<b>Value</b>
$Q$ (m <sup>3</sup> /s)	5.00E-05
$D_h$ (m)	1.00E-02
$A$ (m <sup>2</sup> )	7.85E-05
$\nu$ (m/s)	1.35E-06
$Re$	4.73E+03

The mixing regime was calculated to be in the turbulent regime ( $Re > 4,000$ ) which is desired for flash nanoprecipitation (Saad & Prud'Homme, 2016). The solvent/antisolvent ratio was determined by measuring the decrease in the solvent volume as a function of time using a volumetric cylinder at steady state. The solvent-to-antisolvent ratio was 1:20 on a volume basis. Assuming all the original lignin is in nanoparticle form given the negligible solubility in water, the production of LNPs from an initial lignin concentration of 25 mg/ml was 225 g/hr on a dry basis. This translates to a batch volume of 180 L, which would involve a massive amount of energy for adequate mixing. Therefore, the continuous mixer also has its advantages of scalability over batch methods by minimizing the mixing volume.

## 6.5 Conclusions

In this research, a simple, low-energy method to produce LNPs at a relatively large scale without sacrificing particle quality was introduced. Analysis of lignin nanoparticles formed from fractionated lignin suggests 90% v/v aqueous acetone is the optimal solvent for LNP production. A scalable nanoprecipitation mixer was designed by utilizing the Venturi effect to create a

pressure drop orthogonal to a flow of water, creating a self-generated mixing stream. The only requirement for this mixing apparatus is a steady flow of water. It was shown that the continuous flow mixer was superior in terms of practical scalability as well as particle size reduction compared to a batch pour over method. Future work could optimize this design for effective solvent recovery and mass ratio optimization.

## 7 CONCLUSIONS

Plant life has existed on earth for nearly 700 million years and in that time has evolved to contain materials with great potential with a low environmental impact. In that time, plants have developed to contain a highly structured network of molecules including cellulose, lignin, hemicellulose, and other small molecules. Each of these components play a pivotal role for plant life. Lignin has a unique set of properties that greatly differ from its cellulosic counterparts due to its polyaromatic character. However, lignin valorization has failed due to many challenges related to the heterogeneity and recalcitrance of the polymer. However, lignin has received attention from nanoscience and colloid researchers investigating its viability as a potentially new advanced material resource.

Bioresources have the potential to become the next generation of materials for a more sustainable future. For this to happen, rigorous research must be performed by first learning from nature's creations and creatively engineering new materials from bio-based sources. The focus of this research was transforming lignin into a functional colloidal particle and investigating its application as a nanocarrier/stabilizer of antibacterial compounds.

In this research, the fundamental concepts driving lignin nanoparticle formation were studied and these concepts were used to develop high-value applications in antimicrobials for food packaging. Many fundamental concepts were visited including a brief introduction into the thermodynamics of nanoparticle formation and how it relates to lignin nanoparticles. It was shown that by forming LNPs from fractionated lignins with various hydrophilic/hydrophobic characteristics, we can achieve a deeper understanding of the interparticle and particle-solvent interactions. It was determined that there is an inverse relationship of hydrophilicity with molecular weight that translates to an expanded particle form. Conversely, highly hydrophobic

lignin fractions showed higher degrees of aggregation, likely due to the higher surface energy in aqueous media.

From an applications perspective, it was shown that lignin can form a nanocomplex with an essential oil compound, isoeugenol with added stability and improved antibacterial activity. Additionally, it was shown that this added stability and antibacterial efficacy in solution can be translated to the dry state on food packaging simulated surfaces. This was performed based on the motivation provided by our work of tracking the viability of foodborne bacterial pathogens on paper-based materials. It was shown that *S. Typhimurium* and *L. innocua* can survive on these materials for more up to 40 days with little reduction in viable populations. The effect of lignin content in the paper was also investigated and it was determined that the hydrophobicity provided by lignin may assist in the accessibility of nutrients for bacteria on paper surfaces.

Finally, a Venturi mixed design was implemented to produce colloidal lignin particle suspensions at scale using low-energy methods such as a Venturi mixer design. This design proved superior to a batch design. Additionally, the Venturi design is a continuous design that requires only a flow of water to propel the production of lignin nanoparticles with an average particle size as low as 28 nm.

## 8 FUTURE WORK

At the inception of this research, little research had been performed on understanding and applying the synthesis of lignin-based nanomaterials. Since then, a global effort has put lignin nanoparticles at the forefront of biobased material design. We believe that there are endless applications of colloidal lignin materials, but a few prospects will be discussed here.

In producing lignin nanocomplexes with essential oil compounds, it became apparent the versatility of lignin as a dispersant and stabilizer. Therefore, it would be interesting to entertain various formulations of lignin with plant-based small molecules for encapsulated drug-delivery systems. This could also be the entrapment of ionophores such as quercetin to enhance the delivery of ionic compounds such as zinc or iron.

One major gap in the literature understanding the behavior of lignins in solution. Technical lignins are highly heterogeneous and will have an array of interactions with various solvents, as shown through lignin fractionation. However, this knowledge gap can be remedied with more advanced polymer and colloid analysis. For instance, small-angle X-ray scattering and small-angle neutron scattering experiment are underway for characterizing lignin nanoparticles and have shown to be an additive resource to dynamic light scattering in describing the particle morphologies of LNPs. Although, this same technique can be used for the elucidation of the solution structure of lignin. This technique can give information of the radius of gyration, absolute molecular weight, supramolecular porosity, and other conformational information. In addition to the described particle analysis methods, nanoparticle tracking analysis can be performed to determine the kinetics of nucleation and growth of LNPs or LNCs. This would become invaluable in the future engineering of nanomaterials from lignin and may help solve the recalcitrance issue of lignin in pulping. Furthermore, with the increased interest in alternative

pulping processes such as ethanol solvent pulping, the solution structure of lignin could be very important in the fluid dynamics of the effluent streams.

## 9 REFERENCES

- Abbati De Assis, C., Greca, L. G., Ago, M., Balakshin, M. Y., Jameel, H., Gonzalez, R., & Rojas, O. J. (2018). Techno-Economic Assessment, Scalability, and Applications of Aerosol Lignin Micro- and Nanoparticles. *ACS Sustainable Chemistry and Engineering*, 6(9), 11853–11868. <https://doi.org/10.1021/acssuschemeng.8b02151>
- Adley, C. C., & Ryan, M. P. (2016). The Nature and Extent of Foodborne Disease. In *Antimicrobial Food Packaging*. Elsevier Inc. <https://doi.org/10.1016/B978-0-12-800723-5.00001-2>
- Ago, M., Huan, S., Borghei, M., Raula, J., Kauppinen, E. I., & Rojas, O. J. (2016). High-Throughput Synthesis of Lignin Particles (~30 nm to ~2 µm) via Aerosol Flow Reactor: Size Fractionation and Utilization in Pickering Emulsions. *ACS Applied Materials and Interfaces*, 8(35), 23302–23310.
- Ago, M., Tardy, B. L., Wang, L., Guo, J., Khakalo, A., & Rojas, O. J. (2017). Supramolecular assemblies of lignin into nano- and microparticles. *MRS Bulletin*, 42(5), 371–378. <https://doi.org/10.1557/mrs.2017.88>
- Agrillo, B., Balestrieri, M., Gogliettino, M., Palmieri, G., Moretta, R., Proroga, Y. T. R., Rea, I., Cornacchia, A., Capuano, F., Smaldone, G., & De Stefano, L. (2019). Functionalized polymeric materials with bio-derived antimicrobial peptides for “active” packaging. *International Journal of Molecular Sciences*, 20(3), 1–14. <https://doi.org/10.3390/ijms20030601>
- Alqahtani, M. S., Alqahtani, A., Kazi, M., Ahmad, M. Z., Alahmari, A., Alsenaidy, M. A., & Syed, R. (2020). Wound-healing potential of curcumin loaded lignin nanoparticles. *Journal of Drug Delivery Science and Technology*, 60. <https://doi.org/10.1016/j.jddst.2020.102020>
- Alzagameem, A., Klein, S. E., Bergs, M., Do, X. T., Korte, I., Dohlen, S., Hüwe, C., Kreyenschmidt, J., Kamm, B., Larkins, M., & Schulze, M. (2019). Antimicrobial activity of lignin and lignin-derived cellulose and chitosan composites against selected pathogenic and spoilage microorganisms. *Polymers*, 11(4). <https://doi.org/10.3390/polym11040670>
- Anderson, C. J., & Kendall, M. M. (2017). Salmonella enterica serovar typhimurium strategies for host adaptation. In *Frontiers in Microbiology* (Vol. 8, Issue OCT). Frontiers Media S.A. <https://doi.org/10.3389/fmicb.2017.01983>

- Andino, A., & Hanning, I. (2015). Salmonella enterica: Survival, colonization, and virulence differences among serovars. *Scientific World Journal*, 2015(Table 3).  
<https://doi.org/10.1155/2015/520179>
- Argyropoulos, D. S. (1994). Quantitative phosphorus-31 nmr analysis of lignins, a new tool for the lignin chemist. *Journal of Wood Chemistry and Technology*, 14(1), 45–63.  
<https://doi.org/10.1080/02773819408003085>
- Balasubramaniam, B., Prateek, Ranjan, S., Saraf, M., Kar, P., Singh, S. P., Thakur, V. K., Singh, A., & Gupta, R. K. (2021). Antibacterial and Antiviral Functional Materials: Chemistry and Biological Activity toward Tackling COVID-19-like Pandemics. *ACS Pharmacology and Translational Science*, 4(1), 8–54. <https://doi.org/10.1021/acspsci.0c00174>
- Balloux, F., & van Dorp, L. (2017). Q&A: What are pathogens, and what have they done to and for us? *BMC Biology*, 15(1), 91. <https://doi.org/10.1186/s12915-017-0433-z>
- Balouiri, M., Sadiki, M., & Ibsouda, S. K. (2016). Methods for in vitro evaluating antimicrobial activity: A review. In *Journal of Pharmaceutical Analysis* (Vol. 6, Issue 2, pp. 71–79). Xi'an Jiaotong University. <https://doi.org/10.1016/j.jpha.2015.11.005>
- Barbarossa, C., & De Pelsmacker, P. (2016). Positive and Negative Antecedents of Purchasing Eco-friendly Products: A Comparison Between Green and Non-green Consumers. *Journal of Business Ethics*, 134(2), 229–247. <https://doi.org/10.1007/s10551-014-2425-z>
- Barman, A., Das, R., & De, P. K. (2021). Impact of COVID-19 in food supply chain: Disruptions and recovery strategy. *Current Research in Behavioral Sciences*, 2, 100017.  
<https://doi.org/10.1016/j.crbeha.2021.100017>
- Bastarrachea, L. J., Wong, D. E., Roman, M. J., Lin, Z., & Goddard, J. M. (2015). Active packaging coatings. In *Coatings* (Vol. 5, Issue 4, pp. 771–791). MDPI AG.  
<https://doi.org/10.3390/coatings5040771>
- Beisl, S., Friedl, A., & Miltner, A. (2017). Lignin from micro- To nanosize: Applications. *International Journal of Molecular Sciences*, 18(11). <https://doi.org/10.3390/ijms18112367>
- Beisl, S., Miltner, A., & Friedl, A. (2017). Lignin from micro- to nanosize: Production methods. In *International Journal of Molecular Sciences* (Vol. 18, Issue 6). MDPI AG.  
<https://doi.org/10.3390/ijms18061244>
- Benazzouz, A., Moity, L., Pierlot, C., Molinier, V., & Aubry, J. M. (2014). Hansen approach versus COSMO-RS for predicting the solubility of an organic UV filter in cosmetic

- solvents. *Colloids and Surfaces A: Physicochemical and Engineering Aspects*, 458(1), 101–109. <https://doi.org/10.1016/j.colsurfa.2014.03.065>
- Bhuiyan, N. H., Selvaraj, G., Wei, Y., & King, J. (2009). Role of lignification in plant defense. *Plant Signaling and Behavior*, 4(2), 158–159. <https://doi.org/10.4161/psb.4.2.7688>
- Biji, K. B., Ravishankar, C. N., Mohan, C. O., & Srinivasa Gopal, T. K. (2015). Smart packaging systems for food applications: a review. *Journal of Food Science and Technology*, 52(10), 6125–6135. <https://doi.org/10.1007/s13197-015-1766-7>
- Bourrel, M., & Schechter, R. S. (2010). *Microemulsions and related systems: formulation, solvency, and physical properties* (2nd ed.). Editions Technip, Paris, France.
- Brandwein, M., Al-Quntar, A., Goldberg, H., Mosheyev, G., Goffer, M., Marin-Iniesta, F., López-Gómez, A., & Steinberg, D. (2016). Mitigation of biofilm formation on corrugated cardboard fresh produce packaging surfaces using a novel thiazolidinedione derivative integrated in acrylic emulsion polymers. *Frontiers in Microbiology*, 7(FEB), 1–9. <https://doi.org/10.3389/fmicb.2016.00159>
- Brick, M. C., Palmer, H. J., & Whitesides, T. H. (2003). Formation of colloidal dispersions of organic materials in aqueous media by solvent shifting. *Langmuir*, 19(16), 6367–6380. <https://doi.org/10.1021/la034173o>
- Buendía-Moreno, L., Ros-Chumillas, M., Navarro-Segura, L., Sánchez-Martínez, M. J., Soto-Jover, S., Antolinos, V., Martínez-Hernández, G. B., & López-Gómez, A. (2019). Effects of an Active Cardboard Box Using Encapsulated Essential Oils on the Tomato Shelf Life. *Food and Bioprocess Technology*, 12(9), 1548–1558. <https://doi.org/10.1007/s11947-019-02311-0>
- Bullón, J., Márquez, L., Fernández, J. A., Scorzza, C., Scorza, J. V., Rodríguez, J., Cordero, A., Vejar, F., Khatib, S. K., & Forgiarini, A. (2021). A Promising Cutaneous Leishmaniasis Treatment with a Nanoemulsion-Based Cream with a Generic Pentavalent Antimony (Ulamina) as the Active Ingredient. *Cosmetics*, 8(115). <https://doi.org/10.3390/cosmetics8040115>
- Bullón, J., Molina, J., Márquez, R., Véjar, F., Scorzza, C., & Forgiarini, A. (2007). Nano-emulsión de aceites triglicéridos para uso parenteral mediante un método de baja energía. *Revista Técnica de La Facultad de Ingeniería Universidad Del Zulia*, 30, 428–437.

- Buzby, J. C., Roberts, T., Lin, C.-T. J., & MacDonald, J. M. (1996). *USDA ERS - Bacterial Foodborne Disease: Medical Costs and Productivity Losses*.  
<https://www.ers.usda.gov/publications/pub-details/?pubid=40728>
- Calo, J. R., Crandall, P. G., O'Bryan, C. A., & Ricke, S. C. (2015). Essential oils as antimicrobials in food systems - A review. In *Food Control* (Vol. 54, pp. 111–119). Elsevier Ltd. <https://doi.org/10.1016/j.foodcont.2014.12.040>
- Carpentier, B., & Cerf, O. (1993). Biofilms and their consequences, with particular reference to hygiene in the food industry. *Journal of Applied Bacteriology*, 75(6), 499–511.  
<https://doi.org/10.1111/j.1365-2672.1993.tb01587.x>
- Chakar, F. S., & Ragauskas, A. J. (2004). *Review of current and future softwood kraft lignin process chemistry*. 20, 131–141. <https://doi.org/10.1016/j.indcrop.2004.04.016>
- Chelliah, R., Ramakrishnan, S. R., Khan, I., Ganesan, P., Oh, D.-H., & Kwon, J.-H. (2019). Nanoencapsulation of Plant-Based Oils and Its Applications in Food and Food Packaging Bioavailability. In G. Molina, F. M. Pelissari, & A. M. Asiri (Eds.), *Food Applications of Nanotechnology* (p. 38). CRC Press, Taylor & Francis, Boca Raton, USA.
- Chen, N., Dempere, L. A., & Tong, Z. (2016). Synthesis of pH-Responsive Lignin-Based Nanocapsules for Controlled Release of Hydrophobic Molecules. *ACS Sustainable Chemistry and Engineering*, 4(10), 5204–5211.  
<https://doi.org/10.1021/acssuschemeng.6b01209>
- Chen, R., Zhang, L., Zang, D., & Shen, W. (2016). Wetting and Drying of Colloidal Droplets: Physics and Pattern Formation. In *Advances in Colloid Science*. IntechOpen.  
<https://doi.org/10.5772/65301>
- Chin, A. W. H., Chu, J. T. S., Perera, M. R. A., Hui, K. P. Y., Yen, H.-L., Chan, M. C. W., Peiris, M., & Poon, L. L. M. (2020). Stability of SARS-CoV-2 in different environmental conditions. *The Lancet Microbe*, 0–4. [https://doi.org/10.1016/s2666-5247\(20\)30003-3](https://doi.org/10.1016/s2666-5247(20)30003-3)
- Chu, J., Cheng, Y. L., Rao, A. V., Nouraei, M., Zarate-Muñoz, S., & Acosta, E. J. (2014). Lecithin-linker formulations for self-emulsifying delivery of nutraceuticals. *International Journal of Pharmaceutics*, 471(1–2), 92–102. <https://doi.org/10.1016/j.ijpharm.2014.05.001>
- Coalescence in Colloid Chemistry. (2008). *IUPAC Compendium of Chemical Terminology*, 577, 2014. <https://doi.org/10.1351/goldbook.c01119>

- Contreras, C. B., Charles, G., Toselli, R., & Strumia, M. C. (2018). Antimicrobial Active Packaging. *Biopackaging, August 2018*, 36–58. <https://doi.org/10.1201/9781315152349-3>
- Contreras, S., Gaspar, A. R., Guerra, A., Lucia, L. A., & Argyropoulos, D. S. (2008). Propensity of lignin to associate: Light scattering photometry study with native lignins. *Biomacromolecules*, 9(12), 3362–3369. <https://doi.org/10.1021/bm800673a>
- Corsaro, C., Neri, G., Mezzasalma, A. M., & Fazio, E. (2021). Weibull modeling of controlled drug release from Ag-PMA nanosystems. *Polymers*, 13(17). <https://doi.org/10.3390/polym13172897>
- Cruz, R. M. S., Alves, V., Khmelinskii, I., & Vieira, M. C. (2018). Chapter 2 - New Food Packaging Systems. In *Food Packaging and Preservation*. Elsevier Inc. <https://doi.org/10.1016/B978-0-12-811516-9/00002-6>
- Culbertson, C., Treasure, T., Venditti, R., Jameel, H., & Gonzalez, R. (n.d.). Life Cycle Assessment of lignin extraction in a softwood kraft pulp mill. In *Nordic Pulp & Paper Research Journal* (Vol. 31, Issue 1).
- Dagtepe, P., & Chikan, V. (2010). Quantized Ostwald ripening of colloidal nanoparticles. *Journal of Physical Chemistry C*, 114(39), 16263–16269. <https://doi.org/10.1021/jp105071a>
- Dai, L., Liu, R., Hu, L. Q., Zou, Z. F., & Si, C. L. (2017). Lignin Nanoparticle as a Novel Green Carrier for the Efficient Delivery of Resveratrol. *ACS Sustainable Chemistry and Engineering*, 5(9), 8241–8249. <https://doi.org/10.1021/acssuschemeng.7b01903>
- Das, S., Horváth, B., Šafranko, S., Jokić, S., Széchenyi, A., & Kőszegi, T. (2019). Antimicrobial Activity of Chamomile Essential Oil: Effect of Different Formulations. In *Molecules* (Vol. 24, Issue 23). <https://doi.org/10.3390/molecules24234321>
- Das, S., Horváth, B., Šafranko, S., Jokić, S., Széchenyi, A., & Kőszegi, T. (2019). Antimicrobial activity of chamomile essential oil: Effect of different formulations. *Molecules*, 24(23). <https://doi.org/10.3390/molecules24234321>
- Dean, R., Van Kan, J. A. L., Pretorius, Z. A., Hammond-Kosack, K. E., Di Pietro, A., Spanu, P. D., Rudd, J. J., Dickman, M., Kahmann, R., Ellis, J., & Foster, G. D. (2012). The Top 10 fungal pathogens in molecular plant pathology. *Molecular Plant Pathology*, 13(4), 414–430. <https://doi.org/10.1111/j.1364-3703.2011.00783.x>

- Destrée, C., & B.Nagy, J. (2006). Mechanism of formation of inorganic and organic nanoparticles from microemulsions. *Advances in Colloid and Interface Science*, 123–126(SPEC. ISS.), 353–367. <https://doi.org/10.1016/j.cis.2006.05.022>
- Dickinson, E. (2010). Food emulsions and foams: Stabilization by particles. *Current Opinion in Colloid and Interface Science*, 15(1–2), 40–49. <https://doi.org/10.1016/j.cocis.2009.11.001>
- Duval, A., & Lawoko, M. (2014). A review on lignin-based polymeric, micro- and nano-structured materials. *Reactive and Functional Polymers*, 85, 78–96. <https://doi.org/10.1016/j.reactfunctpolym.2014.09.017>
- EPA - United States Environmental Protection Agency. (2020). Advancing Sustainable Materials Management : Facts 2018 Tables and Figures. Assessing Trends in Materials Generation and Management in The United States. *Advancing Sustainable Materials Management : Facts and Figure 2018, December*.
- Espinoza-Acosta, J. L., Torres-Chávez, P. I., Ramírez-Wong, B., López-Saiz, C. M., & Montaña-Leyva, B. (2016). Antioxidant, antimicrobial, and antimutagenic properties of technical lignins and their applications. *BioResources*, 11(2), 5452–5481. [https://doi.org/10.15376/biores.11.2.Espinoza\\_Acosta](https://doi.org/10.15376/biores.11.2.Espinoza_Acosta)
- Espitia, P. J. P., Otoni, C. G., & Soares, N. F. F. (2016). Zinc Oxide Nanoparticles for Food Packaging Applications. In *Antimicrobial Food Packaging*. Elsevier Inc. <https://doi.org/10.1016/B978-0-12-800723-5.00034-6>
- Fasihi, H., Noshirvani, N., Hashemi, M., Fazilati, M., Salavati, H., & Coma, V. (2019). Antioxidant and antimicrobial properties of carbohydrate-based films enriched with cinnamon essential oil by Pickering emulsion method. *Food Packaging and Shelf Life*, 19, 147–154. <https://doi.org/10.1016/j.fpsl.2018.12.007>
- FDA. (2020). *Outbreaks of Foodborne Illness | FDA*.
- Figueiredo, P., Lintinen, K., Hirvonen, J. T., Kostianen, M. A., & Santos, H. A. (2018). Properties and chemical modifications of lignin: Towards lignin-based nanomaterials for biomedical applications. *Progress in Materials Science*, 93, 233–269. <https://doi.org/10.1016/j.pmatsci.2017.12.001>
- Food Packaging Market Worth \$456.6 Billion By 2027*. (n.d.).

- Forgiarini, A., Esquena, J., González, C., & Solans, C. (2001). Formation of Nano-emulsions by Low-Energy Emulsification Methods at Constant Temperature. *Langmuir*, *17*(7), 2076–2083. <https://doi.org/10.1021/la001362n>
- Forgiarini, A., Marquez, R., & Salager, J.-L. (2021). Formulation improvements in the applications of surfactant-oil-water systems using the HLDN approach with extended surfactant structure. *Molecules*, *26*(12), 3771. <https://doi.org/10.3390/molecules26123771>
- Francis, G. A., & O’Beirne, D. (1998). Effects of the indigenous microflora of minimally processed lettuce on the survival and growth of *Listeria innocua*. *International Journal of Food Science and Technology*, *33*(5), 477–488. <https://doi.org/10.1046/j.1365-2621.1998.00199.x>
- Froio, F., Mosaddik, A., Morshed, M. T., Paolino, D., Fessi, H., & Elaissari, A. (2019). Edible Polymers for Essential Oils Encapsulation: Application in Food Preservation. In *Industrial and Engineering Chemistry Research* (Vol. 58, Issue 46, pp. 20932–20945). American Chemical Society. <https://doi.org/10.1021/acs.iecr.9b02418>
- Fuciños, C., Fuciños, P., Amado, I. R., Míguez, M., Fajardo, P., Pastrana, L. M., & Rúa, M. L. (2016). Smart Nanohydrogels for Controlled Release of Food Preservatives. In *Antimicrobial Food Packaging* (pp. 349–362). Elsevier Inc. <https://doi.org/10.1016/B978-0-12-800723-5.00028-0>
- Ganachaud, F., & Katz, J. L. (2005). Nanoparticles and nanocapsules created using the ouzo effect: Spontaneous emulsification as an alternative to ultrasonic and high-shear devices. In *ChemPhysChem* (Vol. 6, Issue 2, pp. 209–216). Wiley-VCH Verlag. <https://doi.org/10.1002/cphc.200400527>
- Gellerstedt, G., & Henriksson, G. (n.d.). Lignins : Major Sources , Structure and Properties. *Business*.
- Glasser, W. G., Davé, V., & Frazier, C. E. (1993a). Molecular weight distribution of (semi-) commercial lignin derivatives. *Journal of Wood Chemistry and Technology*, *13*(4), 545–559. <https://doi.org/10.1080/02773819308020533>
- Glasser, W. G., Davé, V., & Frazier, C. E. (1993b). Molecular weight distribution of (semi-) commercial lignin derivatives. *Journal of Wood Chemistry and Technology*, *13*(4), 545–559. <https://doi.org/10.1080/02773819308020533>

- Gonçalves, J., da Silva, P. G., Reis, L., Nascimento, M. S. J., Koritnik, T., Paragi, M., & Mesquita, J. R. (2021). Surface contamination with SARS-CoV-2: A systematic review. *Science of The Total Environment*, 798, 149231. <https://doi.org/https://doi.org/10.1016/j.scitotenv.2021.149231>
- Granata, A., & Argyropoulos, D. S. (1995). 2-Chloro-4,4,5,5-tetramethyl-1,3,2-dioxaphospholane, a Reagent for the Accurate Determination of the Uncondensed and Condensed Phenolic Moieties in Lignins. *Journal of Agricultural and Food Chemistry*, 43(6), 1538–1544. <https://doi.org/10.1021/jf00054a023>
- Greening, G. E., & Cannon, J. L. (2016). Human and Animal Viruses in Food (Including Taxonomy of Enteric Viruses). In S. M. Goyal & J. L. Cannon (Eds.), *Viruses in Foods* (pp. 5–57). Springer International Publishing, Berlin, Germany. [https://doi.org/10.1007/978-3-319-30723-7\\_2](https://doi.org/10.1007/978-3-319-30723-7_2)
- Groves, M. J. (1978). *Spontaneous emulsification*. 12. <https://doi.org/https://doi.org/>
- Guerra, A., Gaspar, A. R., Contreras, S., Lucia, L. A., Crestini, C., & Argyropoulos, D. S. (2007). On the propensity of lignin to associate: A size exclusion chromatography study with lignin derivatives isolated from different plant species. *Phytochemistry*, 68(20), 2570–2583. <https://doi.org/10.1016/j.phytochem.2007.05.026>
- Guimarães, A. C., Meireles, L. M., Lemos, M. F., Guimarães, M. C. C., Endringer, D. C., Fronza, M., & Scherer, R. (2019). Antibacterial activity of terpenes and terpenoids present in essential oils. *Molecules*, 24(13). <https://doi.org/10.3390/molecules24132471>
- Guo, X., Zhang, S., & Shan, X. quan. (2008). Adsorption of metal ions on lignin. *Journal of Hazardous Materials*, 151(1), 134–142. <https://doi.org/10.1016/j.jhazmat.2007.05.065>
- Halonen, N., Pálvölgyi, P. S., Bassani, A., Fiorentini, C., Nair, R., Spigno, G., & Kordas, K. (2020). Bio-Based Smart Materials for Food Packaging and Sensors – A Review. In *Frontiers in Materials* (Vol. 7). Frontiers Media S.A. <https://doi.org/10.3389/fmats.2020.00082>
- Hamaguchi, M., Cardoso, M., & Vakkilainen, E. (2012). Alternative technologies for biofuels production in kraft pulp mills-potential and prospects. In *Energies* (Vol. 5, Issue 7, pp. 2288–2309). MDPI AG. <https://doi.org/10.3390/en5072288>
- Hanning, I. B., Nutt, J. D., & Ricke, S. C. (n.d.). *Salmonellosis Outbreaks in the United States Due to Fresh Produce: Sources and Potential Intervention Measures*. [www.liebertpub.com](http://www.liebertpub.com)

- Hanning, I. B., Nutt, J. D., & Ricke, S. C. (2009). Salmonellosis outbreaks in the united states due to fresh produce: sources and potential intervention measures. *Foodborne Pathogens and Disease*, 6(6), 635–648. <https://doi.org/10.1089/fpd.2008.0232>
- Harris, L. J., Farber, J. N., Beuchat, L. R., Parish, M. E., Suslow, T. V., Garrett, E. H., & Busta, F. F. (2003). Outbreaks associated with fresh produce: Incidence, growth, and survival of pathogens in fresh and fresh-cut produce. *Comprehensive Reviews in Food Science and Food Safety*, 2(1 SUPPL.), 78–141. <https://doi.org/10.1111/j.1541-4337.2003.tb00031.x>
- Hayes, D. J., Schulz, L. L., Hart, C. E., & Jacobs, K. L. (2021). A descriptive analysis of the COVID-19 impacts on U.S. pork, turkey, and egg markets. *Agribusiness*, 37(1), 10.1002/agr.21674. <https://doi.org/10.1002/agr.21674>
- Helou, C., Marier, D., Jacolot, P., Abdennebi-Najar, L., Niquet-Léridon, C., Tessier, F. J., & Gadonna-Widehem, P. (2014). Microorganisms and Maillard reaction products: A review of the literature and recent findings. *Amino Acids*, 46(2), 267–277. <https://doi.org/10.1007/s00726-013-1496-y>
- Hollertz, R., Arwin, H., Faure, B., Zhang, Y., Bergström, L., & Wågberg, L. (2013). Dielectric properties of lignin and glucomannan as determined by spectroscopic ellipsometry and Lifshitz estimates of non-retarded Hamaker constants. *Cellulose*, 20(4), 1639–1648. <https://doi.org/10.1007/s10570-013-9980-9>
- Hu, Z., Du, X., Liu, J., Chang, H. M., & Jameel, H. (2016). Structural Characterization of Pine Kraft Lignin: BioChoice Lignin vs Indulin AT. *Journal of Wood Chemistry and Technology*, 36(6), 432–446. <https://doi.org/10.1080/02773813.2016.1214732>
- Hua, L., Yong, C., Zhanquan, Z., Boqiang, L., Guozheng, Q., & Shiping, T. (2018). Pathogenic mechanisms and control strategies of *Botrytis cinerea* causing post-harvest decay in fruits and vegetables. *Food Quality and Safety*, 2(3), 111–119. <https://doi.org/10.1093/fqsafe/fyy016>
- Hyldgaard, M., Mygind, T., Piotrowska, R., Foss, M., & Meyer, R. L. (2015). Isoeugenol has a non-disruptive detergent-like mechanism of action. *Frontiers in Microbiology*, 6(JUL). <https://doi.org/10.3389/fmicb.2015.00754>
- Iravani, S. (2020). Biomedical applications of lignin-based nanoparticles. In *Nanoparticles and their Biomedical Applications* (pp. 217–224). Springer Singapore. [https://doi.org/10.1007/978-981-15-0391-7\\_8](https://doi.org/10.1007/978-981-15-0391-7_8)

- Israelachvili, J. (2011). Intermolecular and Surface Forces. In *Intermolecular and Surface Forces*. <https://doi.org/10.1016/C2009-0-21560-1>
- Jardim, J. M., Hart, P. W., Lucia, L., Jameel, H., & Chang, H. (2020). Lignin precipitation: HW vs. SW. In *BioResources* (Vol. 15, Issue 3).
- Jeon, H. R., Kwon, M. J., & Yoon, K. S. (2018). Control of *Listeria innocua* biofilms on food contact surfaces with slightly acidic electrolyzed water and the risk of biofilm cells transfer to duck meat. *Journal of Food Protection*, *81*(4), 582–592. <https://doi.org/10.4315/0362-028X.JFP-17-373>
- Jiang, C., He, H., Jiang, H., Ma, L., & Jia, D. M. (2013). Nano-lignin filled natural rubber composites: Preparation and characterization. *Express Polymer Letters*, *7*(5), 480–493. <https://doi.org/10.3144/expresspolymlett.2013.44>
- Jiang, X., Liu, J., Du, X., Hu, Z., Chang, H. M., & Jameel, H. (2018a). Phenolation to Improve Lignin Reactivity toward Thermosets Application. *ACS Sustainable Chemistry and Engineering*, *6*(4), 5504–5512. <https://doi.org/10.1021/acssuschemeng.8b00369>
- Jiang, X., Liu, J., Du, X., Hu, Z., Chang, H. M., & Jameel, H. (2018b). Phenolation to Improve Lignin Reactivity toward Thermosets Application. *ACS Sustainable Chemistry and Engineering*, *6*(4), 5504–5512. <https://doi.org/10.1021/acssuschemeng.8b00369>
- Jiang, X., Savithri, D., Du, X., Pawar, S., Jameel, H., Chang, H. M., & Zhou, X. (2017). Fractionation and Characterization of Kraft Lignin by Sequential Precipitation with Various Organic Solvents. *ACS Sustainable Chemistry and Engineering*, *5*(1), 835–842. <https://doi.org/10.1021/acssuschemeng.6b02174>
- Johnson, G. T., Loehle, C., Zhou, S. S., Chiossone, C., Palumbo, J., & Wiegand, P. (2021). Evaluation of the Survivability of SARS-CoV-2 on Cardboard and Plastic Surfaces and the Transferability of Virus from Surface to Skin. *Occupational Diseases and Environmental Medicine*, *09*(02), 63–73. <https://doi.org/10.4236/odem.2021.92006>
- Ju, J., Chen, X., Xie, Y., Yu, H., Guo, Y., Cheng, Y., Qian, H., & Yao, W. (2019). Application of essential oil as a sustained release preparation in food packaging. In *Trends in Food Science and Technology* (Vol. 92, pp. 22–32). Elsevier Ltd. <https://doi.org/10.1016/j.tifs.2019.08.005>

- Kabalnov, A. (1998). Thermodynamic and theoretical aspects of emulsions and their stability. *Current Opinion in Colloid and Interface Science*, 3(3), 270–275.  
[https://doi.org/10.1016/S1359-0294\(98\)80071-X](https://doi.org/10.1016/S1359-0294(98)80071-X)
- Kabalnov, A. (2001). Ostwald Ripening and Related Phenomena. In *J. Dispersion Science and Technology* (Vol. 22, Issue 1). [www.dekker.com](http://www.dekker.com)
- Kämäräinen, T., Ago, M., Seitsonen, J., Raula, J., Kauppinen, E. I., Ruokolainen, J., & Rojas, O. J. (2018a). Harmonic analysis of surface instability patterns on colloidal particles. *Soft Matter*, 14(17), 3387–3396. <https://doi.org/10.1039/c8sm00383a>
- Kämäräinen, T., Ago, M., Seitsonen, J., Raula, J., Kauppinen, E. I., Ruokolainen, J., & Rojas, O. J. (2018b). Harmonic analysis of surface instability patterns on colloidal particles. *Soft Matter*, 14(17), 3387–3396. <https://doi.org/10.1039/c8sm00383a>
- Karatutlu, A., Barhoum, A., & Sapelkin, A. (2018). Theories of nanoparticle and nanostructure formation in liquid phase. In *Emerging Applications of Nanoparticles and Architectural Nanostructures: Current Prospects and Future Trends* (pp. 597–619). Elsevier Inc.  
<https://doi.org/10.1016/B978-0-323-51254-1.00020-8>
- Karumathil, D. P., Upadhyay, A., & Venkitanarayanan, K. (2016). Antimicrobial Packaging for Poultry. In *Antimicrobial Food Packaging*. Elsevier Inc. <https://doi.org/10.1016/B978-0-12-800723-5.00019-X>
- Kitz, R., Walker, T., Charlebois, S., & Music, J. (2021). Food Packaging During the COVID-19 Pandemic: Consumer Perceptions. *International Journal of Consumer Studies*, March, 1–15. <https://doi.org/10.1111/ijcs.12691>
- Komaiko, J., & McClements, D. J. (2015). Low-energy formation of edible nanoemulsions by spontaneous emulsification: Factors influencing particle size. *Journal of Food Engineering*, 146, 122–128. <https://doi.org/10.1016/j.jfoodeng.2014.09.003>
- Koopmans, M., & Duizer, E. (2004). Foodborne viruses: an emerging problem. *International Journal of Food Microbiology*, 90(1), 23–41. [https://doi.org/10.1016/S0168-1605\(03\)00169-7](https://doi.org/10.1016/S0168-1605(03)00169-7)
- Kramer, A., Schwebke, I., & Kampf, G. (2006). How long do nosocomial pathogens persist on inanimate surfaces? A systematic review. *BMC Infectious Diseases*, 6, 1–8.  
<https://doi.org/10.1186/1471-2334-6-130>

- Krogsgård Nielsen, C., Kjems, J., Mygind, T., Snabe, T., Schwarz, K., Serfert, Y., & Meyer, R. L. (2016). Enhancing the antibacterial efficacy of isoeugenol by emulsion encapsulation. *International Journal of Food Microbiology*, 229, 7–14.  
<https://doi.org/10.1016/j.ijfoodmicro.2016.04.002>
- Kumar, S., Mukherjee, A., & Dutta, J. (2020). Chitosan based nanocomposite films and coatings: Emerging antimicrobial food packaging alternatives. *Trends in Food Science and Technology*, 97(August 2019), 196–209. <https://doi.org/10.1016/j.tifs.2020.01.002>
- Kun, D., & Pukánszky, B. (2017). Polymer/lignin blends: Interactions, properties, applications. *European Polymer Journal*, 93(April 2017), 618–641.  
<https://doi.org/10.1016/j.eurpolymj.2017.04.035>
- Kusumaningrum, H. D., Riboldi, G., Hazeleger, W. C., & Beumer, R. R. (2003). Survival of foodborne pathogens on stainless steel surfaces and cross-contamination to foods. *International Journal of Food Microbiology*, 85(3), 227–236.  
[https://doi.org/10.1016/S0168-1605\(02\)00540-8](https://doi.org/10.1016/S0168-1605(02)00540-8)
- Lam, S., Velikov, K. P., & Velev, O. D. (2014). Pickering stabilization of foams and emulsions with particles of biological origin. In *Current Opinion in Colloid and Interface Science* (Vol. 19, Issue 5, pp. 490–500). Elsevier Ltd. <https://doi.org/10.1016/j.cocis.2014.07.003>
- Lamer, V. K., & Dinegar, R. H. (1950). Theory, Production and Mechanism of Formation of Monodispersed Hydrosols. *Journal of the American Chemical Society*, 72(11), 4847–4854.  
<https://doi.org/10.1021/ja01167a001>
- Lammari, N., Louaer, O., Meniai, A. H., & Elaissari, A. (2020). Encapsulation of essential oils via nanoprecipitation process: Overview, progress, challenges and prospects. *Pharmaceutics*, 12(5), 1–21. <https://doi.org/10.3390/pharmaceutics12050431>
- Lepeltier, E., Bourgaux, C., & Couvreur, P. (2014a). Nanoprecipitation and the “Ouzo effect”: Application to drug delivery devices. *Advanced Drug Delivery Reviews*, 71, 86–97.  
<https://doi.org/10.1016/j.addr.2013.12.009>
- Lepeltier, E., Bourgaux, C., & Couvreur, P. (2014b). Nanoprecipitation and the “Ouzo effect”: Application to drug delivery devices. In *Advanced Drug Delivery Reviews* (Vol. 71, pp. 86–97). Elsevier. <https://doi.org/10.1016/j.addr.2013.12.009>
- Leskinen, T., Smyth, M., Xiao, Y., Lintinen, K., Mattinen, M. L., Kostianen, M. A., Oinas, P., & Österberg, M. (2017a). Scaling Up Production of Colloidal Lignin Particles. *Nordic Pulp*

- and Paper Research Journal*, 32(4), 586–596. [https://doi.org/10.3183/npprj-2017-32-04\\_p586-596\\_leskinen](https://doi.org/10.3183/npprj-2017-32-04_p586-596_leskinen)
- Leskinen, T., Smyth, M., Xiao, Y., Lintinen, K., Mattinen, M.-L., Kostainen, M. A., Oinas, P., & Österberg, M. (2017b). Scaling Up Production of Colloidal Lignin Particles - OPEN ACCESS. *Nordic Pulp and Paper Research Journal*, 32(04), 586–596. <https://doi.org/10.3183/npprj-2017-32-04-p586-596>
- Leskinen, T., Smyth, M., Xiao, Y., Lintinen, K., Mattinen, M.-L., Kostainen, M. A., Oinas, P., Österberg, M., & Kostainen, M. (n.d.). Scaling Up Production of Colloidal Lignin Particles. In *SPECIAL ISSUE LIGNIN Nordic Pulp & Paper Research Journal* (Vol. 32).
- Li, B., Deng, A., Li, K., Hu, Y., Li, Z., Xiong, Q., Liu, Z., Guo, Q., Zou, L., Zhang, H., Zhang, M., Ouyang, F., Su, J., Su, W., Xu, J., Lin, H., Sun, J., Peng, J., Jiang, H., ... Lu, J. (2021). Viral infection and transmission in a large, well-traced outbreak caused by the SARS-CoV-2 Delta variant. *MedRxiv*, 2021.07.07.21260122.
- Li, J., Xu, X., Chen, Z., Wang, T., Lu, Z., Hu, W., & Wang, L. (2018). Zein / gum Arabic nanoparticle-stabilized Pickering emulsion with thymol as an antibacterial delivery system. *Carbohydrate Polymers*, 200(August), 416–426. <https://doi.org/10.1016/j.carbpol.2018.08.025>
- Lievonen, M., Valle-Delgado, J. J., Mattinen, M. L., Hult, E. L., Lintinen, K., Kostainen, M. A., Paananen, A., Szilvay, G. R., Setälä, H., & Österberg, M. (2016). A simple process for lignin nanoparticle preparation. *Green Chemistry*, 18(5), 1416–1422. <https://doi.org/10.1039/c5gc01436k>
- Lifshitz, I. M., & Slyzov, V. V. (1961). THE KINETICS OF PRECIPITATION FROM SUPERSATURATED SOLID SOLUTIONS\*. *Physics and Chemistry of Solids*, 19(1), 35–50. <https://doi.org/10.4324/9781315634227>
- Lignin extraction process*. (n.d.). Retrieved July 20, 2022, from <https://www.valmet.com/pulp/other-value-adding-processes/lignin-extraction/lignoboost-process/>
- Lim, L. T. (2019). Active and intelligent packaging materials. *Comprehensive Biotechnology*, 2011, 688–702. <https://doi.org/10.1016/B978-0-444-64046-8.00248-2>

- Lin, N., Verma, D., Saini, N., Arbi, R., Munir, M., Jovic, M., & Turak, A. (2021). Antiviral nanoparticles for sanitizing surfaces: a roadmap to self-sterilizing against COVID-19. *Nano Today*, 101267. <https://doi.org/10.1016/j.nantod.2021.101267>
- List of Selected Multistate Foodborne Outbreak Investigations | Foodborne Outbreaks | Food Safety | CDC.* (n.d.). Retrieved September 1, 2021, from <https://www.cdc.gov/foodsafety/outbreaks/multistate-outbreaks/outbreaks-list.html>
- Liz-Marzán, L. M., Correa-Duarte, M. A., Pastoriza-Santos, I., Mulvaney, P., Ung, T., Giersig, M., & Kotov, N. A. (2001). Core-Shell Nanoparticles and Assemblies Thereof. *Handbook of Surfaces and Interfaces of Materials*, 3, 189–237. <https://doi.org/10.1016/b978-012513910-6/50038-4>
- Lizundia, E., Sipponen, M. H., Greca, L. G., Balakshin, M., Tardy, B. L., Rojas, O. J., & Puglia, D. (2021). Multifunctional lignin-based nanocomposites and nanohybrids. In *Green Chemistry* (Vol. 23, Issue 18, pp. 6698–6760). Royal Society of Chemistry. <https://doi.org/10.1039/d1gc01684a>
- Ma, M., Dai, L., Xu, J., Liu, Z., & Ni, Y. (2020). A simple and effective approach to fabricate lignin nanoparticles with tunable sizes based on lignin fractionation. *Green Chemistry*, 22(6), 2011–2017. <https://doi.org/10.1039/d0gc00377h>
- Malhotra, B., Keshwani, A., & Kharkwal, H. (2015). Antimicrobial food packaging: Potential and pitfalls. *Frontiers in Microbiology*, 6(JUN), 1–9. <https://doi.org/10.3389/fmicb.2015.00611>
- Mallakpour, S., Azadi, E., & Hussain, C. M. (2021). Recent breakthroughs of antibacterial and antiviral protective polymeric materials during COVID-19 pandemic and after pandemic: Coating, packaging, and textile applications. *Current Opinion in Colloid & Interface Science*, 55, 101480. <https://doi.org/10.1016/j.cocis.2021.101480>
- Marchese, A., Barbieri, R., Coppo, E., Orhan, I. E., Daglia, M., Nabavi, S. F., Izadi, M., Abdollahi, M., Nabavi, S. M., & Ajami, M. (2017). Antimicrobial activity of eugenol and essential oils containing eugenol: A mechanistic viewpoint. In *Critical Reviews in Microbiology* (Vol. 43, Issue 6, pp. 668–689). Taylor and Francis Ltd. <https://doi.org/10.1080/1040841X.2017.1295225>

- Marquez, R., Tolosa, L., & Celis, M. T. (2021). Understanding COVID-19 effect on the U.S. supply chain of strategic products: important factors, current situation, and future perspective. *Ciencia e Ingenieria*, 42(1), 53–62.
- Marquez, R., Zwilling, J., Zambrano, F., Tolosa, L., Marquez, M. E., Venditti, R., Jameel, H., & Gonzalez, R. (2022). Nanoparticles and essential oils with antiviral activity on packaging and surfaces: An overview of their selection and application. *Journal of Surfactants and Detergents*. <https://doi.org/10.1002/jsde.12609>
- Marqusee, J. A., & Ross, J. (1984). Theory of Ostwald ripening: Competitive growth and its dependence on volume fraction. *The Journal of Chemical Physics*, 80(1), 536–543. <https://doi.org/10.1063/1.446427>
- Marzoli, F., Bortolami, A., Pezzuto, A., Mazzetto, E., Piro, R., Terregino, C., Bonfante, F., & Belluco, S. (2021). A systematic review of human coronaviruses survival on environmental surfaces. *Science of The Total Environment*, 778, 146191. <https://doi.org/https://doi.org/10.1016/j.scitotenv.2021.146191>
- Maurya, A., Prasad, J., Das, S., & Dwivedy, A. K. (2021). Essential Oils and Their Application in Food Safety. *Frontiers in Sustainable Food Systems*, 5(May). <https://doi.org/10.3389/fsufs.2021.653420>
- McClements, D. J., & Rao, J. (2011). Food-Grade nanoemulsions: Formulation, fabrication, properties, performance, Biological fate, and Potential Toxicity. *Critical Reviews in Food Science and Nutrition*, 51(4), 285–330. <https://doi.org/10.1080/10408398.2011.559558>
- Millet, Y., Jouglard, J., Steinmetz, M. D., Tognetti, P., Joanny, P., & Arditti, J. (1981). Toxicity of Some Essential Plant Oils. Clinical and Experimental Study. *Clinical Toxicology*, 18(12), 1485–1498. <https://doi.org/10.3109/15563658108990357>
- Mishra, P. K., & Ekielski, A. (2019). The Self-Assembly of Lignin and Its Application in Nanoparticle Synthesis: A Short Review. *Nanomaterials*, 9(2), 243. <https://doi.org/10.3390/nano9020243>
- Moreno, A., & Sipponen, M. H. (2020). Lignin-based smart materials: A roadmap to processing and synthesis for current and future applications. *Materials Horizons*, 7(9), 2237–2257. <https://doi.org/10.1039/d0mh00798f>
- Moreno, L. B., José, M., Martínez, S., Antolinos, V., Chumillas, M. R., Segura, L. N., Jover, S. S., Benito, G., Hernández, M., & Gómez, A. L. (2020). Active cardboard box with a coating

- including essential oils entrapped within cyclodextrins and / or halloysite nanotubes . A case study for fresh tomato storage. *Food Control*, 107(July 2019), 106763.  
<https://doi.org/10.1016/j.foodcont.2019.106763>
- National Center for Biotechnology Information. (2020a). *PubChem Compound Summary for CID 180, Acetone*. <https://pubchem.ncbi.nlm.nih.gov/compound/Acetone>.
- National Center for Biotechnology Information. (2020b). *PubChem Compound Summary for CID 702, Ethanol*.
- National Center for Biotechnology Information. (2020c). *PubChem Compound Summary for CID 8028, Tetrahydrofuran*. <https://pubchem.ncbi.nlm.nih.gov/compound/Tetrahydrofuran>.
- Nicholson, R. L., & Hammerschmidt, R. (1992). *Phenolic compounds and their role in disease resistance*.
- Nypelö, T. E., Carrillo, C. A., & Rojas, O. J. (2015). Lignin supracolloids synthesized from (W/O) microemulsions: Use in the interfacial stabilization of Pickering systems and organic carriers for silver metal. *Soft Matter*, 11(10), 2046–2054.  
<https://doi.org/10.1039/c4sm02851a>
- Oliveira, M. B. S., Valentim, I. B., Rocha, T. S., Santos, J. C., Pires, K. S. N., Tanabe, E. L. L., Borbely, K. S. C., Borbely, A. U., & Goulart, M. O. F. (2020). Schinus terebenthifolius Raddi extracts: From sunscreen activity toward protection of the placenta to Zika virus infection, new uses for a well-known medicinal plant. *Industrial Crops and Products*, 152, 112503. <https://doi.org/10.1016/j.indcrop.2020.112503>
- Ontiveros, J. F., Pierlot, C., Catté, M., Molinier, V., Pizzino, A., Salager, J.-L., & Aubry, J. M. (2013). Classification of ester oils according to their Equivalent Alkane Carbon Number (EACN) and asymmetry of fish diagrams of C10E4/ester oil/water systems. *Journal of Colloid and Interface Science*, 403, 67–76. <https://doi.org/10.1016/j.jcis.2013.03.071>
- Österberg, M., Sipponen, M. H., Mattos, B. D., & Rojas, O. J. (2020). Spherical lignin particles: A review on their sustainability and applications. In *Green Chemistry* (Vol. 22, Issue 9, pp. 2712–2733). Royal Society of Chemistry. <https://doi.org/10.1039/d0gc00096e>
- Ostwald ripening. (2008). *IUPAC Compendium of Chemical Terminology*, 1801, 4348.  
<https://doi.org/10.1351/goldbook.o04348>
- Otter, J. A., Yezli, S., Salkeld, J. A. G., & French, G. L. (2013). Evidence that contaminated surfaces contribute to the transmission of hospital pathogens and an overview of strategies

- to address contaminated surfaces in hospital settings. *American Journal of Infection Control*, 41(5 SUPPL.), S6. <https://doi.org/10.1016/j.ajic.2012.12.004>
- Pang, T., Wang, G., Sun, H., Wang, L., Liu, Q., Sui, W., Parvez, A. M., & Si, C. (2020a). Lignin Fractionation for Reduced Heterogeneity in Self-Assembly Nanosizing: Toward Targeted Preparation of Uniform Lignin Nanoparticles with Small Size. *ACS Sustainable Chemistry and Engineering*, 8(24), 9174–9183. <https://doi.org/10.1021/acssuschemeng.0c02967>
- Pang, T., Wang, G., Sun, H., Wang, L., Liu, Q., Sui, W., Parvez, A. M., & Si, C. (2020b). Lignin Fractionation for Reduced Heterogeneity in Self-Assembly Nanosizing: Toward Targeted Preparation of Uniform Lignin Nanoparticles with Small Size. *ACS Sustainable Chemistry and Engineering*, 8(24), 9174–9183. <https://doi.org/10.1021/acssuschemeng.0c02967>
- Papadopoulou, V., Kosmidis, K., Vlachou, M., & Macheras, P. (2006). On the use of the Weibull function for the discernment of drug release mechanisms. *International Journal of Pharmaceutics*, 309(1–2), 44–50. <https://doi.org/10.1016/j.ijpharm.2005.10.044>
- Patrignani, F., Siroli, L., Gardini, F., & Lanciotti, R. (2016). Contribution of two different packaging material to microbial contamination of peaches: Implications in their microbiological quality. *Frontiers in Microbiology*, 7(JUN), 1–13. <https://doi.org/10.3389/fmicb.2016.00938>
- Pattnaik, S., Subramanyam, V. R., Bapaji, M., & Kole, C. R. (1997). Antibacterial and antifungal activity of aromatic constituents of essential oils. *Microbios*, 89(358), 39–46.
- Peng, R., Yang, D., Qiu, X., Qin, Y., & Zhou, M. (2020). Preparation of self-dispersed lignin-based drug-loaded material and its application in avermectin nano-formulation. *International Journal of Biological Macromolecules*, 151, 421–427. <https://doi.org/10.1016/j.ijbiomac.2020.02.114>
- Petrović, T., & D'Agostino, M. (2016). Viral Contamination of Food. *Antimicrobial Food Packaging*, 65–79. <https://doi.org/10.1016/B978-0-12-800723-5.00005-X>
- Piombino, C., Lange, H., Sabuzi, F., Galloni, P., Conte, V., & Crestini, C. (2020). Lignosulfonate microcapsules for delivery and controlled release of thymol and derivatives. *Molecules*, 25(4). <https://doi.org/10.3390/molecules25040866>
- Pitt, J. I., & Hocking, A. D. (2009a). Fungi and food spoilage. In *Fungi and Food Spoilage*. Springer US. <https://doi.org/10.1007/978-0-387-92207-2>

- Pitt, J. I., & Hocking, A. D. (2009b). Fungi and food spoilage. In *Fungi and Food Spoilage*. Springer US. <https://doi.org/10.1007/978-0-387-92207-2>
- Poulson, B. G., Alsulami, Q. A., Sharfalddin, A., El Agammy, Emam. F., Mouffouk, F., Emwas, A.-H., Jaremko, L., & Jaremko, M. (2022). Cyclodextrins: Structural, Chemical, and Physical Properties, and Applications. In *Polysaccharides* (Vol. 3, Issue 1). <https://doi.org/10.3390/polysaccharides3010001>
- Pradhan, A. K., Li, M., Li, Y., Kelso, L. C., Costello, T. A., & Johnson, M. G. (2012). A modified weibull model for growth and survival of listeria innocua and salmonella typhimurium in chicken breasts during refrigerated and frozen storage. *Poultry Science*, *91*(6), 1482–1488. <https://doi.org/10.3382/ps.2011-01851>
- Prakash, A., Baskaran, R., Paramasivam, N., & Vadivel, V. (2018). Essential oil based nanoemulsions to improve the microbial quality of minimally processed fruits and vegetables : A review. *Food Research International*, *111*(December 2017), 509–523. <https://doi.org/10.1016/j.foodres.2018.05.066>
- Prasad, R., Ashok, B., Oinas, P., Lintinen, K., Sarwar, G., Kostianen, M. A., Österberg, M., Ashok, R. P. B., Oinas, P., Lintinen, K., Golam, S., Kostianen, M. A., & Österberg, M. (2018). Techno-economic assessment for the large-scale production of colloidal lignin particles. *Green Chemistry*, 4911–4919. <https://doi.org/10.1039/C8GC02805B>
- Pylypchuk, I. V., Lindén, P. A., Lindström, M. E., & Sevastyanova, O. (2020). New Insight into the Surface Structure of Lignin Nanoparticles Revealed by <sup>1</sup>H Liquid-State NMR Spectroscopy. *ACS Sustainable Chemistry and Engineering*, *8*(36), 13805–13812. <https://doi.org/10.1021/acssuschemeng.0c05119>
- Pylypchuk, I. v., Riazanova, A., Lindström, M. E., & Sevastyanova, O. (2021). Structural and molecular-weight-dependency in the formation of lignin nanoparticles from fractionated soft- And hardwood lignins. *Green Chemistry*, *23*(8), 3061–3072. <https://doi.org/10.1039/d0gc04058d>
- Qian, Y., Lü, L., Qiu, X., Deng, Y., Zhao, H., & Wang, B. (2016). Hollow lignin azo colloids encapsulated avermectin with high anti-photolysis and controlled release performance. *Industrial Crops and Products*, *87*, 191–197. <https://doi.org/10.1016/j.indcrop.2016.03.056>
- Qian, Y., Qiu, X., Zhong, X., Zhang, D., Deng, Y., Yang, D., & Zhu, S. (2015). Lignin Reverse Micelles for UV-Absorbing and High Mechanical Performance Thermoplastics. *Industrial*

- and Engineering Chemistry Research*, 54(48), 12025–12030.  
<https://doi.org/10.1021/acs.iecr.5b03360>
- Qian, Y., Qiu, X., & Zhu, S. (2015). Lignin: A nature-inspired sun blocker for broadspectrum Sunscreens. *Green Chemistry*, 17(1), 320–324. <https://doi.org/10.1039/c4gc01333f>
- Queste, S., Salager, J. L., Strey, R., & Aubry, J. M. (2007). The EACN scale for oil classification revisited thanks to fish diagrams. *Journal of Colloid and Interface Science*, 312(1), 98–107. <https://doi.org/10.1016/j.jcis.2006.07.004>
- Ragnar, M., Lindgren, C. T., & Nilvebrant, N. O. (2000). pKa-values of guaiacyl and syringyl phenols related to lignin. *Journal of Wood Chemistry and Technology*, 20(3), 277–305. <https://doi.org/10.1080/02773810009349637>
- Rahman, O. U., Shi, S., Ding, J., Wang, D., Ahmad, S., & Yu, H. (2018). Lignin nanoparticles: Synthesis, characterization and corrosion protection performance. *New Journal of Chemistry*, 42(5), 3415–3425. <https://doi.org/10.1039/c7nj04103a>
- Rai, S., Dutta, P. K., Mehrotra, G. K., Helanto, K., Matikainen, L., Talj, R., & Rojas, O. J. (2017). Lignin incorporated antimicrobial chitosan film for food packaging application. *Journal of Polymer Materials*, 34(1), 171–183. <https://doi.org/10.15376/biores.14.2.Helanto>
- Ratke, L., & Voorhees, P. W. (2002). Growth and coarsening: Ostwald ripening in materials processing. *Choice Reviews Online*, 117–118. <https://doi.org/10.5860/choice.39-6445>
- Ravindran Chandrasekaran, A., Yoke Jia, C., Sheau Theng, C., Muniandy, T., Muralidharan, S., & Arumugam Dhanaraj, S. (n.d.). Invitro studies and evaluation of metformin marketed tablets-Malaysia. *Journal of Applied Pharmaceutical Science*, 2011(05), 214–217.
- Rawdkuen, S., Punbusayakul, N., & Lee, D. S. (2016). Antimicrobial Packaging for Meat Products. *Antimicrobial Food Packaging*, 229–241. <https://doi.org/10.1016/B978-0-12-800723-5.00017-6>
- Razzini, K., Castrica, M., Menchetti, L., Maggi, L., Negroni, L., Orfeo, N. V, Pizzoccheri, A., Stocco, M., Muttini, S., & Balzaretto, C. M. (2020). SARS-CoV-2 RNA detection in the air and on surfaces in the COVID-19 ward of a hospital in Milan, Italy. *Science of The Total Environment*, 742, 140540. <https://doi.org/10.1016/j.scitotenv.2020.140540>
- Reichardt, C., & Welton, T. (2010). Solvents and Solvent Effects in Organic Chemistry: Fourth Edition. In *Solvents and Solvent Effects in Organic Chemistry: Fourth Edition*. <https://doi.org/10.1002/9783527632220>

- Ribeiro, C., Lee, E. J. H., Longo, E., & Leite, E. R. (2005). A Kinetic model to describe nanocrystal growth by the oriented attachment mechanism. *ChemPhysChem*, 6(4), 690–696. <https://doi.org/10.1002/cphc.200400505>
- Richter, A. P., Bharti, B., Armstrong, H. B., Brown, J. S., Plemmons, D., Paunov, V. N., Stoyanov, S. D., & Velev, O. D. (2016). Synthesis and characterization of biodegradable lignin nanoparticles with tunable surface properties. *Langmuir*, 32(25), 6468–6477. <https://doi.org/10.1021/acs.langmuir.6b01088>
- Richter, A. P., Brown, J. S., Bharti, B., Wang, A., Gangwal, S., Houck, K., Cohen Hubal, E. A., Paunov, V. N., Stoyanov, S. D., & Velev, O. D. (2015a). An environmentally benign antimicrobial nanoparticle based on a silver-infused lignin core. *Nature Nanotechnology*, 10, 817–824. <https://doi.org/10.1038/NNANO.2015.141>
- Richter, A. P., Brown, J. S., Bharti, B., Wang, A., Gangwal, S., Houck, K., Cohen Hubal, E. A., Paunov, V. N., Stoyanov, S. D., & Velev, O. D. (2015b). An environmentally benign antimicrobial nanoparticle based on a silver-infused lignin core. *Nature Nanotechnology*, 10(9), 817–823. <https://doi.org/10.1038/nnano.2015.141>
- Roberts, T. (1986). A Retrospective Assessment of Human Health Protection Benefits from Removal of Tuberculous Beef 1. In *Journal of Food Protection* (Vol. 49, Issue 4). [http://meridian.allenpress.com/jfp/article-pdf/49/4/293/1657031/0362-028x-49\\_4\\_293.pdf](http://meridian.allenpress.com/jfp/article-pdf/49/4/293/1657031/0362-028x-49_4_293.pdf)
- Rokka, J., & Uusitalo, L. (2008). Preference for green packaging in consumer product choices – Do consumers care? *International Journal of Consumer Studies*, 32(5), 516–525. <https://doi.org/10.1111/j.1470-6431.2008.00710.x>
- Saad, W. S., & Prud'Homme, R. K. (2016). Principles of nanoparticle formation by flash nanoprecipitation. *Nano Today*, 11(2), 212–227. <https://doi.org/10.1016/j.nantod.2016.04.006>
- Salager, J.-L., Antón, R. E., Bullón, J., Forgiarini, A., & Marquez, R. (2020). How to Use the Normalized Hydrophilic-Lipophilic Deviation (HLDN) Concept for the Formulation of Equilibrated and Emulsified Surfactant-Oil-Water Systems for Cosmetics and Pharmaceutical Products. *Cosmetics*, 7(3), 57. <https://doi.org/10.3390/cosmetics7030057>
- Salager, J.-L., Antón, R. E., Sabatini, D. A., Harwell, J. H., Acosta, E. J., & Tolosa, L. I. (2005). Enhancing solubilization in microemulsions - State of the art and current trends. *Journal of Surfactants and Detergents*, 8(1), 3–21. <https://doi.org/10.1007/s11743-005-0328-4>

- Salager, J.-L., Forgiarini, A., & Marquez, R. (2019). Extended Surfactants Including an Alkoxylated Central Part Intermediate Producing a Gradual Polarity Transition—A Review of the Properties Used in Applications Such as Enhanced Oil Recovery and Polar Oil Solubilization in Microemulsions. *Journal of Surfactants and Detergents*, 22(5), 935–972. <https://doi.org/10.1002/jsde.12331>
- Salager, J.-L., Marquez, R., Bullon, J., & Forgiarini, A. (2022). Formulation in Surfactant Systems: From-Winsor-to-HLDN. *Encyclopedia*, 2(2). <https://doi.org/10.3390/encyclopedia2020054>
- Scallan, E., Hoekstra, R. M., Angulo, F. J., Tauxe, R. V., Widdowson, M. A., Roy, S. L., Jones, J. L., & Griffin, P. M. (2011). Foodborne illness acquired in the United States—Major pathogens. *Emerging Infectious Diseases*, 17(1), 7–15. <https://doi.org/10.3201/eid1701.P11101>
- Schubert, S., Delaney, J. T., & Schubert, U. S. (2011). Nanoprecipitation and nanoformulation of polymers: From history to powerful possibilities beyond poly(lactic acid). In *Soft Matter* (Vol. 7, Issue 5, pp. 1581–1588). <https://doi.org/10.1039/c0sm00862a>
- Schuerch, C. (1952a). *Solvent Properties of Liquids : Relation to Fractionation of Lignin 5061 The Solvent Properties of Liquids and Their Relation to the Solubility, Swelling, Isolation and Fractionation of Lignin*. <https://pubs.acs.org/sharingguidelines>
- Schuerch, C. (1952b). The Solvent Properties of Liquids and Their Relation to the Solubility, Swelling, Isolation and Fractionation of Lignin. *Journal of the American Chemical Society*, 74(20), 5061–5067. <https://doi.org/10.1021/ja01140a020>
- Setälä, H., Alakomi, H. L., Paananen, A., Szilvay, G. R., Kellock, M., Lievonen, M., Liljeström, V., Hult, E. L., Lintinen, K., Österberg, M., & Kostiainen, M. (2019). Lignin nanoparticles modified with tall oil fatty acid for cellulose functionalization. *Cellulose*, 9, 273–284. <https://doi.org/10.1007/s10570-019-02771-9>
- Shi, X., & Zhu, X. (2009). Biofilm formation and food safety in food industries. *Trends in Food Science and Technology*, 20(9), 407–413. <https://doi.org/10.1016/j.tifs.2009.01.054>
- Sipponen, M. H., Henn, A., Penttilä, P., & Österberg, M. (2020). Lignin-fatty acid hybrid nanocapsules for scalable thermal energy storage in phase-change materials. *Chemical Engineering Journal*, 393. <https://doi.org/10.1016/j.cej.2020.124711>

- Sipponen, M. H., Lange, H., Ago, M., & Crestini, C. (2018a). Understanding Lignin Aggregation Processes. A Case Study: Budesonide Entrapment and Stimuli Controlled Release from Lignin Nanoparticles [Research-article]. *ACS Sustainable Chemistry and Engineering*, 6(7), 9342–9351. <https://doi.org/10.1021/acssuschemeng.8b01652>
- Sipponen, M. H., Lange, H., Ago, M., & Crestini, C. (2018b). Understanding Lignin Aggregation Processes. A Case Study: Budesonide Entrapment and Stimuli Controlled Release from Lignin Nanoparticles. *ACS Sustainable Chemistry and Engineering*, 6(7), 9342–9351. <https://doi.org/10.1021/acssuschemeng.8b01652>
- Sipponen, M. H., Lange, H., Crestini, C., Henn, A., & Österberg, M. (2019). Lignin for Nano- and Microscaled Carrier Systems: Applications, Trends, and Challenges. *ChemSusChem*, 12(10), 2039–2054. <https://doi.org/10.1002/cssc.201900480>
- Sipponen, M. H., Smyth, M., Leskinen, T., Johansson, L. S., & Österberg, M. (2017). All-lignin approach to prepare cationic colloidal lignin particles: Stabilization of durable Pickering emulsions. *Green Chemistry*, 19(24), 5831–5840. <https://doi.org/10.1039/c7gc02900d>
- Siracusa, V. (2016). Packaging Material in the Food Industry. In *Antimicrobial Food Packaging*. Elsevier Inc. <https://doi.org/10.1016/B978-0-12-800723-5.00007-3>
- Siroli, L., Patrignani, F., Serrazanetti, D. I., Chiavari, C., Benevelli, M., Grazia, L., & Lanciotti, R. (2017a). Survival of spoilage and pathogenic microorganisms on cardboard and plastic packaging materials. *Frontiers in Microbiology*, 8(DEC), 1–10. <https://doi.org/10.3389/fmicb.2017.02606>
- Siroli, L., Patrignani, F., Serrazanetti, D. I., Chiavari, C., Benevelli, M., Grazia, L., & Lanciotti, R. (2017b). Survival of spoilage and pathogenic microorganisms on cardboard and plastic packaging materials. *Frontiers in Microbiology*, 8(DEC), 1–10. <https://doi.org/10.3389/fmicb.2017.02606>
- Siroli, L., Patrignani, F., Serrazanetti, D. I., Chiavari, C., Benevelli, M., Grazia, L., & Lanciotti, R. (2017c). Survival of spoilage and pathogenic microorganisms on cardboard and plastic packaging materials. *Frontiers in Microbiology*, 8(DEC), 1–10. <https://doi.org/10.3389/fmicb.2017.02606>
- Sirsat, S. A. (2020a). The persistence of foodborne pathogens on produce box cartons. *Journal of Environmental Health*, 82(6), 16–21.

- Sirsat, S. A. (2020b). The persistence of foodborne pathogens on produce box cartons. *Journal of Environmental Health*, 82(6), 16–21.
- Sirsat, S. A., Choi, J. K. K., Almanza, B. A., & Neal, J. A. (2013). Persistence of Salmonella and E. Coli on the surface of restaurant menus. *Journal of Environmental Health*, 75(7), 8–14.
- Sizun, J., Yu, M. W. N., & Talbot, P. J. (2000). Survival of human coronaviruses 229E and OC43 in suspension and after drying on surfaces: A possible source of hospital-acquired infections. *Journal of Hospital Infection*, 46(1), 55–60.  
<https://doi.org/10.1053/jhin.2000.0795>
- Slavova, T. G., Radulova, G. M., Kralchevsky, P. A., & Danov, K. D. (2020). Encapsulation of fragrances and oils by core-shell structures from silica nanoparticles, surfactant and polymer: Effect of particle size. *Colloids and Surfaces A Physicochemical and Engineering Aspects*, 606, 125558. <https://doi.org/10.1016/j.colsurfa.2020.125558>
- Slomkowski, S., Alemán, J. V., Gilbert, R. G., Hess, M., Horie, K., Jones, R. G., Kubisa, P., Meisel, I., Mormann, W., Penczek, S., & Stepto, R. F. T. (2011). Terminology of polymers and polymerization processes in dispersed systems (IUPAC recommendations 2011). *Pure and Applied Chemistry*, 83(12), 2229–2259. <https://doi.org/10.1351/PAC-REC-10-06-03>
- Snyder, A. B., & Worobo, R. W. (2018). Fungal spoilage in food processing. In *Journal of Food Protection* (Vol. 81, Issue 6, pp. 1035–1040). International Association for Food Protection. <https://doi.org/10.4315/0362-028X.JFP-18-031>
- Stull, D. R. (1947). Vapor Pressure of Pure Substances. *Organic and Inorganic Compounds. Ind. Eng. Chem.*, 39(4), 517–540. <https://doi.org/10.1021/ie50448a022>
- Sun, H., Li, S., Chen, S., Wang, C., Liu, D., & Li, X. (2020). Antibacterial and antioxidant activities of sodium starch octenylsuccinate-based Pickering emulsion films incorporated with cinnamon essential oil. *International Journal of Biological Macromolecules*, 159, 696–703. <https://doi.org/10.1016/j.ijbiomac.2020.05.118>
- Sung, S. Y., Sin, L. T., Tee, T. T., Bee, S. T., Rahmat, A. R., Rahman, W. A. W. A., Tan, A. C., & Vikhraman, M. (2013). Antimicrobial agents for food packaging applications. *Trends in Food Science and Technology*, 33(2), 110–123. <https://doi.org/10.1016/j.tifs.2013.08.001>
- Suominen, I., Suihko, M. L., & Salkinoja-Salonen, M. (1997). Microscopic study of migration of microbes in food-packaging paper and board. *Journal of Industrial Microbiology and Biotechnology*, 19(2), 104–113. <https://doi.org/10.1038/sj.jim.2900424>

- Suprani, C., Gonçalves, S., Diirr, L., Irene, M., Carlos, J., Freitas, C. De, & Fernandes, D. (2019).  $\beta$ -Cyclodextrin inclusion complexes with essential oils : Obtention , characterization , antimicrobial activity and potential application for food preservative sachets. *Food Research International*, *119*(October 2018), 499–509.  
<https://doi.org/10.1016/j.foodres.2019.01.016>
- Takeda, Y., Jamsransuren, D., Matsuda, S., Crea, R., & Ogawa, H. (2021). The SARS-CoV-2-Inactivating Activity of Hydroxytyrosol-Rich Aqueous Olive Pulp Extract (HIDROX®) and Its Use as a Virucidal Cream for Topical Application. In *Viruses* (Vol. 13, Issue 2).  
<https://doi.org/10.3390/v13020232>
- Talapin, D. V., Rogach, A. L., Haase, M., & Weller, H. (2001). Evolution of an ensemble of nanoparticles in a colloidal solution: Theoretical study. *Journal of Physical Chemistry B*, *105*(49), 12278–12285. <https://doi.org/10.1021/jp012229m>
- Tang, C.-H., Chin, C.-Y., & Lee, Y.-H. (2021). Coronavirus disease outbreak and supply chain disruption: Evidence from Taiwanese firms in China. *Research in International Business and Finance*, *56*, 101355. <https://doi.org/10.1016/j.ribaf.2020.101355>
- Tang, Q., Qian, Y., Yang, D., Qiu, X., Qin, Y., & Zhou, M. (2020). Lignin-based nanoparticles: A review on their preparations and applications. *Polymers*, *12*(11), 1–22.  
<https://doi.org/10.3390/polym12112471>
- TAPPI T205 sp-02. (2006). Forming handsheets for physical tests of pulp. *TAPPI Press*, 1–9.
- TAPPI Test Methods. (1996). Kappa number of pulp - T236 cm-85. *TAPPI Press*.
- Tardy, B. L., Richardson, J. J., Guo, J., Lehtonen, J., Ago, M., & Rojas, O. J. (2018). Lignin nano- and microparticles as template for nanostructured materials: Formation of hollow metal-phenolic capsules. *Green Chemistry*, *20*(6), 1335–1344.  
<https://doi.org/10.1039/c8gc00064f>
- Thanh, N. T. K., Maclean, N., & Mahiddine, S. (2014). Mechanisms of nucleation and growth of nanoparticles in solution. *Chemical Reviews*, *114*(15), 7610–7630.  
<https://doi.org/10.1021/cr400544s>
- Tian, D., Hu, J., Bao, J., Chandra, R. P., Saddler, J. N., & Lu, C. (2017). Lignin valorization: Lignin nanoparticles as high-value bio-additive for multifunctional nanocomposites. *Biotechnology for Biofuels*, *10*(1), 1–11. <https://doi.org/10.1186/s13068-017-0876-z>

- Tirumkudulu, M. S. (2018). Buckling of a drying colloidal drop. *Soft Matter*, 14, 7455.  
<https://doi.org/10.1039/c8sm01324a>
- Upadhyay, A., Upadhyaya, I., Kollanoor-Johny, A., & Venkitanarayanan, K. (2013). Antibiofilm effect of plant derived antimicrobials on *Listeria monocytogenes*. *Food Microbiology*, 36(1), 79–89. <https://doi.org/10.1016/j.fm.2013.04.010>
- U.S. Department of Commerce. (2021). QUARTERLY RETAIL E-COMMERCE SALES 1st Quarter 2021 Estimated Measures of Sampling Variability for Quarterly U . S . Retail Sales Estimates : Total and E-commerce. In *U.S. Census Bureau News* (Issue 301).
- US EPA. (2018). *Containers and Packaging: Product-Specific Data | Facts and Figures about Materials, Waste and Recycling | US EPA*. <https://www.epa.gov/facts-and-figures-about-materials-waste-and-recycling/containers-and-packaging-product-specific-data>
- USDA ERS - *Cost Estimates of Foodborne Illnesses*. (n.d.). Retrieved September 13, 2021, from <https://www.ers.usda.gov/data-products/cost-estimates-of-foodborne-illnesses/>
- Valmet LignoBoost - *lignin extraction*. (n.d.). Retrieved July 24, 2022, from <https://www.valmet.com/pulp/other-value-adding-processes/lignin-extraction/>
- van Doremalen, N., Bushmaker, T., Morris, D. H., Holbrook, M. G., Gamble, A., Williamson, B. N., Tamin, A., Harcourt, J. L., Thornburg, N. J., Gerber, S. I., Lloyd-Smith, J. O., de Wit, E., & Munster, V. J. (2020a). Aerosol and Surface Stability of SARS-CoV-2 as Compared with SARS-CoV-1. *New England Journal of Medicine*, NEJMc2004973.  
<https://doi.org/10.1056/NEJMc2004973>
- van Doremalen, N., Bushmaker, T., Morris, D. H., Holbrook, M. G., Gamble, A., Williamson, B. N., Tamin, A., Harcourt, J. L., Thornburg, N. J., Gerber, S. I., Lloyd-Smith, J. O., de Wit, E., & Munster, V. J. (2020b). Aerosol and Surface Stability of SARS-CoV-2 as Compared with SARS-CoV-1. *New England Journal of Medicine*, NEJMc2004973.  
<https://doi.org/10.1056/NEJMc2004973>
- Vance, C. P., Kirk, T. K., & Sherwood, R. T. (1980). Lignification as a mechanism of disease resistance. *Annual Review of Phytopathology*, 1.
- Varona, S., Rodríguez Rojo, S., Martín, Á., Cocero, M. J., Serra, A. T., Crespo, T., & Duarte, C. M. M. (2013). Antimicrobial activity of lavandin essential oil formulations against three pathogenic food-borne bacteria. *Industrial Crops and Products*, 42, 243–250.  
<https://doi.org/10.1016/j.indcrop.2012.05.020>

- Vieira, A., & Boyer, M. (2015). *Foodborne Illness Source Attribution Estimates for Salmonella , Escherichia coli O157 ( E . coli O157 ), Listeria monocytogenes ( Lm ), and Campylobacter using Outbreak Surveillance Data Report Interagency Food Safety Analytics Collaboration ( IFSAC ) Pro. 157*(February), 1–12.
- Vitale, S. A., & Katz, J. L. (2003). Liquid droplet dispersions formed by homogeneous liquid-liquid nucleation: “The ouzo effect.” *Langmuir*, *19*(10), 4105–4110.  
<https://doi.org/10.1021/la026842o>
- Vlosky, R. P., Ozanne, L. K., & Fontenot, R. J. (1999). A conceptual model of US consumer willingness-to-pay for environmentally certified wood products. *Journal of Consumer Marketing*, *16*(2), 122–136. <https://doi.org/10.1108/07363769910260498>
- Wang, J., Qian, Y., Li, L., & Qiu, X. (2020). Atomic Force Microscopy and Molecular Dynamics Simulations for Study of Lignin Solution Self-Assembly Mechanisms in Organic–Aqueous Solvent Mixtures. *ChemSusChem*, 1–9.  
<https://doi.org/10.1002/cssc.201903132>
- Webster, A. J., & Cates, M. E. (1998). *Stabilization of Emulsions by Trapped Species*.  
<https://pubs.acs.org/sharingguidelines>
- Wei, Z., Yang, Y., Yang, R., & Wang, C. (2012). Alkaline lignin extracted from furfural residues for pH-responsive Pickering emulsions and their recyclable polymerization. *Green Chemistry*, *14*(11), 3230–3236. <https://doi.org/10.1039/c2gc36278c>
- WHO. (n.d.). *Food safety*.
- WHO. (2019). *Primary health care on the road to universal health coverage: 2019 global monitoring report*. World Health Organization.  
<https://apps.who.int/iris/bitstream/handle/10665/344057/9789240004276-eng.pdf?sequence=2>
- Wilks, S. A., Michels, H. T., & Keevil, C. W. (2006). Survival of *Listeria monocytogenes* Scott A on metal surfaces: Implications for cross-contamination. *International Journal of Food Microbiology*, *111*(2), 93–98. <https://doi.org/10.1016/j.ijfoodmicro.2006.04.037>
- Winsor, P. (1954). *Solvent properties of amphiphilic compounds*. Butterworths Scientific Publications.
- Won, G., & Lee, J. H. (2017). *Salmonella Typhimurium*, the major causative agent of foodborne illness inactivated by a phage lysis system provides effective protection against lethal

- challenge by induction of robust cell-mediated immune responses and activation of dendritic cells. *Veterinary Research*, 48(1). <https://doi.org/10.1186/s13567-017-0474-x>
- Yadav, E., Kumar, S., Mahant, S., Khatkar, S., & Rao, R. (2017). Tea tree oil: a promising essential oil. *Journal of Essential Oil Research*, 29(3), 201–213. <https://doi.org/10.1080/10412905.2016.1232665>
- Yahaya, W. A. W., Almajano, M. P., Yazid, N. A., & Azman, N. A. M. (2019). Antioxidant activities and total phenolic content of Malaysian herbs as components of active packaging film in beef patties. *Antioxidants*, 8(7). <https://doi.org/10.3390/antiox8070204>
- Yang, W., Owczarek, J. S., Fortunati, E., Kozanecki, M., Mazzaglia, A., Balestra, G. M., Kenny, J. M., Torre, L., & Puglia, D. (2016). Antioxidant and antibacterial lignin nanoparticles in polyvinyl alcohol/chitosan films for active packaging. *Industrial Crops and Products*, 94, 800–811. <https://doi.org/10.1016/j.indcrop.2016.09.061>
- Yasuda, T. (1991). Medical application of liposomes. In *Rinsho byori. The Japanese journal of clinical pathology: Vol. Suppl 91*. [https://doi.org/10.1016/0009-8981\(87\)90210-5](https://doi.org/10.1016/0009-8981(87)90210-5)
- Yearla, S. R., & Padmasree, K. (2016). Preparation and characterisation of lignin nanoparticles: evaluation of their potential as antioxidants and UV protectants. *Journal of Experimental Nanoscience*, 11(4), 289–302. <https://doi.org/10.1080/17458080.2015.1055842>
- Yildirim, S., Röcker, B., Pettersen, M. K., Nilsen-Nygaard, J., Ayhan, Z., Rutkaite, R., Radusin, T., Suminska, P., Marcos, B., & Coma, V. (2018). Active Packaging Applications for Food. In *Comprehensive Reviews in Food Science and Food Safety* (Vol. 17, Issue 1, pp. 165–199). Blackwell Publishing Inc. <https://doi.org/10.1111/1541-4337.12322>
- Zambrano, F., Marquez, R., Jameel, H., Venditti, R., & Gonzalez, R. (2021). Upcycling strategies for old corrugated containerboard to attain high-performance tissue paper: A viable answer to the packaging waste generation dilemma. *Resources, Conservation and Recycling*, 175(May), 105854. <https://doi.org/10.1016/j.resconrec.2021.105854>
- Zambrano, F., Wang, Y., Zwilling, J. D., Venditti, R., Jameel, H., Rojas, O., & Gonzalez, R. (2021). Micro- and nanofibrillated cellulose from virgin and recycled fibers: A comparative study of its effects on the properties of hygiene tissue paper. *Carbohydrate Polymers*, 254(August 2020), 117430. <https://doi.org/10.1016/j.carbpol.2020.117430>

- Zhang, W., He, H., Zhu, L., Liu, G., & Wu, L. (2021). Food Safety in Post-COVID-19 Pandemic: Challenges and Countermeasures. *Biosensors*, *11*(3), 71. <https://doi.org/10.3390/bios11030071>
- Zhao, C. (2016). *PARTICLE FORMATION AND GROWTH FOR SMALL MOLECULES AND POLYMERS BY NANOPRECIPIATION*.
- Zhao, W., Simmons, B., Singh, S., Ragauskas, A., & Cheng, G. (2016a). From lignin association to nano-/micro-particle preparation: Extracting higher value of lignin. In *Green Chemistry* (Vol. 18, Issue 21, pp. 5693–5700). <https://doi.org/10.1039/c6gc01813k>
- Zhao, W., Simmons, B., Singh, S., Ragauskas, A., & Cheng, G. (2016b). From lignin association to nano-/micro-particle preparation: Extracting higher value of lignin. In *Green Chemistry* (Vol. 18, Issue 21, pp. 5693–5700). Royal Society of Chemistry. <https://doi.org/10.1039/c6gc01813k>
- Zhou, Y., Sun, S., Bei, W., Zahi, M. R., Yuan, Q., & Liang, H. (2018). Preparation and antimicrobial activity of oregano essential oil Pickering emulsion stabilized by cellulose nanocrystals. *International Journal of Biological Macromolecules*, *112*, 7–13. <https://doi.org/10.1016/j.ijbiomac.2018.01.102>
- Zikeli, F., Vinciguerra, V., Sennato, S., Scarascia Mugnozza, G., & Romagnoli, M. (2020). Preparation of Lignin Nanoparticles with Entrapped Essential Oil as a Bio-Based Biocide Delivery System. *ACS Omega*, *5*(1), 358–368. <https://doi.org/10.1021/acsomega.9b02793>
- Zou, T., Nonappa, N., Khavani, M., Vuorte, M., Penttilä, P., Zitting, A., Valle-Delgado, J. J., Elert, A. M., Silbernagl, D., Balakshin, M., Sammalkorpi, M., & Österberg, M. (2021). Experimental and Simulation Study of the Solvent Effects on the Intrinsic Properties of Spherical Lignin Nanoparticles. *The Journal of Physical Chemistry B*, *125*(44), 12315–12328. <https://doi.org/10.1021/acs.jpccb.1c05319>
- Zwilling, J. D., Jiang, X., Zambrano, F., Venditti, R. A., Jameel, H., Velev, O. D., Rojas, O. J., & Gonzalez, R. (2021). Understanding lignin micro- And nanoparticle nucleation and growth in aqueous suspensions by solvent fractionation. *Green Chemistry*, *23*(2), 1001–1012. <https://doi.org/10.1039/d0gc03632c>

## 10 APPENDICES

## APPENDIX A: Supplementary Information for Chapter 3

### Short term effects of storage conditions

#### Methods

The paper specimens were stored on the laboratory benchtop in sterile, aerobic plastic petri dishes and inoculated with the bacterial inocula suspended in either TSB+ media or saline solution (NaCl, 8.5 g/L).

#### Results

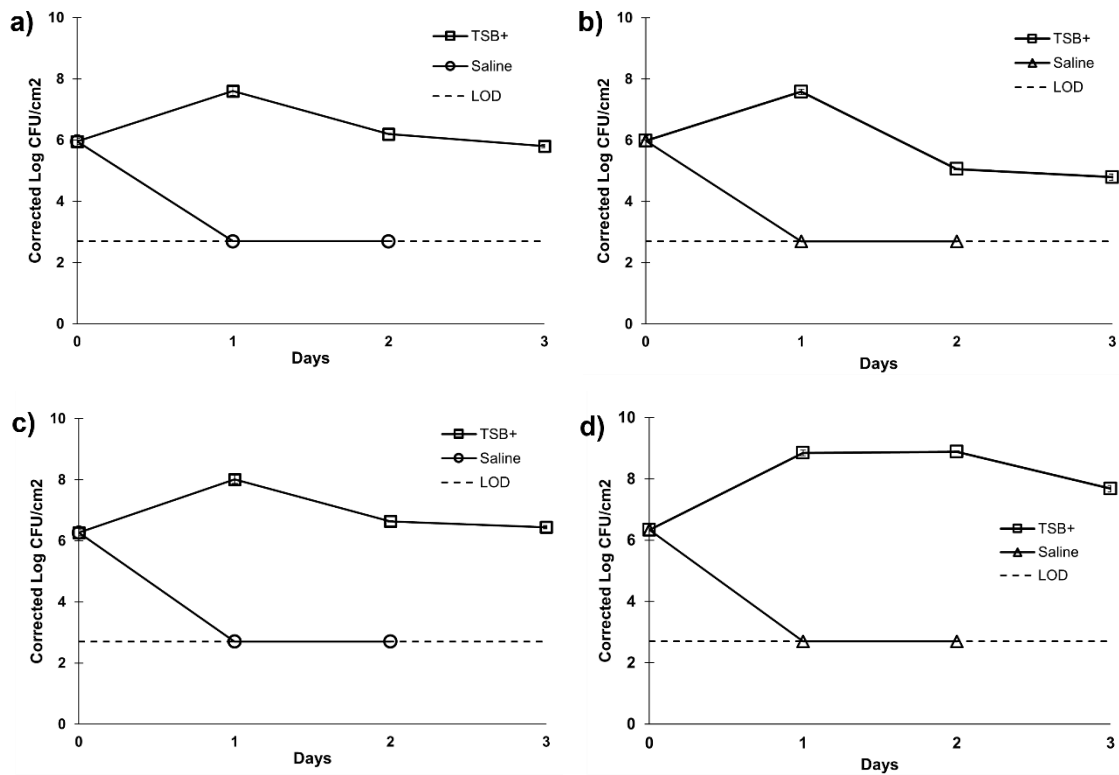


Figure S1: Short term growth and survivability of *Listeria innocua* (a,c) and *Salmonella Typhimurium* (b,d) on bleached (a,b) and unbleached (c,d) paper specimens stored in sterile petri dishes inoculated with nutrient media (TSB+) or saline solution (8.5 g/L NaCl).

## JSL code for comparison of slopes test

```
Fit Model(  
  Y( :Adjusted ),  
  Effects(  
    :BACTERIA,  
    :PAPER,  
    :BACTERIA * :PAPER,  
    :Day,  
    :BACTERIA * :Day,  
    :PAPER * :Day,  
    :BACTERIA * :PAPER * :Day  
  ),  
  Personality( "Standard Least Squares" ),  
  Emphasis( "Minimal Report" ),  
  Run(  
    :Adjusted << { Summary of Fit( 1 ), Analysis of Variance( 1 ),  
    Parameter Estimates( 1 ), Scaled Estimates( 0 ),  
    Plot Actual by Predicted( 0 ), Plot Regression( 0 ),  
    Plot Residual by Predicted( 0 ), Plot Studentized Residuals( 0 ),  
    Plot Effect Leverage( 0 ), Plot Residual by Normal Quantiles( 0 ),  
    Box Cox Y Transformation( 0 ), Custom Test(  
      [0 0 0 0 0 2 2 0,  
        0 0 0 0 0 2 0 2 0,  
        0 0 0 0 0 2 2 0 0,  
        0 0 0 0 0 2 -2 0 0,  
        0 0 0 0 0 2 0 -2 0,  
        0 0 0 0 0 0 2 -2 0],  
      Label( "compare slopes" )  
    )  
  )  
  ),  
  SendToReport(  
    Dispatch(  
      {"Response Adjusted", "Custom Test"},  
      " ",  
      TextBox,  
      {Set Text( "compare slopes" )})  
  )  
)
```

## Non-linear model of bacterial growth and decay

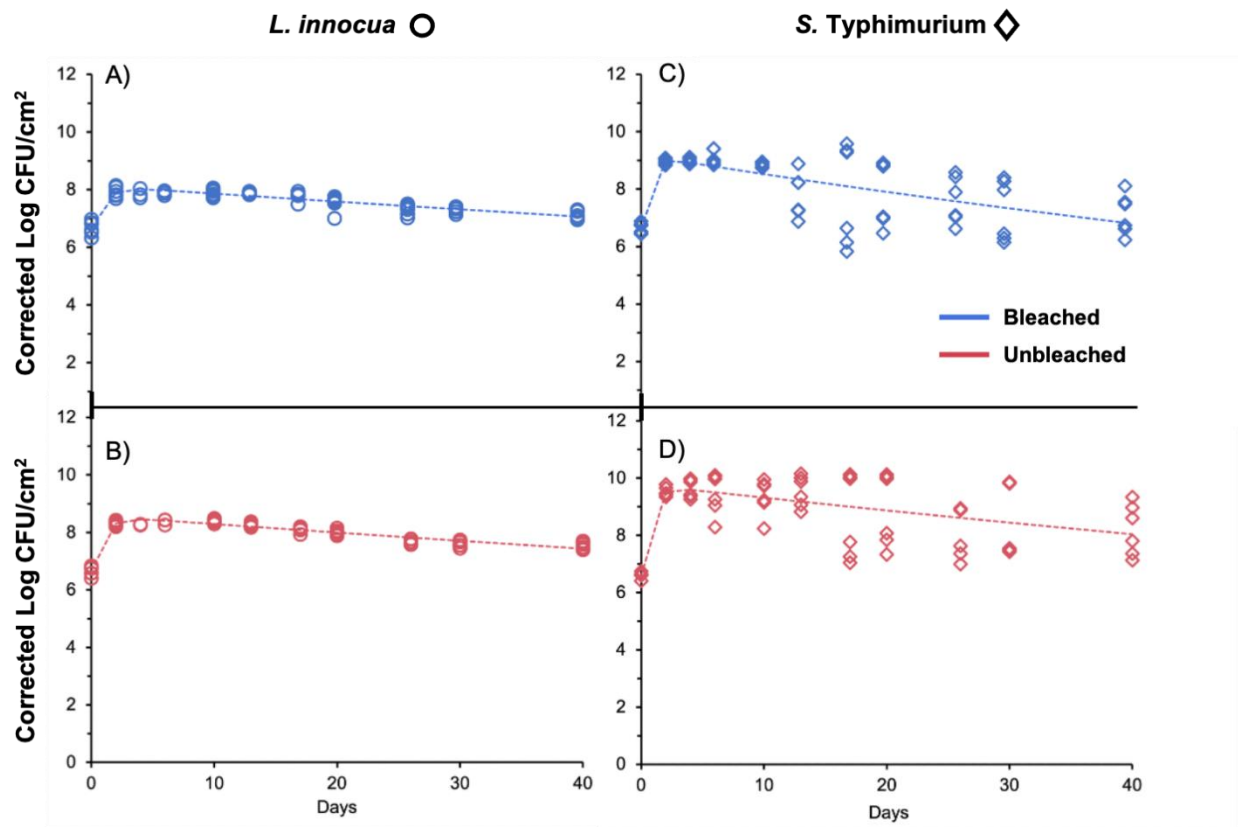


Figure S2: Nonlinear fit model for each of the four conditions (two bacteria, two papers). The average log CFU/m<sup>2</sup> was corrected for the extraction efficiencies ( $\epsilon$ ) as described previously.

Parameter estimates and standard errors are displayed in Table 3-2.

Table S1: Nonlinear model cell growth and mortality parameters calculated using JMP nonlinear modeling program. In Eq. S1,  $y_{max}$  is the estimated maximum bacterial count (log transformed) over the period studied,  $y_0$  is the estimated starting bacterial count. The model was fitted using log-transformed bacterial counts (log CFU). Growth ( $\alpha$ ) and mortality ( $\beta$ ) are constant rate parameters. SE is the standard error of the estimated rate values.

$\frac{y_{max} * y_0}{(y_{max} - y_0) * e^{-t * \alpha} + y_0 * e^{t * \beta}} \quad (S1)$				
<b><i>L. innocua</i></b>				
<b>Parameter</b>	<b>Bleached</b>	<b>SE</b>	<b>Unbleached</b>	<b>SE</b>
$y_{max}$	8.12	0.05	8.59	0.05
$y_0$	6.69	0.06	6.66	0.06
Growth ( $\alpha$ )	1.09	0.21	1.18	0.18
Mortality ( $\beta$ )	0.0036	0.0003	0.0036	0.0003
<b><i>S. Typhimurium</i></b>				
<b>Parameter</b>	<b>Bleached</b>	<b>SE</b>	<b>Unbleached</b>	<b>SE</b>
$y_{max}$	9.19	0.25	9.79	0.24
$y_0$	6.64	0.34	6.61	0.34
Growth ( $\alpha$ )	1.93	2.87	1.65	1.23
Mortality ( $\beta$ )	0.007	0.0013	0.0049	0.0012

## Microscopic images of paper specimens

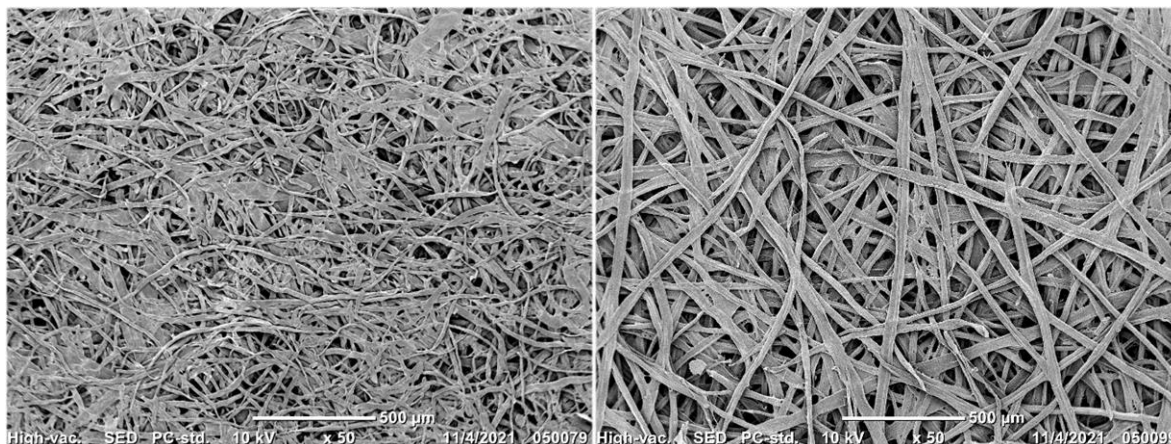


Figure S10-1: Scanning electron microscope image of bleached (left) and unbleached (right) paper specimens. SEM images were taken of the paper specimens with a JEOL JCM-6000 Benchtop SEM. The paper specimens were coated with gold using a sputter coater directly prior to image acquisition.